Stony Brook University

RapidCaP, a mouse model for analysis and therapy of prostate cancer reveals drivers of *Pten*-mutant metastasis.

A Dissertation Presented

by

Hyejin Cho

to

The Graduate School in Partial Fulfillment of the Requirements for the Degree of

Doctor of Philosophy

In

Molecular and Cellular Biology

Stony Brook University

August 2013

Stony Brook University

The Graduate School

Hyejin Cho

We, the dissertation committee for the above candidate for the

Doctor of Philosophy degree, hereby recommend

acceptance of this dissertation.

Dr. Lloyd Trotman – Dissertation Advisor
Associate Professor, CSHL

Dr. Alea Mills - Chairperson
Professor, MCB

Dr. Leemor Joshua-Tor - Co-adviser
Professor, MCB

Dr. Christopher Vakoc - member
Assistant Professor, MCB

Dr. Scott Lowe - outside member
Professor, MSKCC

This dissertation is accepted by the Graduate School

Charles Taber
Interim Dean of the Graduate School

Abstract of the Dissertation

RapidCaP, a mouse model for analysis and therapy of prostate cancer reveals drivers of *Pten*-mutant metastasis.

by

Hyejin Cho

Doctor of Philosophy

in

Molecular and Cellular Biology

Stony Brook University

2013

The functional loss of PTEN through mutations, deletions, or protein degradation has been found at a high frequency in many human cancers. Therefore, the *Pten* gene locus has been targeted to generate clinically relevant mouse models for metastatic prostate cancer. The first two chapters include the development and exploration of RapidCaP, a novel mouse model for prostate cancer metastasis, that is based on surgical gene transfer to overcome the need for extensive animal breeding. Through prostate specific delivery of transgenic virus, model generation times have been reduced from several years to a few weeks. Moreover, non-invasive Xenogen-based imaging can be used to monitor disease progression. Using RapidCaP, it is shown that focal loss of *Pten* and *Trp53* genes in prostate triggers distant metastasis at 56% penetrance by 4 months. Molecular pathology analysis revealed spontaneous Myc activation in metastatic nodules. Importantly, it was confirmed that *Myc* can induce local metastasis using a *Myc*-transgenic RapidCaP model. This demonstrates the identification and functional validation of the system. In castration therapy trials, both primary and metastatic disease respond with regression, but later relapse to produce lethal, castration resistant disease, as seen in human. The RapidCaP system thus introduces a fast and faithful platform for research and therapy of metastatic prostate cancer in genetically engineered mice. The last chapter presents the generation of a dual color reporter system for identification of the regulators of PTEN stability.

Taken together, this thesis introduces novel tools for cancer discovery and their application for understanding prostate metastasis.

Table of Contents

List of Tables

List of Figures

List of Abbreviations

APCs	Antigen presenting cells
AR	Androgen receptor
ARR2	Arrestin 2
BPH	Benign Prostatic Hypertrophy
CARNs	Castration resistant Nkx3.1-expressing cells
CAST	Castration
CHX	Cycloheximide
CK-2	Casein kinase-2
CK8	Cytokeratin 8
CR2	Cryptdin-2
Cre	Cre recombinase
CRPC	Castration-resistant prostate cancer
DOX	Doxycycline
ERG	Ets related gene
FACS	Fluorescence-activated cell sorting
FG	Fetal globin-gamma
GEM	Genetically engineered mouse
GFP	Green fluorescent protein
H&E	Hematoxylin and eosin staining
HER2	Human Epidermal Growth Factor Receptor 2
HPC	Hereditary prostate cancer
IAP	Inhibitor of apoptosis
IF	Immunofluorescence
IGF-1	Insulin-like growth factor 1
IHC	Immunohistochemistry
IRES	Internal ribosome entry site
LKB-1	Liver kinase B1
LSL	LoxP-STOP-LoxP cassette
Luci	Firefly luciferase

LV	Lentivirus
MAT205	Microtubule associated kinase
MEF	Mouse embryonic fibroblast
MLP	MSCV LTR miR30-shRNA Puro IRES GFP vector
MSR1	Macrophage scavenger receptor 1
NEDD 4-1	Neural precursor cell-expressed, developmentally downregulated 4-1
NK	Natural killer
NOD	Non obese Diabetic
NSCLC	Non-small cell lung carcinoma
Pb	Probasin
PIN	Prostatic intraepithelial neoplasia
PSA	Prostate specific antigen
PTEN	Phosphatase and tensin homolog deleted on chromosome ten
RAG	Recombination activating gene
RAK	RhoA-associated kinase
Rb	Retinoblastoma
RLuc	Renilla-Luciferase
RNAi	RNA interference
RNASEL	Ribonuclease L (2',5'-oligoisoadenylate synthetase-dependent)
rPB	Rat probasin promoter
rtTA	reverse tetracycline transactivator protein
RV	Retrovirus
SCID	Severe combined immunodeficiency
SV40	Simian virus 40 (SV40)
Tag	Large tumor antigen
TRAMP	Transgenic Adenocarcinoma of the Mouse Prostate
TRE	Tetracycline responsive element
XIAP	X-linked inhibitor of apoptosis protein

Acknowledgements

Foremost, I would like to express the deepest appreciation to my advisor, Dr. Lloyd Trotman, who has been greatly supportive and encouraged me to have a positive mind. He has been patient, motivated, enthusiastic and knowledgeable. I could not have imagined having a better advisor and mentor for my Ph.D study.

Besides my advisor, I would like to thank my thesis committee: Dr. Alea Mills, Dr. Scott Lowe, Dr. Leemor Joshua-Tor and Dr. Bill Tansey for their encouragement, insightful comments, guidance and encouragement over these years. Your advice and interest in my progress have always been motivative. Without their encouragement and guidance, this project would not have materialized. I also like to thank Dr. Chris Vakoc for accepting to be a member for my thesis defense.

Thank you to past and present members of the Trotman lab, I am grateful to share research experiences with the former member, Martha Zeeman, and with Tali Herzka who helped the launching and improving of the RapidCaP model, Adam Naguib and Dawid Nowak for intense scientific discussion and for forming a nice lab atmosphere, former member Wu Zheng for materials, help and a positive attitude, Dorothy Tsang for her great care for every detail.

I would like to especially thank Johannes Zuber, for teaching all procedures, from the basic to the most sophisticated cloning techniques and screening library development, for spending time to design the whole experiments and for mentoring me in proceeding with the PTEN stability project. Without his guidance and persistent help, Chapter IV would not have been possible.

My sincere thanks also go to my close friends, Nilgun Tasdemir, Young Kyoung Lee and her family, and Marlies Rossman for your faithful friendship. Most of all, without your enormous encouragement and comfort, I might not have been able to continue my Ph.D. research. Also, thank you to Charles Frosch for your patience and great support.

Last but not least, I would like to thank my family: my parents, brothers and sisters for being a constant source of my inspiration and motivation, giving me their immense support throughout, as always, for which my mere expression of thanks likewise does not suffice.

I. Introduction

1. Prostate cancer

A. History

In 1853, John Adams, a surgeon in London hospital, described the first case of prostate cancer (CaP) as a rare disease (Adams, 1853). One hundred sixty years later, it has become the most commonly diagnosed cancer and the second most frequent cause of cancer related deaths in men in the United States. This remarkable increase in CaP incidence can be due to several reasons. First, CaP was not distinguished from other incidences of urinary obstruction until the early 1900's. Second, the incidence of CaP rises with age more than any other cancer type (Greenlee et al., 2001). Therefore, as the average life expectancy has increased, many more CaPs are diagnosed. Third, the rising number of CaP cases is related to the Western lifestyle. The incidence of CaP is notably lower in Asian populations, moreover, case numbers increase in Asian men after they immigrate to Western countries (Ingles et al., 1997). The majority of disease related death is due to the complications, such as infections and hemorrhage, resulting from advanced bone metastasis and multiple treatments. Prostatic metastasis is often found in bone and soft tissues. In the 1940s, Charles Huggins opened the doors to the new era of CaP therapy by discovering that metastatic CaP requires androgen as it responds to castration (Huggins, 1941). Ever since, androgen ablation has remained the most powerful intervention to prevent death from this disease.

B. Diagnosis and disease progression

CaP is a slowly progressing disease. It is not fully understood when a localized cancer will spread and cause clinically manifest problems. Two major advances have led to today's standard for quantification of the disease and its speed of progression:

(1) Gleason scoring

CaP histopathology is closely related to the rate of growth and spread of CaP, therefore it is most commonly recorded using the Gleason grading system, which is based on the architectural pattern of cancerous glands (Gleason and Mellinger, 1974). The most differentiated

Figure 1. Gleason Scale

After biopsy, cancer cells are graded according to the Gleason scale.

* ***Pattern 1*** –The glands are small, well-formed, and closely packed.
* ***Pattern 2*** – The tissues are larger and have more tissue between them.
* ***Pattern 3*** – The tissue still has recognizable glands, but the cells are darker. At high magnification, some of these cells have left the glands and are beginning to invade the surrounding tissue.
* ***Pattern 4*** – The tissue has few recognizable glands. Many cells are invading the surrounding tissue.
* ***Pattern 5*** – The tissue does not have recognizable glands. There are often just sheets of cells throughout the surrounding tissue.

froProstate.net)

Figure 2. Disease-specific survival

According to the Gleason score, the tumors were grouped into four categories, i.e. 4–5, 6, 7 and 8–10. The disease-specific survival of these categories differed significantly (P<0.001); the numbers of patients at risk in the respective categories at 5/10/15 years were 46/30/2, 53/25/6, 30/10/2 and 32/7/1. (Egevad et al., 2002)

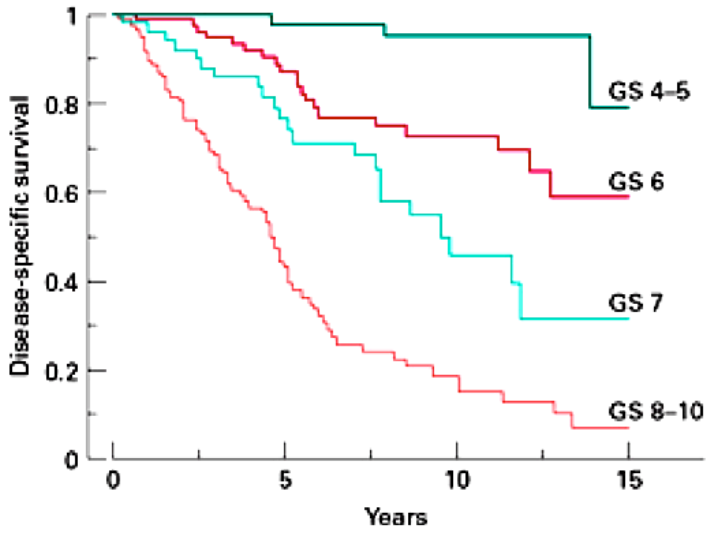

(benign) regions are graded as 1 and the least differentiated as 5 (see **Figure 1**). Due to multi-focality, the overall Gleason score is defined as the sum of the two most prevalent patterns. Individuals with a higher Gleason score tend to have more aggressive cancer and shorter survival. Despite attempts to identify genetic signatures distinguishing low– and high–Gleason grade cancer, different signatures show little overlap between individual genes, and the processes driving the different architectural patterns remain unknown (Kallioniemi et al., 1996). It has been reported that men with low grade CaP (Gleason sum score 2 to 4) had such a low rate of progression that survival over 15 years was very similar to that of age-matched men, who did not have cancer. However, patients with Gleason 8-10 disease show only a 50% survival rate at 5 years (Egevad et al., 2002) (**Figure. 2**), while intermediate progression and death rates are seen in men

with Gleason 6-7 sum scores. In comparison to many types of cancer, CaP is slow to infiltrate adjacent tissues and spread to distant sites.

(2) Prostate specific antigen (PSA) : prediction and surveillance

In 1986, prostate specific antigen (PSA) was approved as a marker to monitor the response to therapy and disease recurrence and it has been the most common standard to diagnosis of disease since 1994. In the last two decades, a number of studies have accumulated evidence that the serum PSA level is closely associated with CaP risk (Aus et al., 2005; Gann et al., 1995; Stenman et al., 1994; Thompson et al., 2004; Ulmert et al., 2008). However, recent reports have proposed that PSA testing causes the over-diagnosing and treatment of harmless cancers (Schroder et al., 2009; Schroder et al., 2012b). Moreover, the evaluation of serum PSA levels can be misleading because the PSA level can be affected by various factors, such as age, race/ethnicity (Richardson and Oesterling, 1997), infectious and inflammatory status, body mass index (Banez et al., 2007) (Werny et al., 2007) (Rundle and Neugut, 2008), hyperplastic status and also by the detection method (Link et al., 2004). In terms of detection of CaP, higher PSA levels than 4 ng/ml are used as direct criteria for performing a biopsy. However, this value has been criticized as a number of studies have shown that the frequency of CaP is not negligible among men with lower than 4 ng/ml PSA level (Thompson et al., 2004). Therefore it has been suggested to include a number of other risk factors to determine CaP probability (Thompson et al., 2006). In contrast, the recurrence of CaP, which is also mostly detected by monitoring PSA, has been undoubtedly beneficial. An increasing PSA level, for example after a radical prostatectomy, is the most valuable indicator for disease recurrence.

On the other hand, novel treatments may have unexpected effects on PSA levels, and so the use of PSA in monitoring castrate-resistant CaP (CRPC) is becoming controversial (Chen et al., 2004). Taken together, identifying new CaP biomarkers that facilitate early cancer detection with high accuracy are still in need, while post-treatment monitoring could also still benefit from improved approaches.

(3) Metastasis

CaP is the second leading cause of cancer deaths of men in the United States (Greenlee et al., 2000). The vast majority of CaP deaths are related to metastatic disease and more than 70%

of deaths are due to complications resulting from late-stage tumors that have spread to distant sites (Zhau et al., 2000). CaP typically first spreads to the tissues immediately adjacent to the prostate, including the seminal vesicles and nearby lymph nodes and then migrates to bone. In a majority of advanced prostate disease, metastasis is found particularly in bone, which is a well known and leading cause of mortality and morbidity. Bone metastasis is most commonly seen in the lower spine, the pelvis, and the upper legs, though CaP can spread to bones anywhere in the body. The second most common CaP metastatic site is liver, followed by the lungs and adrenal glands (Bubendorf et al., 2000). In order to form a metastatic lesion, initiating cells have to retain proliferation properties subsequent to their migration to a secondary site. The simplified presumed sequence of metastasis is initiated by local invasion to seminal vesicles and the lymph nodes, intravasation, survival in circulation, extravasation and colonization of distant organs. For a particular malignancy to progress to metastatic disease a complex series of biological properties must be acquired (Chambers et al., 2002). In this vein, it has been observed that only a small portion of cells from a primary tumor are able to initiate secondary growth (Nguyen et al., 2009)(Chambers et al., 2002). Most intriguingly, there is also evidence that tumor cell dissemination occurs early in disease progression for a variety of cancers, including CaP, but the vast majority of these cells cannot establish metastases. It had indeed been reported that the genetic aberrations in metastatic cells from bone marrow samples did not resemble those in the primary tumor, and this was explained by tumor cells disseminating very early and evolving independently in metastasis and in the primary tumors (Schmidt-Kittler et al., 2003) (Eyles et al., 2010) In contrast however, recent whole genome analysis of CaP evolution suggests a monoclonal origin of lethal metastasis (Liu et al., 2009). In the same vein, single nucleus sequencing to analyze breast cancer evolution has revealed a close relationship between primary and metastatic cells (Navin et al., 2011).

C. Molecular Pathology - Molecular changes associated with CaP

Genetic alterations are observed in over 90% of cancers, some of these are inherited, while others are sporadic, or in response to long-term environmental exposure. The enormous amount of research into CaP has demonstrated a complicated interaction of multiple genes and environmental factors involved in the molecular pathology of CaP. At the time CaP is detected, cancer cells are found to contain various genetic alterations, such as somatic mutations, gene

deletions/amplifications, chromosomal rearrangements and changes in DNA methylation, which are thought to have accumulated for several decades (Baca et al., 2013). With the rapidly growing technology and research tools, an increasing amount of data has revealed genetic variations regulating the initiation, development, and progression of CaP. The recent landmark genetic study on CaP performed at Memorial Sloan Kettering Cancer Center (Taylor et al., 2010) has revealed that a steady increase in copy number alterations (more than gene mutations) is seen in disease progression, resulting in complex patterns in late stage metastasis.

(1) Genetic changes in hereditary CaP

The hereditary component in the risk of CaP has been reported in multiple studies (Schleutker et al., 2000). Most inherited cases which show early onset of CaP were caused by both autosomal dominant and X-linked alleles. So far, three genes of linkage were identified in the first genome wide screen for polymorphic markers, *HPC2/ELAC2* on 17p (Tavtigian et al., 2001), *RNASEL* on 1q25 (Carpten et al., 2002) and *MSR1* on 8p22-23 (Xu et al., 2002). Although *ELAC2*, a metal dependent hydrolase, was first known to be associated with familial CaP in an earlier study (Rebbeck et al., 2000), the significance of *ELAC2* in cancer progression has not been confirmed in other reports (Dong, 2006). The chromosomal region, 1q24-25, assigned as the hereditary CaP (HPC1) gene locus, has been most investigated and shown the strongest linkage to CaP. A putative gene in the HPC1 locus, *RNASEL* (encoding ribonuclease L), is a ubiquitously expressed endoribonuclease associated with the antiviral and pro-apoptotic pathway by degrading viral and cellular RNA (Kerr and Brown, 1978; Zhou et al., 1997). Recent studies have suggested that the reduced enzymatic activity of *RNASEL* is seen in about 13% of CaP cases (Casey et al., 2002) (Rennert et al., 2002) (Rokman et al., 2002). The *MSR1* gene encodes a macrophage scavenger receptor responsible for cellular uptake of molecules. The *MSR1* susceptibility in hereditary CaP has been controversial based on familial studies of hereditary CaP (Wang et al., 2003). An individual harboring an *MSR1* mutation may thus have increased CaP risk due to chronic inflammation, which could indirectly cause or accelerate the disease. Taken together, two inherited susceptibility genes, *RNASEL* and *MSR1*, may primarily have roles in host response to infections, owing to the possibility that prostate infection or inflammation could initiate carcinogenesis.

In the last few years, a number of genome wide analyses have identified more than a dozen germline single nucleotide polymorphisms (SNPs) associated with increased CaP risk. The combination of these SNPs might raise the probability of CaP occurrence (Alvarez-Cubero et al., 2012). Currently, the etiology of CaP remains to be identified since the increasing amounts of research have suggested that the combination of genetic variations and numerous environmental factors can affect CaP progression. Unlike other cancers, for example breast of colorectal, CaP has not so far been associated with a strong hereditary component that could help with early identification of people who are at risk.

(2) Genetic changes in sporadic CaP

Most CaPs are sporadic, developing spontaneous chromosomal rearrangements, some somatic mutations, gene deletions, amplifications and or changes in DNA methylation at the time of diagnosis. Based on studies on CaP onset, these alterations probably accumulate over a period of several decades (Vogelstein et al., 2013).

Copy number changes - Now classic studies have reported somatic genome alterations by using comparative genomic hybridization (CGH). The most frequently found chromosomal abnormalities were gains at 7q, 7p, 8q and Xq, losses at 8p, 10q and 16q (Elo and Visakorpi, 2001). Today, rapid advances in whole genome analysis have validated most of these but added a number of hot spots in the genome (**Figure 3**) These include deletions on chromosomes 13q, and 17p harboring *RB1* and *TP53*, respectively (Taylor et al., 2010).

Translocations - The most common gene fusion in CaP is between *TMPRSS2* (transmembrane protease serine 2) and *ERG* (a member of the erythroblast-transformation specific (ETS) gene family), which has seen in about 50% cases (Tomlins et al., 2005) (Kumar-Sinha et al., 2008; Tomlins et al., 2007). Functional studies in mouse (see below) have demonstrated cooperation of the fusion with other genetic lesions, for example loss of *PTEN*. However, it has emerged that this event is generally more important in tumor initiation than in tumor progression to metastasis.

Methylation/silencing - Another observed somatic change in CaP is DNA methylation. The comparative analysis of genome-wide DNA methylation patterns within tumor and benign prostate samples has revealed greater than 147,000 cancer related epigenetic changes. Interestingly, a significant difference in global methylation was associated with *TMPRSS2-ERG*

fusion free *EZH2* activation, indicating that an altered methylation pattern in rearrangement free tumor might be important for disease progression (Borno et al., 2012).

Figure 3 Global View of the CaP Genome

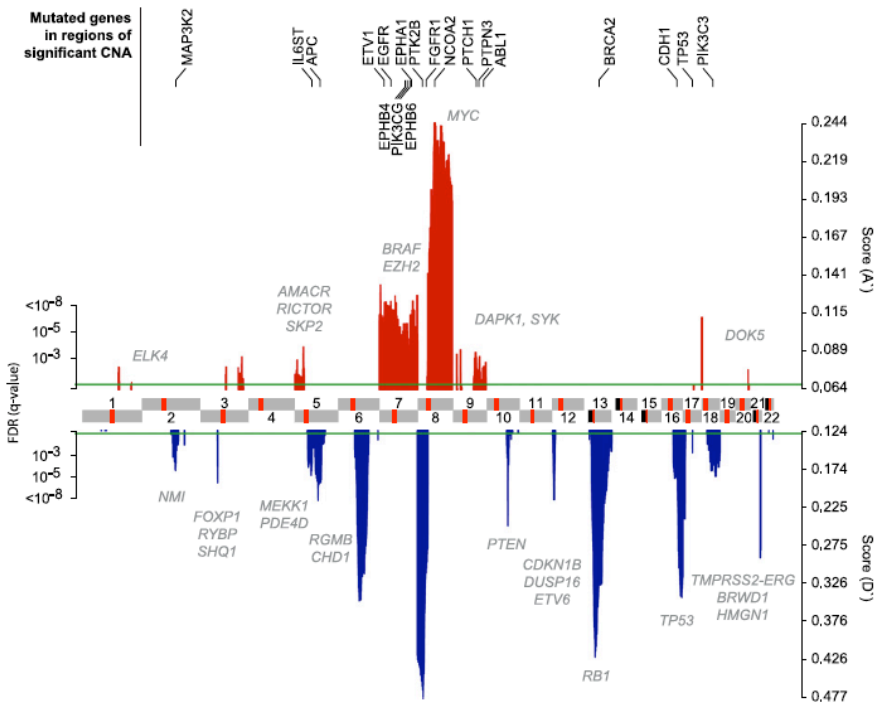

(Taylor et al., 2010)

Tumor suppressor genes

Increasing evidence has led to a revision of the initial requirement that 'tumor suppressor genes are defined by loss of both alleles ("two hit hypothesis" (Knudson, 1971)). Indeed, whole genome studies now reveal that the deletion of validated prostate tumor suppressors is most commonly seen in heterozygosity (see Taylor et al. and TCGA prostate provisional data at http://www.cbioportal.org/public-portal/index.do). The comprehensive genome analysis has found relatively rare somatic point mutations in primary and advanced CaP compared to other cancer types. Also a greater number of deletions than amplifications was seen throughout the genome, suggesting that loss of tumor suppressors might be the major driving force for disease initiation and progression. In addition, single allele deletion in haploinsufficient tumor suppressors, such as PTEN, combined with loss of other tumor suppressors, has been observed to co-operatively affect the PI3K-AKT pathway, at least in primary cancers (Taylor et al., 2010). The best characterized tumor suppressor genes in CaP are summarized below:

PTEN (Phosphatase and Tensin homolog deleted on chromosome Ten (Li et al., 1997), is a dominant prostate tumor suppressor gene. Its protein expression is lost in 75% of CaP (Chen et al., 2011), and gene deletion is found in 50%-63% after CaP progression to metastasis.

As shown in **Figure 3**, co-deletion of both *PTEN* and *NKX3.1* are common in CaP and haploinsufficiency of *PTEN* contributes to active proliferation in prostate cells (Taylor et al., 2010). *PTEN* copy number loss and down regulation of PTEN protein is also correlated with poor prognosis (Cordon-Cardo et al., 1998; Guo et al., 1997). On the other hand, PTEN has been described to regulate the level of p27, encoded by *CDKN1B*. Not only is somatic deletion of *CDKN1B* frequent in primary and metastatic CaP (Taylor et al., 2010) but also the expression and nuclear localization of p27 (Shin et al., 2002) are suppressed by the PI3K-AKT signaling pathway. Therefore, PTEN performs an important role as a tumor suppressor by regulating p27 level in CaP progression (Gottschalk et al., 2001)(Nakamura et al., 2000).

Rb1 (Retinoblastoma 1) is an important tumor suppressor in various human cancers, including CaP. The Rb protein inhibits transcription of various genes involved in cell growth by binding to E2F transcription factors (Bookstein et al., 1990; Brooks et al., 1995). Inactivation mechanisms of Rb have been reported through allelic loss, mutation and decreased transcription (Lalani el et al., 1997; Tricoli et al., 1996).

A relatively low frequency of ***TP53*** mutations as well as rare case of copy number loss was found in early stages of CaP (Taylor et al., 2010). Consistently, no major effects on prostate have been seen in *Trp53*$^{pc-/-}$ mice (Chen et al., 2005). However, the combined loss of *Pten* and *Trp53* showed aggressive invasive CaP. Indeed human metastatic samples with *PTEN*-loss also show *TP53*-deletion prompting us to postulate that *TP53*-loss is a bottleneck for *PTEN*-mutant prostate cancer (Chen et al., 2011).

NKX3-1, located at 8q21, encodes a prostate specific homeobox protein and binds to the *PSA* promoter to repress gene expression (Chen et al., 2002; Steadman et al., 2000). Prostatic epithelial hyperplasia and dysplasia have been shown in mice harboring a disrupted *NKX3-1* allele (Abdulkadir et al., 2002; Bhatia-Gaur et al., 1999). In human studies, loss of 8q21 was shown as an early event during prostate carcinogenesis and also more than 90% of CaP cases have lost heterozygosity at 8q21 (Emmert-Buck et al., 1995). However, due to the broad nature of deletions other tumor suppressors cannot be excluded as the selective factor in the chromosomal loss observed in this region.

Oncogenes

The positive correlation between *c-MYC* expression and CaP has been reported in multiple studies. The *MYC* oncogene is a member of the basic helix-loop-helix-leucine zipper

(bHLHZ) family of transcription factors. c-*MYC* is often found amplified in CaP and is closely linked to worse prognosis (Sato et al., 1999). Mutations of the androgen receptor (AR) are rare at early stages, however, the frequency of mutations dramatically increases in advanced, androgen independent CaP, indicating that AR mutations are associated with tumor progression. Greater than 70 different somatic missense AR mutations have been found in CaP patients (Brooke and Bevan, 2009). Most AR mutations are known to provide growth advantages by altering binding affinities for either AR co-factors or ligands (Gottlieb et al., 2004). Amplification of the *AR* gene has been closely associated with recurrence in CaP patients who failed androgen deprivation therapy (Chen et al., 2008).

D. Advanced prostate cancer and treatment

In 1941, Huggins and Hodges concluded that "Prostatic cancer is influenced by androgenic activity in the body" (see (Huggins and Hodges, 1972)). Ever since, androgen deprivation therapy, or 'hormone therapy', achieved through castration or oalternative mechanisms of androgen neutralization has been the standard care treatment for CaP.

The first-line therapy for localized CaP, prostatectomy or radiation, is however mostly beneficial. Some 20% of patients show recurrence, as detected by a rising serum PSA level after 5 years. Moreover, surgical castration or radiation therapy is not beneficial for patients diagnosed after the cancer has spread. Advanced CaP is almost always treated with androgen deprivation therapy (ADT), achieved by either surgical castration (orchidectomy), estrogen-therapy, luteinizing hormone-releasing hormone (LHRH) agonist therapy, anti-androgens and more recently through gonadotrophin-releasing hormone antagonists. Degarelix, the most actively studied antagonist, has been shown to control testosterone better, and increase survival without biochemical recurrence (PSA rising above 0.2 ng/ml) (Schroder et al., 2012a). Subsequently most patients proceed to a more aggressive disease, now termed castration-resistant prostate cancer (CRPC) because it is still sensitive to AR inhibition (Ryan and Tindall, 2011). Increased AR expression due to gene amplification and mutation has often been found in CRPC. A number of studies with mouse xenograft models have proven that the resistance to ADT can be explained with increased AR levels (Cai et al., 2009; Sun et al., 2010). Therefore, the AR has been the major target for ADT emergence. The first generation AR antagonists, bicalutamide and flutamide, block androgen binding to the AR effectively lowering serum PSA level. In 2012, the

FDA approved a new second generation AR antagonist Enzalutamide, (previously known as MDV3100, and related to ARN509) developed by Charles Sawyers and Michael Jung (at UCLA) to better treat CRPC through higher binding affinity for AR, including mutated or overexpressed AR, and to prevent the nuclear translocation of AR (Tran et al., 2009). In phase I/II clinical trials, these drugs have proved their potential by demonstrating sustained lowered serum PSA levels. Another recently FDA approved drug, Zytiga (Abiraterone) targets the CYP17A enzyme of the testosterone biosynthesis pathway and has also shown significant, 4 month increased, relapse-free survival benefits in CRPC patients (de Bono et al., 2011). However, most likely, patients treated with these drugs will eventually develop resistance with rising PSA levels. Possible mechanisms for drug resistance could be *AR* mutations (truncated or constitutively active), or synthesis of androgens independent of the CYP17A pathway, and crosstalk with other growth pathways (**Figure 4**) (Carver et al., 2011; Craft et al., 1999; Zhu and Kyprianou, 2008). Taken together, efforts to defeat death from prostate cancer are today focused on identifying the molecular mechanisms behind resistance to these second- and third-line therapies of metastatic CRPC.

Figure 4. Promising Targets in Castration-Resistant CaP.
(1) Sipuleucel-T induce the immune system to recognize and kill prostate-cancer cells. (2) Abiraterone blocks androgen synthesis. (3) MDV3100 blocks androgen binding, nuclear translocation of the receptor, and coactivator recruitment to the DNA-binding complex. HSP90 can be blocked by (4) geldanamycin and its congeners. Endothelin receptor antagonists ((5) zibotentan and atrasentan) block by endothelin. RANK ligand inhibitor (6) denosumab. (7) Heregulin and Dasatinib inhibit epidermal growth factor (EGF). (Longo, 2010)

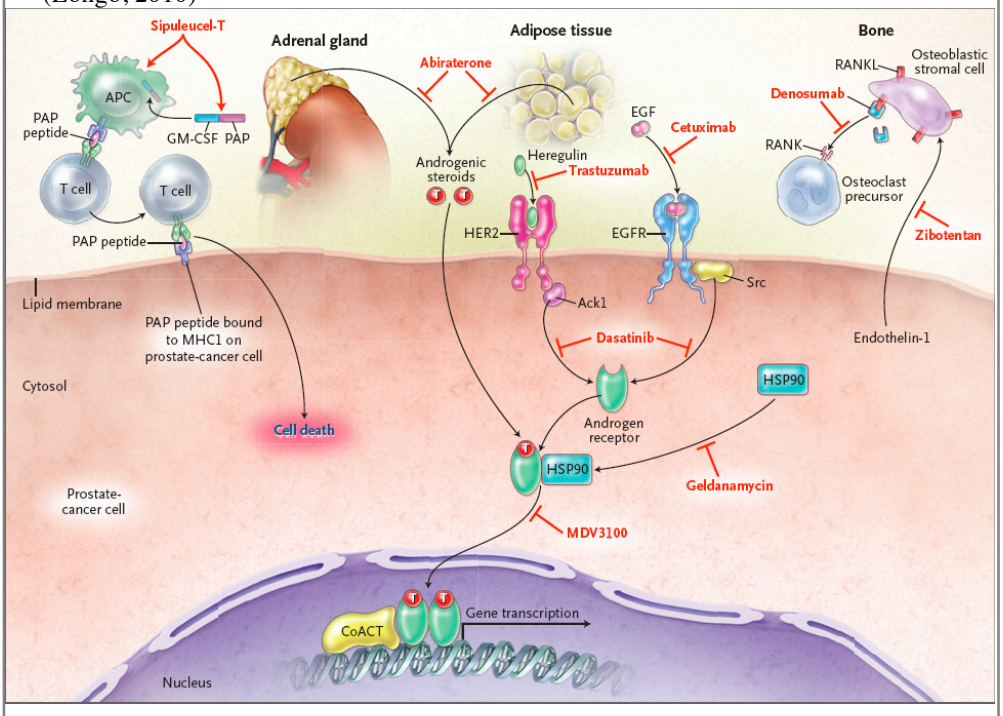

2. Mouse models of CaP

Introduction

Anatomically mouse prostate differs from the human organ. Mouse prostate is divided into four lobes: anterior, ventral, dorsal and lateral (Abate-Shen and Shen, 2002), whereas human prostate has a single globular lobe, which consists of the, central, transitional and peripheral zones. Most human CaPs are found in the peripheral zone, which constitutes almost 75% of the tissue. No clear relationship has emerged between any of the mouse prostate lobes and the zones of human prostate (Shappell et al., 2004). Noticeably, it is known that mouse does not develop spontaneous carcinoma in prostate. In fact, only three large animals are known to spontaneously develop high-grade PIN and CaP at high frequency, humans, dogs and lions.
Hence, a large amount of research has focused on genetically engineering mice to recapitulate human CaP accurately. The mouse model is by far one of the best animal models to study human cancer, as mice can be made tumor-prone by gene manipulation. Importantly, the human and mouse genomes are about 95% identical, and various genes and genomic alterations that were identified in human cancers were also shown to facilitate mouse cancers (de Jong and Maina, 2010; Maser et al., 2007). Genetic engineering is relatively easy in mice and also housing and breeding are relatively affordable due to the small size and short gestation time.

The purpose behind developing a mouse model of human cancer is to identify mechanisms of disease and test new therapies. The ideal CaP mouse model would evolve along the following expected path: early epithelial hyper-proliferation and hyperplasia, resulting in prostatic intraepithelial neoplasia (PIN), which does not invade stroma. Then a region with high grade PIN would develop a locally invasive phenotype, carcinoma, and finally proceed to first local and later distant organ metastasis, such as to bone, lymph nodes and liver. The ideal model would also recapitulate response and resistance to castration therapy, as discussed above. Even though genetic engineering succeeded to recreate primary cancer, the following caveats remain to be solved: 1) absence of metastasis, 2) lethality of primary cancer. Importantly, the commonly observed bone metastasis in human patients has proven difficult, if not impossible, to recapitulate in mouse (Ittmann et al., 2013). Genetically engineered mouse models have been tailored to modify (mutate, delete or over-express) genes of interest in the whole body, the entire prostate epithelial tissue, or in a subset of cells that form the gland. These genetic changes are

typically acquired after puberty in a conditional knockout (cko) approach or through the germline (ko) approach. However, gene alterations in human are thought to most commonly occur in a random single cell of a prostate gland and this is expected to initiate focal disease first.

In order to test therapy efficiently, disease progression needs to be monitored by live, non-invasive imaging. The most commonly used imaging technique use firefly luciferase (bioluminescent imaging), and green fluorescent protein or its derivatives for fluorescence imaging. Recently, transgenic models, expressing firefly luciferase in the prostate in an androgen dependent manner, have been developed (Ellwood-Yen et al., 2006; Hsieh et al., 2005; Lyons et al., 2006). However, the sensitivity of luminescence signal in these models is limited by significant background and relatively weak reporter gene expression in the anterior and dorsolateral lobes of the murine prostate. A slightly different approach has used *Cre- LoxP*-mediated activation of either luciferase or a *GFP* reporter gene combined with conditional *Pten* deletion and revealed live prostate cancer signal but lymph node metastasis in less than 3 out of 120 mice (Liao et al., 2007). The conventional ways of monitoring tumor progression and metastasis of tumor cells are positron emission tomography (PET), magnetic resonance imaging (MRI), and Micro-computed tomography (CT) scanning. However, these techniques are very expensive for routine monitoring of large cohorts and require highly trained staff, a team of radiologists and physicists to run experiments and interpret results.

Various CaP mouse models have been developed over the last few decades, xenograft models and genetically engineered mouse models (GEM models), which both will be discussed below.

A. Xenograft models

Immunodeficient mice have been used as recipients of foreign tissues, such as human tumor tissues, primary cells and cell lines. The first transplantation of a human androgen-responsive prostate tumor was conducted in athymic nude mice in 1980 (Hoehn et al., 1980). These models facilitate human tumor analysis by allowing patient derived tumors or cell lines to engraft and expand *in vivo* so that researchers can test effective treatments. Since it is possible to graft combinations of multiple genetic changes (manipulated *ex vivo*) into immunodeficient mice, the system can be used to study many different genetic modifications.

Nude mice - The first xenotransplantation model used for human CaP tissue was in nude mice (Hoehn et al., 1980). Nude mice are deficient in T lymphocytes due to lack of a thymus caused by a genetically engineered mutation. Subcutaneous and orthotopical injection of a castration resistant CaP cell lines (C4-2) resembles human CaP by metastasizing to the lymph node and bone, as analyzed by histopathology. (Thalmann et al., 1994).

SCID (Severe combined immunodeficiency) mice are deficient in mature B and T cells due to a defect in genetic recombination necessary for lymphoid development (Bosma and Carroll, 1991), however natural killer (NK) cells and myeloid cells are normal. This model was specifically used to study if HER2/NEU mediated the growth of androgen independent CaP (Craft et al., 1999).

NOD (nonobese) -SCID mice are an improved model of SCID mice by crossing to nonobese diabetic (NOD) mice, which are deficient in NK cells, circulating complement, and functional antigen-presenting cells (APCs) (Greiner et al., 1995; Serreze and Leiter, 1988). This model shows a higher success rate of transplantation relative to SCID mice due to high acceptance of foreign tissues (Shultz et al., 1995).

NOG/NSG mice - A further improved model of NOD-SCID mice with complete loss of B, T, and NK cells generated by crossing X-SCID mice, which is lacking interleukin 2 receptor γ (*IL2Rγ*) and NK cells (Cao et al., 1995; Ohbo et al., 1996). Currently this is the most severe immunodeficient model. As such, it shows a higher success rate in xenograft derived tumor growth and no tumor regression has been described in long term monitoring.

RAG mice - deficient in the recombination activating gene (RAG), leading to deficiency in both B and T cells. This model possesses an inflammatory response and NK cell activity. To study specific anti-tumor treatment, TRAMP-C2 (TRAMP model driven prostate epithelial cell line, see below for TRAMP model) cells were injected to RAG mice to establish a link between TGF-beta signaling and immune responses (Zhang et al., 2006).

Patient-derived xenografts (PDX) mice were generated to recapitulate the human tumor microenvironment and heterogeneity better than cell lines. They use direct implants of tumor tissues into immune deficient nude mice. PDX has been accepted as a beneficial model to depict the characteristics of patient's original tumor, such as the expressions of immunohistochemical markers, genetic alterations and representing the response to therapies (Lawrence et al., 2013).

Despite these benefits of the xenograft model, there are severe restrictions to this approach. First, the lack of an immune system can be misleading as it plays a critical role in progression of human CaP and metastasis (Buijs and van der Pluijm, 2009; Eshhar et al., 2005). Second, normal tumor development and evolution of tumor architecture can not be recapitulated in a xenograft model. Therefore, the tumor microenvironment, including vasculature, stromal cells, lymphatic circulation and infiltrating immune cells, is very different from that seen in patients, and may make treatment artificially more successful (Becher and Holland, 2006; Frese and Tuveson, 2007; Sikder et al., 2003). Another major pitfall of xenograft models is the misreading of cells stuck in circulation as metastasis. Moreover, the ability of xenograft models to predict the drug efficiency in human has not been successful. Yet, mouse xenograft models derived from human prostate tumor cells have been used extensively in drug discovery due to their overall practicality and low cost.

B. GEM models of CaP

(1) Transgenic T Antigen models

GEM models have allowed for the development of models carrying genetic modifications similar to those found in human tumors. This has not only validated the importance of these alterations in tumor initiation and progression but has also facilitated the development of improved models for therapeutic testing in several human tumors. The challenge of finding a suitable prostate specific promoter for oncogene expression was first met by choosing expression of the simian virus 40 (SV40) Large T antigen (TAg), as an oncoprotein that can inhibit both p53 and retinoblastoma proteins. The resulting models showed aggressive prostate phenotypes and with some metastatic and castration-resistant characteristics. However, the models have been criticized as too artificial because metastases typically had a neuroendocrine pathology, which is not typical of human metastatic disease. Thus, faithfulness and clinical relevance of these mouse models remained to be determined.

C3(1)-Tag - Researchers targeted the expression of the SV40 large tumor antigen (Tag) to the prostate by using a region of the *C3(1)* gene, which is known as the rat prostatic steroid binding protein gene. Male *C3(1)*-Tag mice developed early (3 month) prostatic epithelial hyperplasia, and the majority of males developed locally invasive adenocarcinoma by 7–11

months. Metastasis was rarely found in this model. The drawback of this model was that expression of SV40 was not prostate specific (Yoshidome et al., 1998).

TRAMP - In this model Norman Greenberg and colleagues, drove the expression of both the large and small SV40 tumor antigens (T/tag) by the prostate-specific rat probasin promoter (*rPB*) (Greenberg et al., 1995). TRAMP mice developed epithelial hyperplasia by 8 weeks of age, progressing to prostatic intraepithelial neoplasia (PIN) by 18 weeks of age, and at 28 weeks old, 100% of the mice developed lymphatic metastases, and approximately two-thirds acquired pulmonary metastases. Thus, TRAMP was the first mouse model to display distant organ metastasis, albeit only rarely to bone. As mentioned above, an issue with the TRAMP model is that metastasis in these mice has been reported to be of neuroendocrine origin (Chiaverotti et al., 2008). Neuroendocrine tumors (NETs) share a common histopathology but are found to originate in a variety of tissues, most famously pancreas, and also intestine (also termed carcinoids) or lung. It has been reported that only about 10% of prostate adenocarcinoma includes neuroendocrine differentiation (McLeod et al., 1992).

FG (fetal globin-γ) Tag - This model was initially designed to study erythroid cells since the *fetal globin-γ* gene was thought to be specifically expressed in embryonic erythroid cells. The mice with human *FG* promoter driven expression of T antigen developed prostate tumors at 50% penetrance after 16 weeks and metastasis to the renal lymph nodes, adrenal glands and kidneys as well as micrometastases to the lung, bone and thymus (Calvo et al., 2010; Chada et al., 1986; Perez-Stable et al., 1997). However, T antigen expression was not exclusively prostate specific and several lines of evidence showed that carcinogenesis was caused by the expression of T antigen in other cell types (Reiner et al., 2007).

CR2 (cryptdin-2) Tag - *CR2*-Tag mice were originally designed to study intestinal epithelial cells (secreting antimicrobial peptides, cryptdins), however, it had been discovered unexpectedly the *CR2*-Tag male mice died harboring large prostate tumors at 5 to 7 months (Garabedian et al., 1998). Locally invasive CaP was found in all male mice by 24 weeks. Mice displayed metastases to the liver, abdominal lymph nodes, lung, and bone marrow. However, Tag expression was also strongly induced in neuroendocrine cells, which formed the basis of tumorigenesis in this model (Hu et al., 2002).

ARR2PB Tag-The Tag construct has been modified by adding *hepsin* since hepsin mRNA was identified to increase CaP (Klezovitch et al., 2004). *PB-hepsin* was also known as *ARR2PB*

owing to the promoter harboring androgen receptor binding site 1 (*ARBS-1*) and 2 (*ARBS-2*) (Zhang et al., 2000) which importantly lead to higher expression of transgenes. *ARR2PB Tag* mice promoted the disruption of epithelial organization, resulting in invasion and distant metastasis in more than half of the males within 21 weeks. However, the majority of metastatic regions obviously contained neuroendocine cells (Garabedian et al., 1998; Klezovitch et al., 2004).

Despite failures to recapitulate some human disease characteristics, these transgenic T antigen models have led to identification of potent prostate specific promotor systems.

(2) Transgenic models and prostate oncogenes

Based on the above promoter results, the later generation of transgenic models have adapted natural oncogenic genes which are often found to be amplified or over-expressed during disease initiation and progression, such as the androgen receptor *(AR), Myc, Ras, Her2/Neu*, and *FGR1*.

PB-mAR- This model was developed to study the effect of androgen receptor (AR) overexpression in prostate epithelium. Most male mice developed hyperproliferation, neoplasia and microinvasive high-grade PIN, proving the role of *AR* in promotion of CaP (Stanbrough et al., 2001). However, the precise role of *AR* in cancer progression still remains to be determined as mouse models with loss of *AR* also showed enhanced epithelial proliferation (Wu et al., 2007).

ARR2PB (PB) -Myc - Increased copy number of *Myc* is seen in approximately 30% of CaP cases. The *PB* and *ARR2PB* promoters were used to generate transgenic mice expressing different levels of *Myc* transgene expression, (Ellwood-Yen et al., 2003). This study has revealed that disease progression was dependent on *Myc* expression levels. No metastasis was observed in this model.

PB -Ras - Ras has been implicated in many cancers. The constitutively active forms (*G12V, G12D and G13D*) of have been used to drive tumorigenesis in multiple models. However, *Ras* mutation is rare and insignificant in CaP although *Ra*s pathway activation is common in human CaP. *PB-Ras* mice were designed to study the effect of *H-Ras* in CaP progression. The *PB-Ras* mice have not developed further than the PIN and this data implicated

Ras may have a role only in early transformation in CaP (Gumerlock et al., 1991; Scherl et al., 2004).

ARR2PB -ERG - The fusion protein, *TMPRSS2-ERG*, between the transmembrane protease, serine 2 (*TMPRSS*2) and *ETS* transcription factor is frequently found in human CaP (Tomlins et al., 2005). The mouse model was generated to validate that the truncated form of *ERG*, the product of the fusion drives cancer under the control of *ARR2PB*. However, low frequency of low grade PIN has been reported in this model. In combination with loss of *PTEN* or activation of PI3K pathways, the model progressed to more aggressive disease. These results suggested that the translocation might depend on PI3K pathway activation for tumorigenesis (Carver et al., 2009; King et al., 2009; Klezovitch et al., 2008).

PB -Akt (MPAKT) - *AKT* activation is often observed with loss of *PTEN*, therefore, *Akt* transgenic mice were designed to determine if CaP can be triggered by activation of *Akt* alone. The *MPAKT* model showed that *Akt1* activation is sufficient to develop PIN but not for invasive prostate carcinoma. These data have demonstrated that additional events are necessary for the progression to adenocarinoma (Majumder et al., 2003).

These transgenic mouse models established potential drivers of the disease. But they mostly displayed mild cancer phenotypes, and hardly any adenocarcinoma. This suggested that other genetic events are critical for cancer and metastasis.

(3) Traditional knockout models and tumor suppressors

Traditional knockout models are great tools to study the roles of tumor suppressor genes or essential DNA regions in CaP. In 1989, the first traditional knockout was introduced to adapt homologous recombination in embryonic stem cells (ESCs). This event was awarded with the 2007 Nobel Prize in Physiology or Medicine (Capecchi, 1989).

PTEN - The *Pten* knockout mouse was created by three different groups in 1998 and 1999 (Di Cristofano et al., 1998; Suzuki et al., 1998)(Podsypanina et al., 1999). *Pten* was found to be essential for early embryonic development, thus, *Pten* heterozygotes animals had to be analyzed in lieu of complete KO animals. In these animals, prostates developed enlarged, hyperplastic glands and high-grade PIN in addition to cancer phenotypes in a number of other organs. These data suggested that *Pten* may be crucial in early prostate carcinogenesis. To study

the disease beyond PIN and the combined effects of tumor suppressors, various other tumor suppressor knockout mice were crossed to *Pten* heterozygotes. Most double knockout mice presented a far more aggressive phenotype than the single knockouts. The *Pten* heterozygote and *p27* knockout developed CaP at 100% penetrance, which supported the cooperation of both genes in the human disease (Di Cristofano et al., 2001). The cross of $Pten^{+/-}$ mice with *ARR2Pb-ERG* resulted in adenocarcinoma confirming cooperation between concomitant loss of *PTEN* and the *EGR* genetic rearrangement in human CaP (Carver et al., 2009). Besides cooperation, a series of *Pten* hypomorphic alleles was used to demonstrate that the levels of Pten protein below heterozygosity trigger prostate cancer (Trotman et al., 2003), demonstrating haploinsufficiency for disease initiation. Taken together, Pten plays a master role in suppressing CaP initiation and also prevents tumor progression in cooperation with other genes.

p27 - Loss of *p27* (the *Cdkn1b* gene) induced high proliferation, enlarged glands and increased fibromuscular stromal cells in prostate and also hyperplasia of various organs, consistent with the aberrant expression pattern of p27 that was detected in human CaP samples (Cordon-Cardo et al., 1998). In histological analysis, prostatic hyperplasia, enlargement of the glands, and increased fibromuscular stromal cells were observed in *p27* knockout mice, demonstrating that they are ideal models for BPH (Benign Prostatic Hyperplasia) but not for CaP. However, the cross with *Pten* heterozygotes did result in aggressive CaP (Di Cristofano et al., 2001).

RB1 - The retinoblastoma gene , the first identified human tumor suppressor, has been shown to be directly involved in various human cancers. Since *the* knockout is embryonic lethal, *Rb1* heterozygotes were crossed to other tumor suppressor mutant mice, such as *Pten*, and *Trp5*3 due to the absence of an obvious phenotype in *Rb* heterozygous mice, resulting in CaP development (Kwabi-Addo et al., 2001; You et al., 2002).

(4) Conditional knockout models

Conditional knockout (cko) modeling was made possible by development of the *Cre-loxP* system, which was developed in the Sternberg laboratory at the National Cancer Institute (Sternberg, 1979; Sternberg and Hamilton, 1981). By using the above discussed promoters (see 'Transgenic Models') for Cre recombinase, it has been possible to generate mouse models with

cell type or tissue specific genetic alterations. Conditional knockout modeling prevents off-target effects and enables the study of tissue specific functions of target genes. Most importantly, it allows deletion of both alleles of embryonic lethal genes. Moreover, cko models resemble the human patient situation more closely than knockout models since the genetic modification is restricted to the target tissue (or a specific cell type) while the rest of the organ and the micro-environment remains normal, in principle.

Probasin-Cre - Two different versions of *Probasin-Cre* have been generated. One was designed with the *PB* promoter –426/+28, known as *PB-Cre* (Maddison et al., 2000). The second one, the *ARR2PB,* known as *PB-Cre4*, is specific for prostate epithelial cells (Wu et al., 2001) and has emerged as the most widely used promoter in CaP conditional knockout models. Conditional *Rb* (*PBCre;Rb*^{flox}) mice (Maddison et al., 2004) and *Trp53* mice were generated separately, however the phenotypes from each mice were observed only hyperplasia.
The *Pten* cko, (*PBCre;Pten*^{flox} and *PBCre4;Pten*^{flox})(Freeman et al., 2003; Trotman et al., 2003) demonstrated complete penetrance of CaP with 6 month latency. The combined cko model for *Pten* and *Trp53* revealed that *Pten*-loss depends on p53 for senescence growth arrest and resulted in the most aggressive early onset CaP with a grossly enlarged lethal prostate phenotype (Chen et al., 2005). The cko for *Pten* and *Smad4* showed an identical prostate phenotype (Ding et al., 2011). Importantly, either *Trp53* or *Smad4* loss on its own showed no disease. Thus, the concept of *Pten*-loss as driver, and Smad4 or Tp53 activation as downstream response elements of tumor suppression has emerged.

Nkx3-1 - CreERT2 - *Nkx3-1* has been known to express only in luminal epithelial stem cells, also called castration resistant *Nkx3-1*-expressing cells (CARNs, (Wang et al., 2009)). The derived *Pten* cko model, *Nkx3-1*^{CreERT2} *; Pten*^{flox}, was generated deletion of *Pten* upon tamoxifen treatment. This model developed PIN and microinvasive carcinoma rapidly, as well as castration resistance (Wang et al., 2009).

In sum, GEM models for prostate cancer have broadly contributed to our understanding of prostate cancer genetics and local progression. However, these models hardly recapitulate the lethal stages of human disease, such as distant metastasis. Another drawback of GEM models is the need for breeding, which makes them unsuitable for pre-clinical trials. For example, the generation of low Pten expressing mice (hypomorphic *Pten*, *Pten*$^{hy/-}$) for Pten stability studies required years of breeding periods and also resulted in infertile mice which could not be

efficiently studied. In addition, cancer researchers are facing hurdles when investigating the biology of metastasis. The major problem is low frequency in prostatic metastasis, together with inadequate monitoring techniques for detecting the disseminated disease with current models. Therefore, at the start of my PhD, there was a strong incentive for producing a mouse model that would circumvent the above issues. The approach that we chose was aimed at generating the fast mouse model by using viral injection, avoiding the problems and complications associated with breeding. The results of this work are presented in chapters II-III.

3. Post-translational regulation of PTEN

PTEN is a critical tumor suppressor gene in many cancers. Using mouse models, it has been shown that *PTEN* heterozygotes develop hyperplasia in endometrium, thyroid, adrenal gland, prostate and liver. In addition, the conditional *PTEN* knockout demonstrated that loss of *PTEN* is sufficient for tumor formation. Furthermore, studies of a hypomorphic series of *Pten* alleles suggested that its levels control prostate and breast cancer initiation (Alimonti et al., 2010; Trotman et al., 2003). In some cancers, *PTEN* deletion and mutation can not explain the low levels or loss of PTEN protein, instead suggesting PTEN to be down-regulated by post-translational degradation (Naguib et al., 2011). The E3-ubiquitin ligase *NEDD4-1* (neural precursor cell-expressed, developmentally down-regulated 4-1) has been identified as a PTEN E3 ligase. Several studies have found NEDD4-1 over-expressed in cancers with low PTEN protein (Amodio et al., 2010; Kim et al., 2008; Yanagawa et al., 2012). Therefore, NEDD4-1 mediated degradation of PTEN is likely a mechanism of PTEN regulation in some cancers. However, further studies suggested that there are also other PTEN E3 ligases, like the E3 ligase, X-linked inhibitor of apoptosis protein (*XIAP*) (Van Themsche et al., 2009). Most importantly, the above E3 ligase genes are not frequently amplified at DNA or RNA level, suggesting that the regulation of PTEN protein may be encoded indirectly by alteration of other genes.

PTEN localization is also regulated by its phosphorylation status. There are several kinases that phosphorylate PTEN and by doing so, they may indirectly increase or decrease PTEN stability (Leslie et al., 2008). Taken together, changes in PTEN post-translational modification are linked to its loss at the protein level, but the identity or causality of the underlying genetic drivers in cancer remain to be established. To address this problem, I decided

to carry out an RNAi based screen for regulators of PTEN stability. The results of this work are discussed in chapter IV.

II. RapidCaP : A therapeutic mouse model for the advanced prostate cancer

Summary

Genetically engineered mouse (GEM) models for *Pten*-deficient Cancers of the Prostate (CaP) have greatly helped us understand the biology of tumor initiation, but their characteristic of developing lethal primary disease is obstructing research and therapy of the advanced metastatic disease stages. Thus, the genetic requirements needed to trigger metastatic prostate cancer have remained ill defined. Here we developed RapidCaP, a GEM modeling approach that uses surgical injection for viral gene delivery. We show that in *Pten*-deficiency, complete loss of the *Trp53* tumor suppressor triggers CaP metastasis to distant sites at greater than 50% penetrance by 4 months, entirely consistent with results from human genome analysis. Through live tracking of the endogenous prostate metastasis via bioluminescence imaging, we find that both primary and metastatic disease first respond to castration, but later relapse to produce lethal, castration resistant disease, as seen in human. To our surprise, analysis of these lesions and of metastatic nodules in lung consistently failed to reveal activation of Akt, the signature oncogene downstream of *Pten*-loss. Instead, these metastases showed strong activation of the Myc oncogene, which was even more pronounced in the castration resistant tumors.

Taken together, these data suggest that an 'Akt-switch' to Myc is a critical event in prostate cancer metastasis and resistance to castration therapy. Thus, the RapidCaP system greatly helps address the hitherto unmet need for analysis, gene validation and therapy of prostate cancer metastasis in genetically engineered mice.

Introduction

Prostate cancer is the most common malignancy in men and the second-leading cause of cancer-related deaths in the Western world. Similar to other solid tumors, metastasis is the major cause of mortality and morbidity of prostate cancer patients (Jemal et al., 2003).

For studying human prostate cancer, genetically engineered mouse (GEM) models are considered the best system due to mouse susceptibility to cancer, 95% genomic identity to human, and a relatively short lifespan, making mice feasible to maintain and breed, hence multiple genetic modifications can be accomplished by breeding. The ultimate goal for developing GEM models is to identify the mechanisms of cancer progression and accelerate preclinical testing of novel drug candidates as well as finding the best therapeutic treatment options for already existing drugs.

To fulfill these purposes, GEM models must recapitulate the critical aspects of human prostate cancer: disease progression to metastasis and emergence of castration resistant metastatic tumors. However, currently no GEM models obviously mimic these features of human prostate cancer (Valkenburg and Williams, 2011). While metastasis could indeed be seen during autopsy of some, the reported penetrance is far too low for pre-clinical studies. Moreover, prostate conditional GEM models expressing common androgen dependent transgenes (eg, probasin promoter driven expression) are incompatible with castration and thus cannot be used for therapeutic trials on castration resistant prostate cancer.

Furthermore, an imaging system for detecting advanced prostate cancer and monitoring the response to therapy is indispensable. Given the small size of the murine prostate, the proximity to the bladder, its variable position and the complicated multi-partite anatomy, imaging prostate has been challenging (Lyons et al., 2006). On top of these high demands, there are only a limited number of genes that can be manipulated within couple of years time to build novel GEM models. The above major shortcomings of classic GEM models have put them hopelessly out of sync with today's speed of human cancer gene discovery and the resulting need for fast validation of candidate oncogenes and tumor suppressors. As a consequence, animal model scientists are actively exploring new approaches.

Here, we propose a new prostate cancer mouse model that is designed for therapeutic trials. Using a surgical process to deliver a viral transgene specifically to prostate, we are able to achieve prostate specific single or multiple gene alternations, such as knockout, knockdown and over-expression without cross breeding of multiple animals harboring engineered alleles. In addition, introduction of a luciferase marker together with target genes enables live imaging and monitoring of disease progression as a function of the delivered target genes.

Results

1. Injection based recombination of Pten and Trp53 results in focal proliferation in the prostate epithelium

After showing the feasibility of viral transgene delivery to prostate (see Supplemental figure 2.1), Lentiviral Cre-luciferase virus (LV-Cre/Luci) was injected into prostates of *Pten*$^{loxp/loxp}$*; Trp53*$^{loxp/loxp}$ mice to examine recombination. As shown (Figure 2.1 A) LV-Cre/Luci injected mice typically show a strong luciferase signal in the genitourinary (GU) region. Post-mortem analysis (69 days post injection) reveals that the injected anterior prostate and associated seminal vesicle are the source. In contrast, 62% of LV-Luci virus injected mice demosntrated loss of signal within 78 days (not shown). PCR analysis of genomic DNA from prostate revealed recombination of the tumor suppressors, *Pten* and *Trp53*, specifically in LV-Cre/Luci injected right anterior prostate (AP, Figure 2.1 B, *ΔPten, Δp53*). The immunohistochemistry (IHC) analysis with indicated antibodies revealed the focal nature of disease initiation in this model: only a small region showed increased proliferation, loss of Pten and strong AKT activation, while the majority of tissue in the prostate retained normal morphology and staining for these proteins. Furthermore, we observed no immunogenicity of the viral injection procedure as shown by CD3 staining in various settings (see, Supplemental figure 2.2 B). These data demonstrated that surgery based viral delivery triggered highly focal disease initiation, which is thought to be a normal feature of the human disease process. Note that classic conditional knockout systems in contrast delete target genes in every cell of the prostate epithelium (Chen et al., 2005; Ding et al., 2011; Trotman et al., 2003).

2. Pten/Trp53 deletion triggers disease dissemination

Analysis of the human prostate cancer genome has revealed that *PTEN* and *TP53* are co-deleted in half of all metastatic samples (Chen et al., 2011). In mouse however, the complete *Pten* and *Trp53* deletion in prostate resulted in massive and lethal tumor growth (Chen et al., 2005; Ding et al., 2011). In order to investigate disease progression in the RapidCaP model system (LV-Cre/Luci injection into *Pten*$^{loxp/loxp}$*; Trp53*$^{loxp/loxp}$ prostate), mice were monitored for a

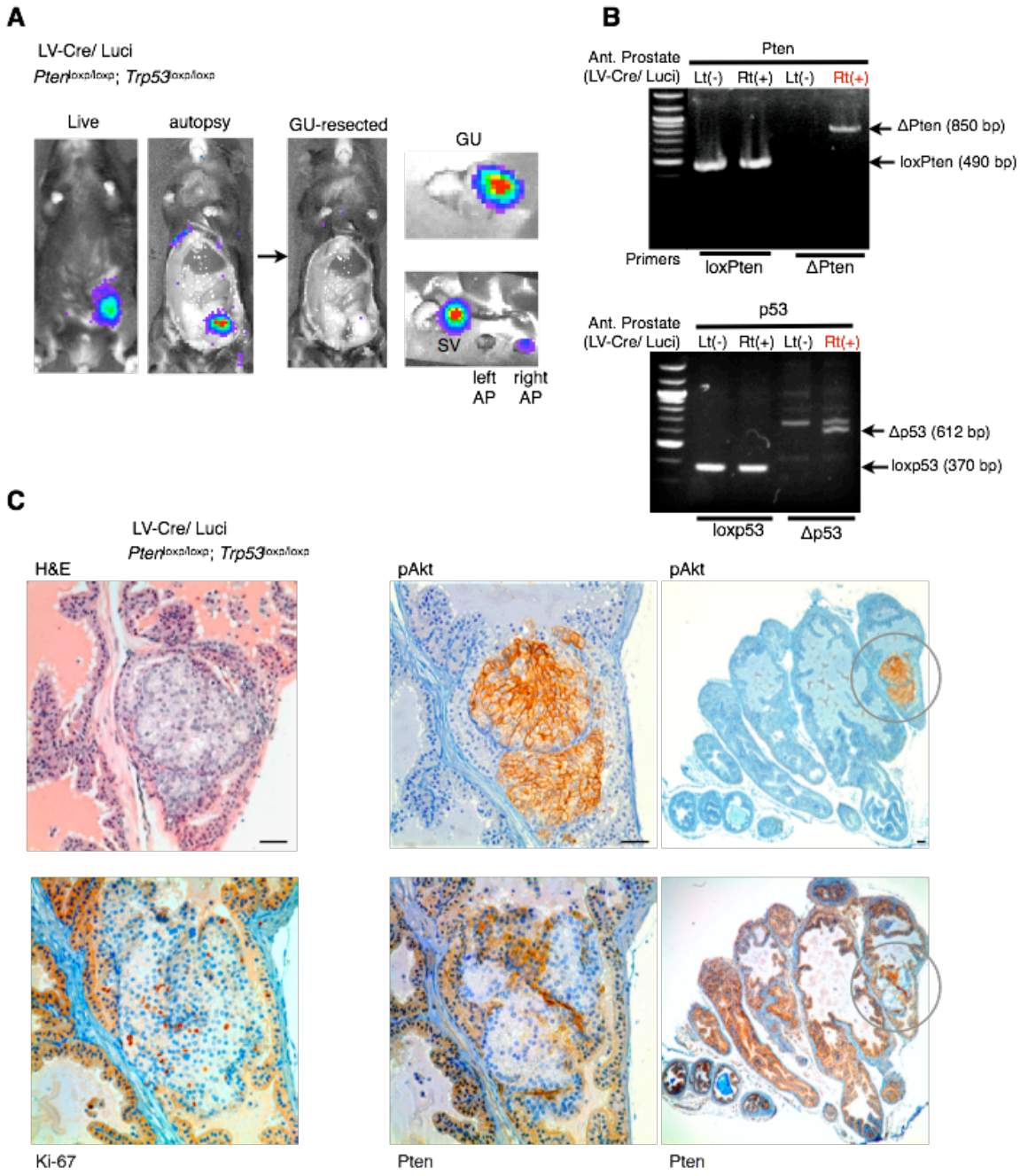

Figure 2.1 Prostate specific LV-Cre/ Luci delivery results in focal disease. A. Live and post-mortem images of LV-Cre/Luci injected *Pten*$^{loxp/loxp}$*; Trp53*$^{loxp/loxp}$ mouse at 69 days post injection. Dissection reveals similar distribution to that shown in S2.1C. Luminescence signal was displayed in LV-Cre/Luci injected prostate and seminal vesicle. B. PCR analysis confirms recombination of *Pten* and *Trp53* in LV-Cre/luci injected *Pten*$^{loxp/loxp}$*; Trp53*$^{loxp/loxp}$ specifically in the injected right (Rt) anterior prostate. C. Immunohistochemistry analysis of LV-Cre/luci injected *Pten*$^{loxp/loxp}$*; Trp53*$^{loxp/loxp}$ prostate reveals a focal lesion in the luminal epithelium of one gland (H&E), which also displays increased proliferation, specific to epithelial cells (Ki-67). Loss of Pten expression and activation of Akt (pAkt) and high proliferation are also found in this region (middle panels), which is a unique focus of disease in the cross section of the entire anterior prostate (right panels). Note that surrounding stroma remains unaffected in all panels. Scale bars, 100 µm (top right), 50 µm (all other panels).

period of several months. As shown in Figure 2.3 A, the luminescence signal was initially observed in the lower abdominal region (up to 25 days post injection, p.i.). Later however, a signal spread was detected to the upper and mid body (72d to 140d p.i.). Typically, the signal first disseminated to below the neck and later to the mid-abdomen, as shown (Figure 2.2 A). Quantification of whole body, primary and secondary signal and illustrated in graph (Figure 2.2 B), revealed how both primary and secondary signals increased over time. Importantly, no spreading of luminescence signal was observed in any of the control injection cohorts as most (62%) of the non-gene modifying control injections showed loss of primary luciferase signal within 78 days (see Figure 2.2 C)

Overall (see Figure 2.2 C), 50% of animals showed dissemination 4 months post injection. Using *post mortem* analysis, secondary signals were confirmed in lymph nodes (mediastinal, lumbar and caudal), spleen and liver (Figure 2.2 D), while often pancreas and lung as well as organs near the GU tract were also signal positive (not shown). Importantly, LV-Cre/Luci injected prostate was macroscopically indistinguishable from the non-injected prostate (Figure 2.2 D, nl, inj), consistent with absence of inflammatory responses of the procedure shown above (Supplemental figure 2.2 B). Note that seminal vesicles were luminescence positive also in control injections. However, we found neither a phenotypic change by IHC analysis nor could we isolate marker gene positive cells by flow sorting (not shown), suggesting that the signal does not come from intact cells. Recombination of *Pten* and *Trp53* in the signal positive secondary organ sites was confirmed by recombination PCR (Figure 2.2 E). Histopathological examination of prostates revealed local invasion as shown by the focal budding of epithelial cells (Figure 2.2 F).

3. Histopathological analysis confirms metastatic disease

To investigate if the signal dissemination in the RapidCaP mouse is really prostate metastasis, histopathological analysis was performed. As shown in Figure 2.3A, lungs of RapidCaP animals were often luciferase positive. First, we defined markers for mutant cancer cells based on prostate analysis. As expected, focal regions in prostate lost Pten expression. As shown, the epithelial markers, cytokeratin-8 (CK-8) and androgen receptor (AR), were absent specifically in regions where Pten (and Trp53) was no longer expressed (Figure 2.3 B, arrows) consistent with previous reports (Carver et al., 2011). Using these negative markers in the lung,

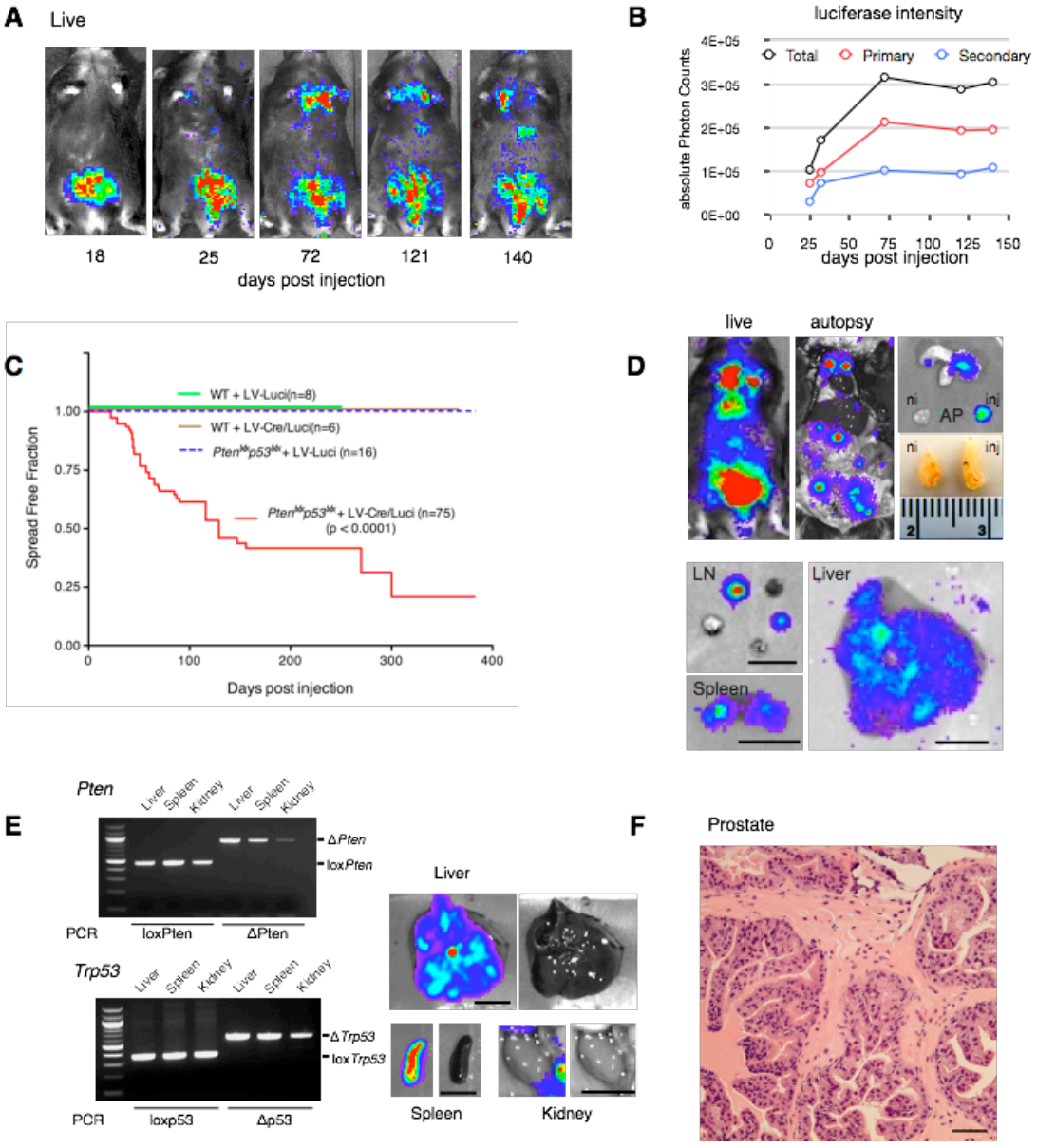

Figure 2.2 *Pten/Trp53* deletion triggers disease dissemination. A. Time course of a typical RapidCaP experiment (showing one LV-Cre/Luci injected *Pten*$^{loxp/loxp}$*; Trp53*$^{loxp/loxp}$ mouse) reveals disease spreading to distant sites starting at 72 days post injection. B. Quantification of the luminescence signal intensity from mouse shown in Fig. 3A. Total body, secondary and primary signal measurements are shown. C. Kaplan-Meier analysis of disease dissemination reveals early onset and high penetrance, specifically in *Pten*$^{loxp/loxp}$*; Trp53*$^{loxp/loxp}$ mice (p<0.0001). D. Live (at 219 days post injection) and *post-mortem* autopsy of an LV-Cre/Luci injected *Pten*$^{loxp/loxp}$*; Trp53*$^{loxp/loxp}$ mouse reveals luciferase positive secondary organ sites (lymph-nodes, LN, spleen and liver) and a minor difference in size of prostate lobes (injected, inj. vs. non-injected, ni). Scale bar, 1 cm. E. PCR analysis reveals *Pten*/ *Trp53* recombination in the secondary tissues (weakest in kidney). Scale bar, 1 cm. F. H&E staining of an LV-Cre/Luci injected *Pten*$^{loxp/loxp}$*; Trp53*$^{loxp/loxp}$ prostate lesion (192 days post injection) reveals a typical budding gland with features of focal invasion. Scale bar, 50 µm.

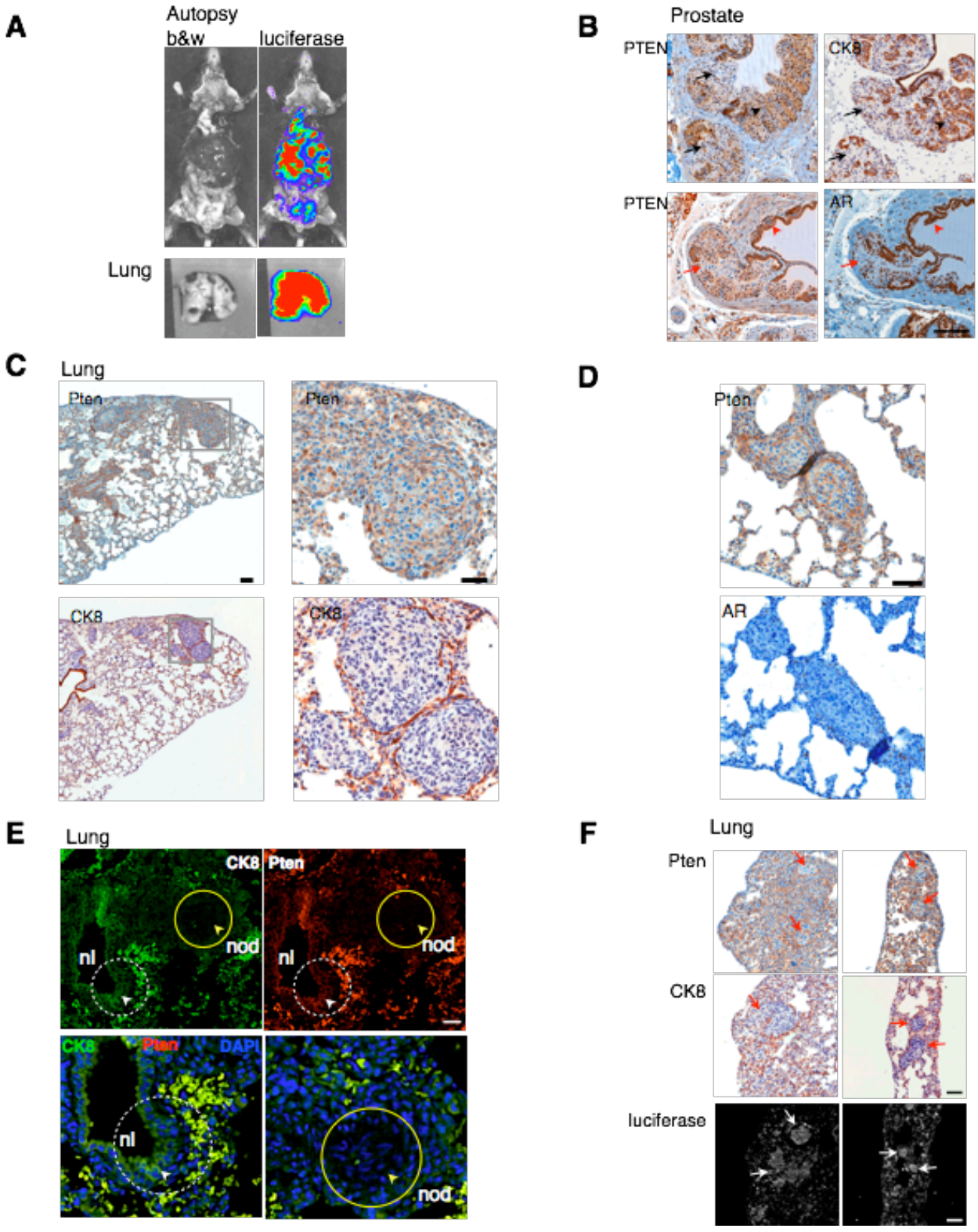

Figure 2.3 Immunohistology analysis confirms prostate cancer metastasis to lung.

Figure 2.3. Immunohistology analysis confirms prostate cancer metastasis to lung. A. Autopsy imaging of the mock-castrated RapidCaP mouse from Fig. 2.4 reveals disease dissemination to lung, lymph nodes,spleen and liver at the trial endpoint (10 month post injection). B. Identification of histogenic markers that define prostate cancer cells by immunohistochemistry (IHC) analysis of prostate in animal from A: Pten & CK8 (black arrows, see black arrowhead for region with normal protein levels) and Pten & AR (red arrows, see red arrowhead for region with normal protein levels). Note that 'loss' of AR staining is a hallmark of *Pten*/*p53*-null prostate (see also Carver BS. et al., Cancer Cell. 2011 Aug 16;20(2):173-86). Scale bar, 100 µm. C, D. IHC analysis of lung from above mouse reveals metastatic nodules that are Pten-, CK8- and AR-negative with low magnification (left panel) of lung stained with Pten and CK8 and the images with high magnification (right panel) of the area displayed nodules negative for both Pten and CK8 (area in the block box). Scale bars, 100 µm (top left), 50 µm (all other panels). E. Double-immunofluorescence (IF) labeling confirms double-negativity for Pten and CK8 in a metastatic lung nodules (nod) shown in (C-D) (yellow circles & arrowheads). Note that in contrast, co-labeling of Pten and CK8 in adjacent normal lung epithelia (nl, white dashed circles and arrowheads) shows double positive staining. Scale bar, 50 µm. F. Anti-luciferase antibody staining and IF analysis of lung from (C-F) confirms that metastatic nodules are luciferase positive (white arrows), and it correlates with Pten-CK8 deficiency (red arrowheads). Scale bar, 100 µm.

we observed that this organ was littered with nodules of cancerous cells, that clearly separated them from surrounding lung tissue, confirming their metastatic histology. (Figure 2.3 C and D). Importantly, the metastatic nodules stood out from lung tissue, as they retained the loss of Pten, Ck8 and AR which were all characteristically absent from the primary cancer as well. In order to confirm the that metastatic cells were truly double negative for Pten and Ck8, double immunofluorescence (IF) labeling was performed on lung sections (see Figure 2.3 E). Indeed, metastatic nodules in lung (nod) were negative for both Pten and CK8 (Figure 2.3 E, yellow circle and arrowhead) while normal lung epithelium (nl) stained positively for both proteins. Finally, IF analysis revealed that metastatic nodules are readily detected by luciferin antibodies. Taken together, our analysis confirmed widespread prostate cancer metastasis to lung in RapidCaP.

4. RapidCaP metastasis responds to castration

Androgen ablation therapy is the standard of care for advanced prostate cancer causing widespread atrophy of prostate cells. Surgical castration was conducted on mice with secondary signals and bioluminescence imaging was continued once per week on two untreated control (one mock castrated) and two castrated animals (Figure 2.4 A).

In both castrated animals, partial (cast-1) or complete (cast-2) responses were seen at 7 weeks post castration, importantly in both the primary and secondary signals. However, regression was followed by aggressive relapse of both primary and secondary signals, now growing much more rapidly than prior to castration (see Figure 2.4 A and quantification in 2.4 C, whole body), a hallmark of human castration resistance. In contrast (see Figure 2.4 B), both control animals showed steadily increasing signal intensity, requiring sacrificed in order to prevent excessive tumor burden. Separate quantification confirmed the sharp increase in intensity for both primary and secondary disease, resulting in the typical 'hockey stick' growth behavior (Figure 2.4 C, compare pre-castration to post-castration growth), with massive cell expansion just prior to termination due to obvious signs of morbidity, palpable tumors, low activity, hunched backs, and rough hair coat among other adverse phenotypes. These data indicated that the disseminated disease was also dependent on androgen. A closer analysis of regression and breakdown into primary and secondary disease (Figure 2.4 D) illustrates how prostate and

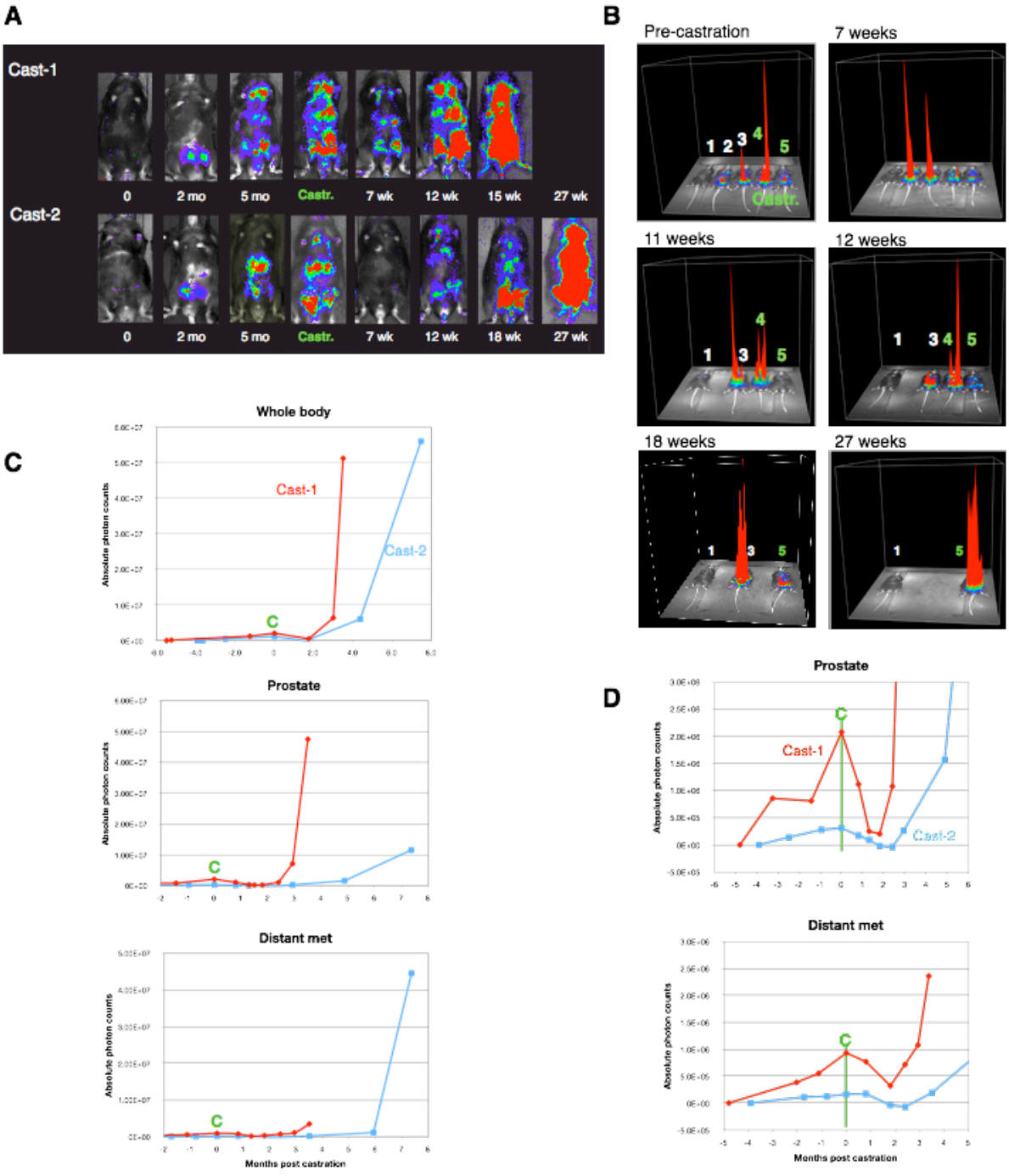

Figure 2.4. Secondary signals respond to castration. A. Live imaging time course of two castrated RapidCaP mice (LV-Cre/Luci injected *Pten*$^{loxp/loxp}$*; Trp53*$^{loxp/loxp}$ mouse). Surgical castration (Castr.) was performed at 5 months post injection on mice harboring distant secondary disease. Analysis reveals differential response and recurrence of disease post castration. B. 3D signal intensity time course from (A), including control mice: 1, wt untreated mouse- 2, RapidCaP mouse- 3, RapidCaP mouse mock-castrated- 4&5, castrated RapidCaP mice. C. Quantification of luminescence signals in castrated animals reveals a sharp increase in the rate of disease progression after relapse. “C” denotes castration. D. Close-up analysis of graphs from (C) shows that both primary and secondary disease respond to castration, confirming their hormone dependence.

metastatic signals in both animals responded to castration, confirming the metastatic nature of all luminescent cells.

Post-mortem analysis of a castration resistant animal (#4, Figure 2.4 B) revealed metastatic disease in various secondary organs, including lymph node, liver, spleen and pancreas. Most notably, prostate was massively enlarged spanning close to 3 cm in diameter, as opposed to the 5-7 mm typically seen for wt prostate (not shown). IHC analysis of this prostate confirmed loss of PTEN, AR and CK8, consistent with the staining result obtained on non-castrated mice (Figure 2.3 B). Surprisingly however (see Supplemental figure 2.4 C), Akt was not activated prostate in spite of *Pten*-loss. However, there was strong c-Myc activation that went beyond what is observed in normal prostate (see Supplemental figure 2.4 C). These data suggested that c-Myc and not phospho-Akt may be driving the castration resistant cancer, unlike during disease initiation (compare pAkt, Figure 2.1 C).

Taken together, the castration experiments confirmed that RapidCaP mice developed prostate metastatic disease, which initially respond to androgen deprivation and eventually relapsed to form castration resistant prostate cancer that contains a new driver pathway signature.

Discussion

Strategy

The RapidCaP system presents us with new technology for the exploration of metastatic prostate cancer and its therapy. The injection based technique combines rapid gene modification driven by viral Cre delivery with monitoring of disease progression by live bioluminescence imaging. The time- and labor-consuming breeding process to generate prostate conditional knockout mouse lines is a serious obstruction to establishing pre-clinical GEM models.

The striking characteristic of this model compared to the germline Probasin-Cre driven counterpart is that the viral mediated deletion of *Pten* and *Trp53* suffices to trigger frequent metastatic disease within a few months. Indeed, disease dissemination occurs surprisingly early compared with the current GEM models where the secondary diseases is rarely observed (Chen et al., 2005; Ding et al., 2011). It has been previously reported that tumor cells disseminated to distant organs early during development of a primary tumor in model systems of several cancer types, including breast cancer. (Chambers et al., 2002; Nguyen et al., 2009). These findings

support that the genetically altered cells in RapidCaP were dispersed to the other tissues in early stage of disease hence, the model shortens the lag time for developing metastatic disease and thus early applications of the therapeutic trials are possible. This feature of RapidCaP clearly distinguishes it from the invasive adenocarcinoma observed already at 11 weeks in the prostate conditional *Pten*$^{pc-/-}$; *Trp53*$^{pc-/-}$ mice. In addition, these mice survived only for about 7 months when the prostate cancer is so large that it obstructs bladder function and little or no metastasis is found (Chen et al., 2005; Ding et al., 2011). The two most striking differences between the models are therefore in the primary cancer size and the frequency of metastasis. Several reasons may explain this difference. First, sensitive BLI imaging facilitates the detection of metastases thus resulting in more metastatic cells that are sufficiently bright for detection in RapidCaP. In our hands, as few as 1000 luciferase positive cells could easily be detected in live prostate (not shown), yet these could easily be missed by histopathology analysis. Second, RapidCaP mice survive longer due to non-lethality of their primary disease, thus enhancing the chances to detect metastasis by luciferase. While both of these explanations look convincing at first glance, they cannot fully explain the discrepancy. Importantly, a third explanation has recently emerged through studies in our own lab. After losing *Pten* and *Trp53*, cells release IL6, which activates Stat3 signaling and paracrine proliferation. In the *Pten*$^{pc-/-}$;*Trp53*$^{pc-/-}$ mice, this results in massive stromal expansion occurring on top of the epithelial cell proliferation (D. Nowak, et al. in preparation). The stromal expansion in these animals is a hallmark of the model (Chen et al., 2005) and not typically seen in human. The RapidCaP system does not show this stromal proliferation (see Figure 2.1 C and 2.2 F), which may facilitate the metastatic escape of the mutant epithelial cells.

Taken together, the RapidCaP system may reveal an unknown requirement for metastasis of *Pten/Trp53* mutant prostate cells.

New Biology

Using the RapidCaP system, we have seen that metastatic disease is still androgen dependent, thus the model will be suitable to design therapeutic strategies against castration resistant prostate cancer, and also to study the drivers for metastasis by genomic analysis. These properties are likely to greatly contribute to advances in treating CRPC if human and mouse have similar drug responses and genetic events.

Importantly, there are RapidCaP cases that do not react to castration. Typically, this happened when therapy was started in mice with very high secondary signals (see also Figure 2.4). It will be very important investigate whether these variations are due to the different genetic events, accumulated along with disease progression.

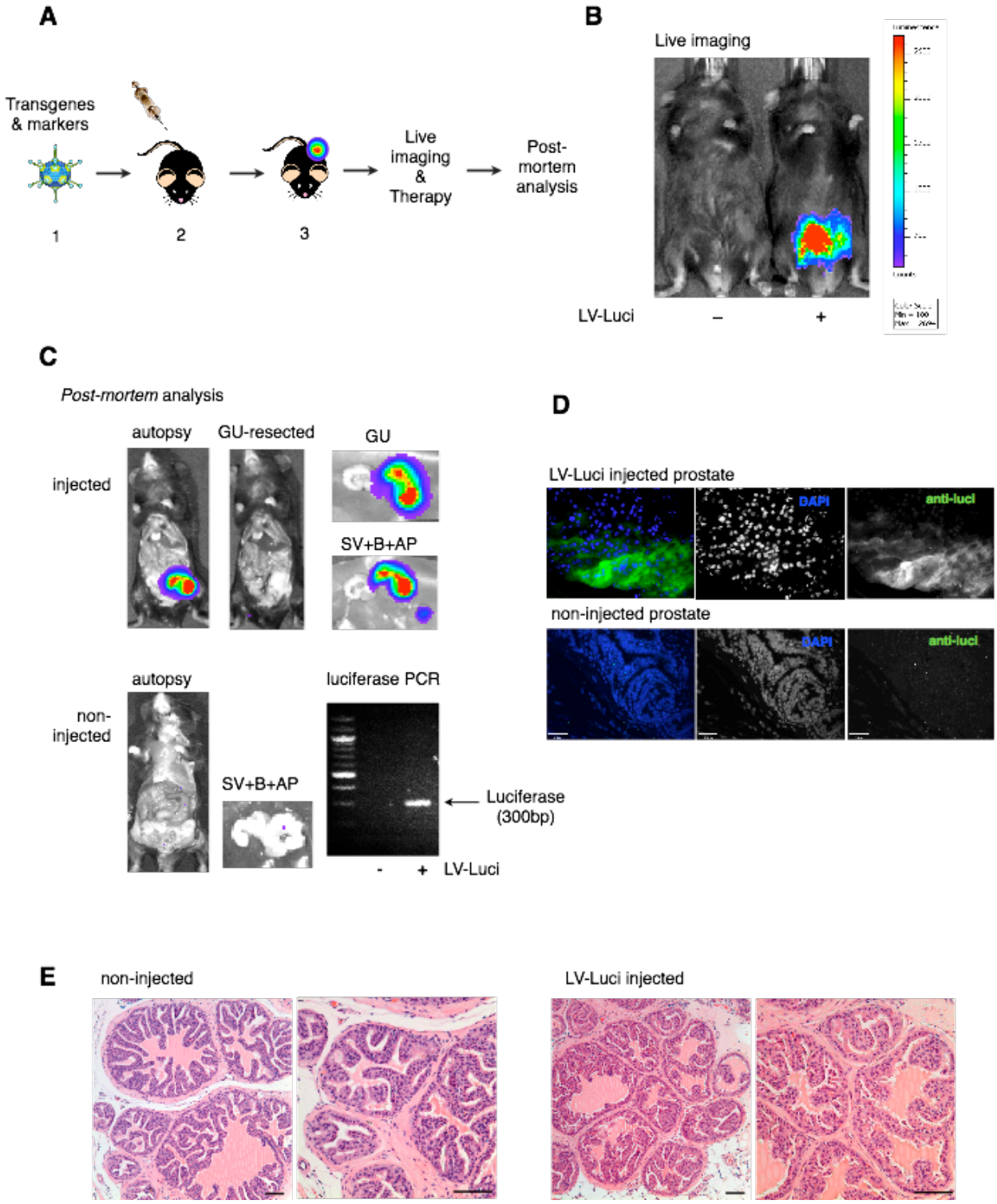

Supplemental figure 2.1 Stable transgene delivery to epithelial prostate cells by virus injection.

Supplemental figure 2.1 Stable transgene delivery to epithelial prostate cells by virus injection. A. The RapidCaP system. 1- Design and production of virus harboring candidate cancer genes and marker genes. 2- Surgical injection of virus directly into anterior prostate gland. 3- Non-invasive bioluminescence imaging to monitor disease progression and therapeutic effects. B. Live imaging of lentiviral luciferase (LV-Luci) injected Bl6 mice and non-injected control at 60 days post injection demonstrates persistent transgene expression. C. *Post-mortem* autopsy imaging of LV-Luci and non-injected control mice at 98 days post injection. The genito-urinary (GU) tract comprises bladder (B), seminal vesicle (SV) and anterior prostate (AP). Luminescence signal is found in the (injected) right anterior prostate lobe and also in the seminal vesicle. Note that FACS sorting experiments fail to identify infected (tomato-FP) seminal vesicle cells, potentially suggesting SV signal to be extracellular, while our technique infects between 1-4% of the ~100 million anterior prostate cells by FACS analysis (not shown). PCR of prostate genomic DNA reveals the luciferase transgene (300 bp) only in the LV-Luci injected prostate lobe. D. Anti-luciferase immunofluorescence on LV-Luci- and control-injected prostate reveals luciferase expression in prostate luminal epithelium (note that while infection of other cell types cannot be excluded, whole body knockout mouse studies have revealed that epithelial cells specifically respond to *Pten*-suppression with proliferation). Scale bar, 47 µm. E. H&E staining of LV-Luci injected and non-injected control prostate reveals retention of normal glandular architecture. Scale bar, 100 µm.

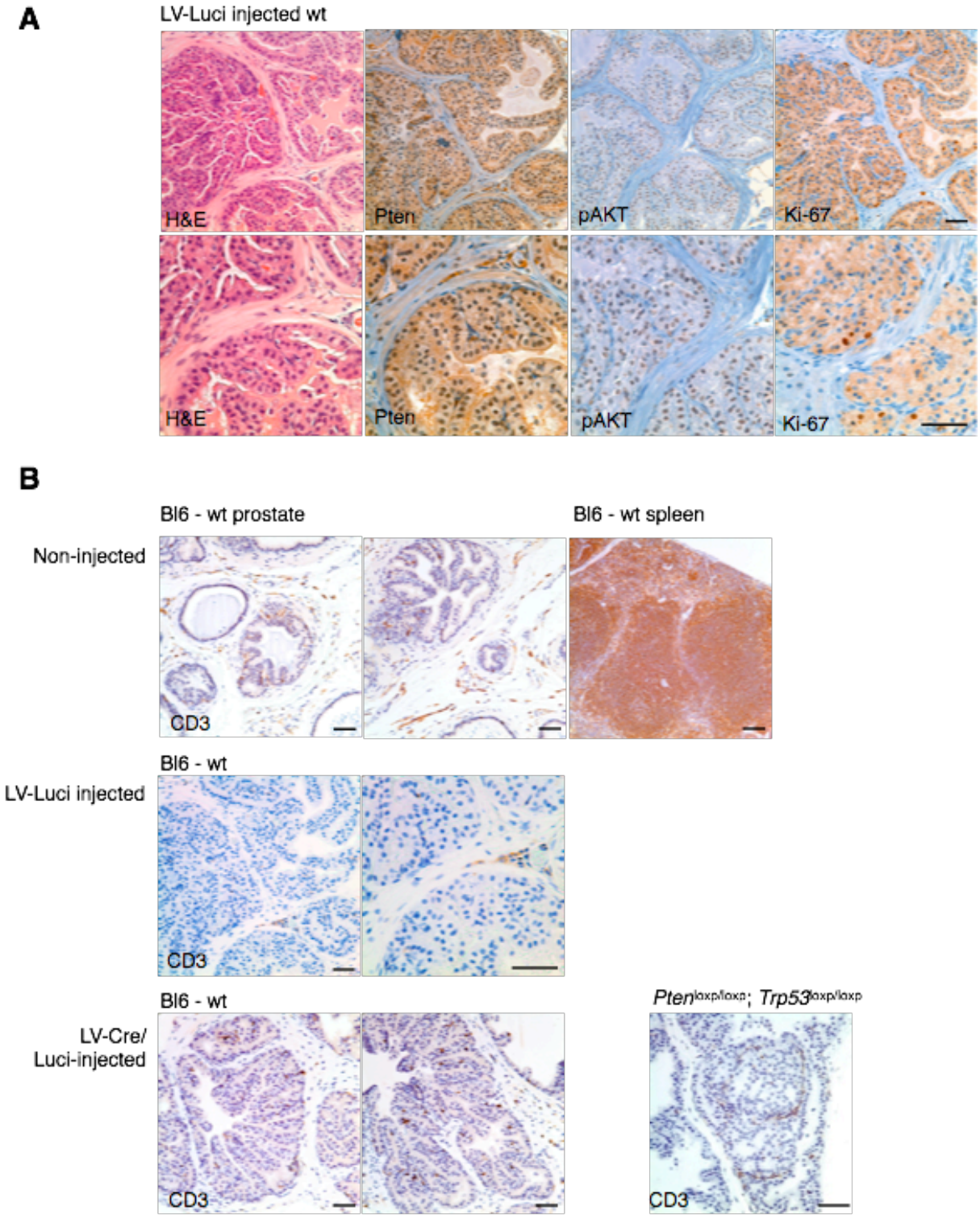

Supplemental figure 2.2 Immunohistological analysis of LV-luci injected wt mice. A. IHC analysis reveals normal Pten, pAkt and Ki-67 staining in LV-Luci injected wt (Bl6) prostate. Scale bars, 50 µm. B. Injection procedures do not trigger an inflammatory response as measured by CD3 staining of indicated tissues. Scale bars, 50 µm (middle panel, bottom right), 100 µm (all other panels).

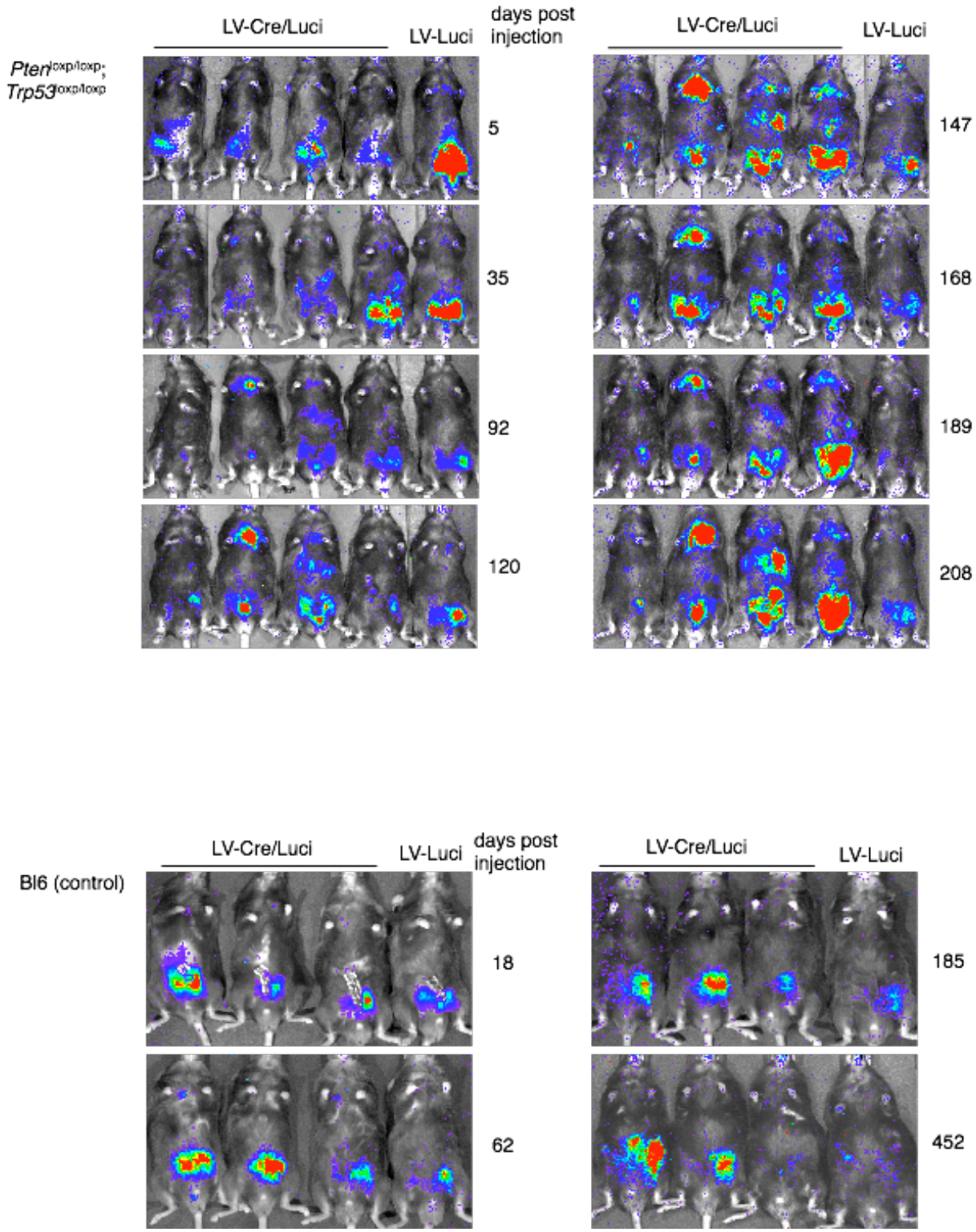

Supplemental Figure 2.3 Typical examples of RapidCaP experiments and bioluminescense visualization of disease progression over time.

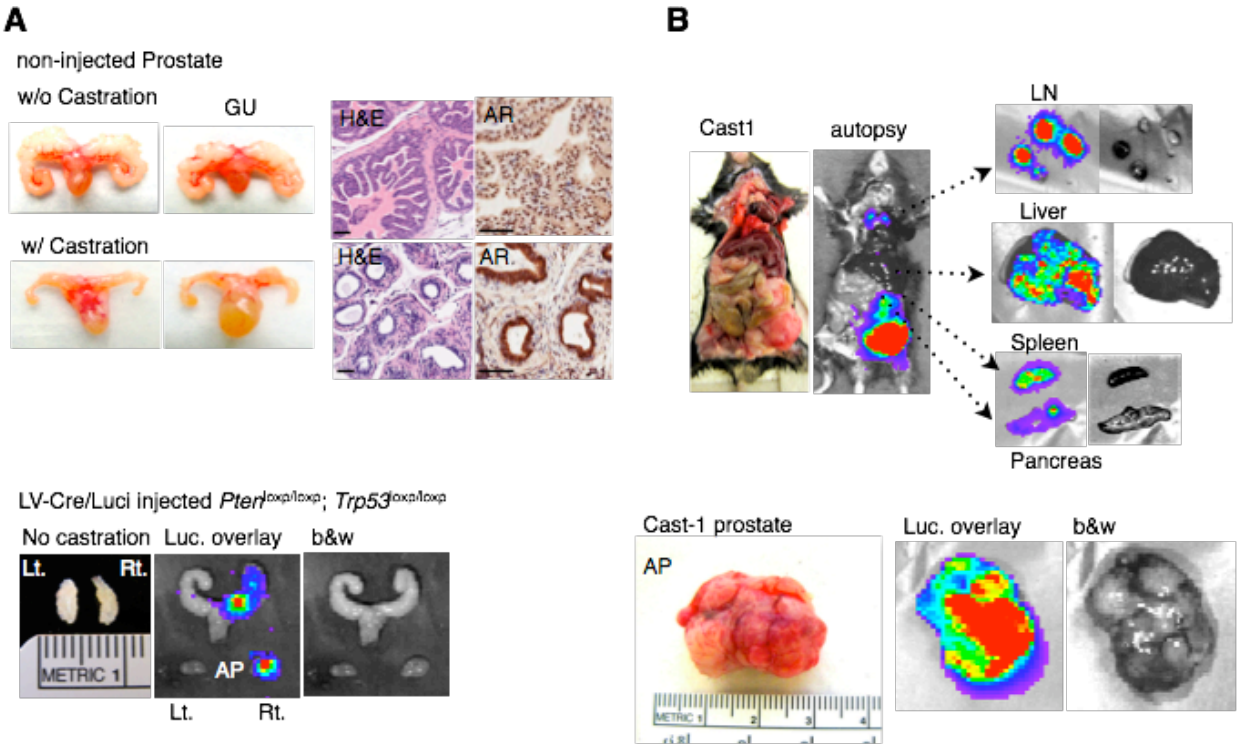

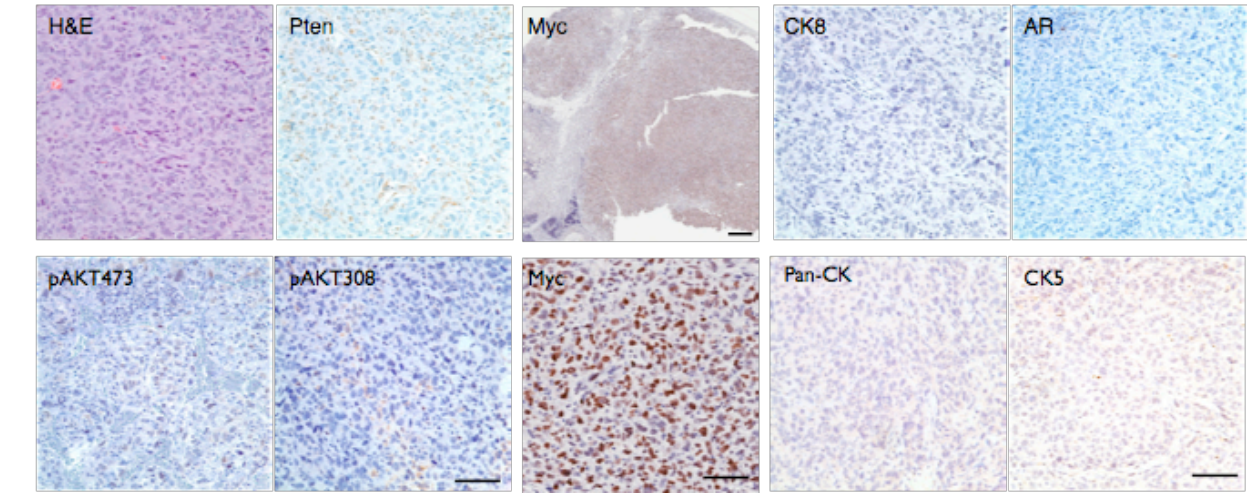

Supplemental figure 2.4 Analysis of castration resistant prostate cancer. A. Castration results in prostate epithelium atrophy and diffuse cytoplasmic AR staining (upper panels). Note that *Pten/Trp53*-loss in RapidCaP model does not cause a significant increase in prostate size (lower panels). Scale bar, 100 µm. B. *Post mortem* analysis of Cast-1 (see Figure 2.4) animal after relapse (see Fig. 4A) shows metastasis to distant organs and massive prostate enlargement. C. IHC analysis of Cast-1 prostate shows loss of Akt activation, loss of cytokeratin epithelial and basal cell markers CK8 and CK5, respectively. In contrast, there is strong activation of c-Myc in tumor cells throughout the therapy-resistant prostate tumor. Scale bars, 1 mm (top panel, Myc), 50 µm (all other panels).

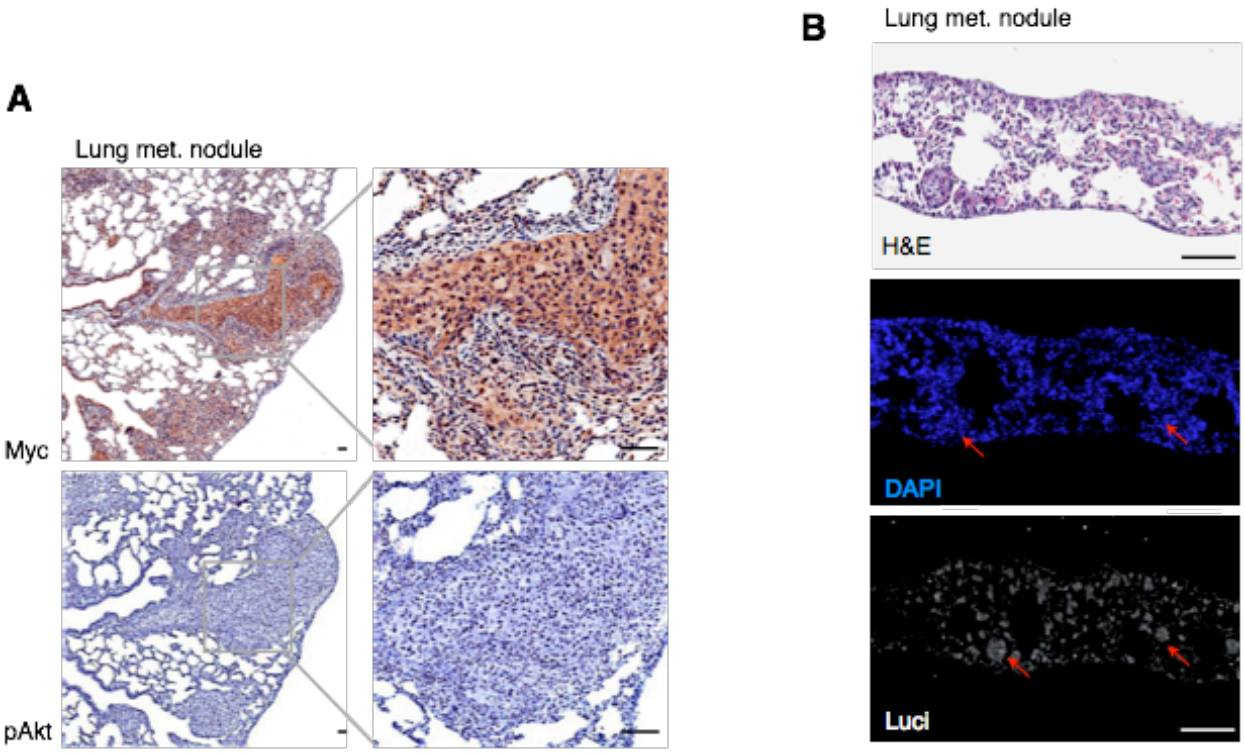

Supplemental figure 2.5 Myc succeeds Akt activation in metastasis and can drive local dissemination of prostate cancer. A. IHC analysis of phospho-Akt (Ser473) in metastatic lung nodule reveals absence of activation. In contrast, Myc is strongly increased, especially in the cytoplasm (compared to prostate, Fig. S6E). Note the apparent further Myc increase in castration resistant prostate (Fig. 5C), when compared to this mock-castrated metastasis). Scale bar, 50 μm. B. Identification of metastatic prostate cancer nodules (red arrows) in lung using staining with luciferase antibody. Scale bar, 100 μm.

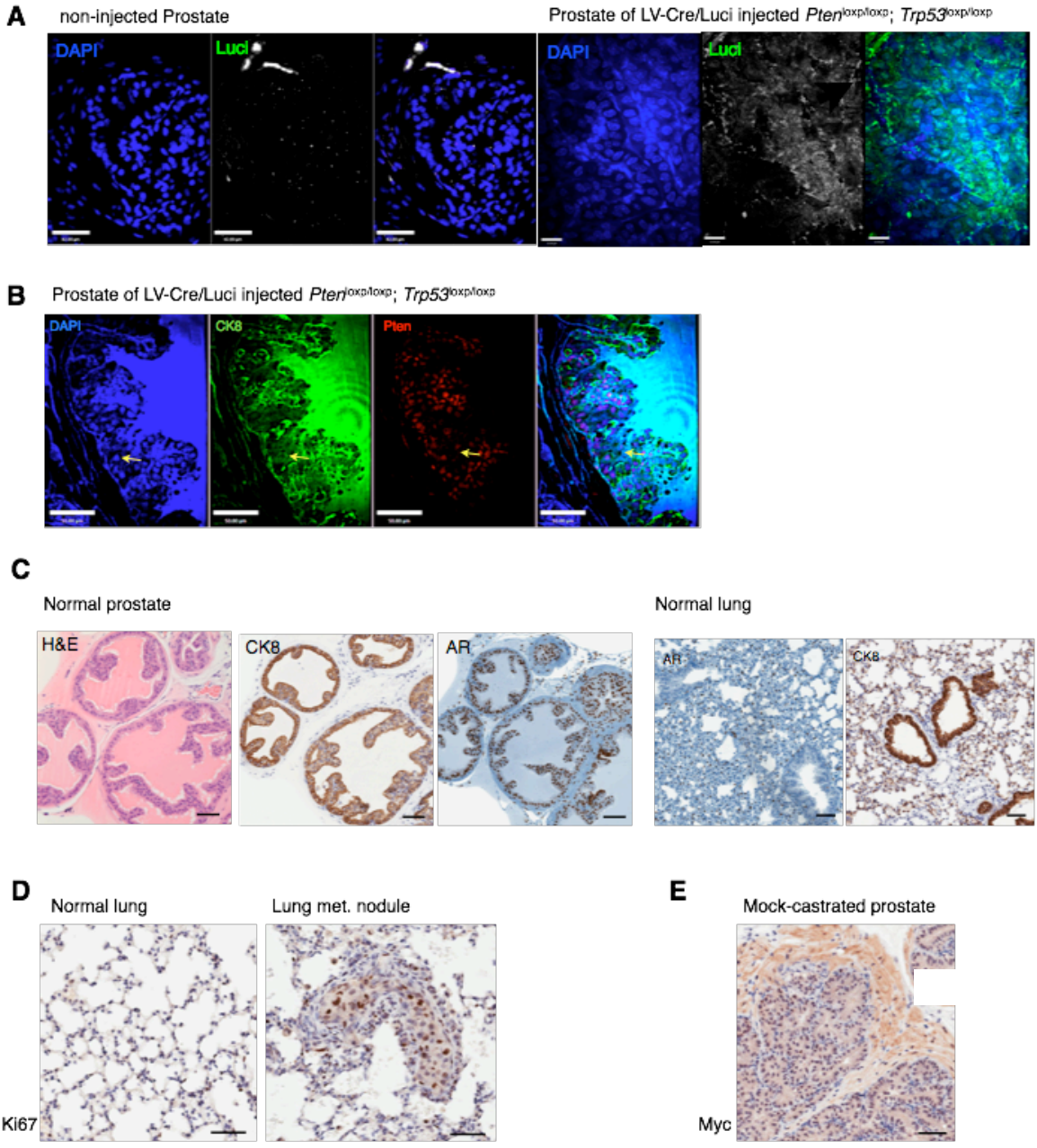

Supplemental figure 2.6 Immunohistological analysis of RapidCaP. A. IF analysis of prostates after injection shows specificity of luciferase expression as probed with anti-luciferase antibodies. Scale bars, 42 µm (left panel), 15 µm (right panel). B. Double-immunofluorescence (IF) labeling confirms double-negativity for Pten & CK8 in LV-Cre/Luci injected *Pten*$^{loxp/loxp}$; *Trp53*$^{loxp/loxp}$ prostate (yellow arrows). Note that in contrast, co-labeling of Pten and CK8 in adjacent normal prostate epithelium shows double positive staining. Scale bar, 50 µm. C. Cytokeratin-8 (CK8) shows membrane associated staining in normal prostate epithelium while androgen receptor is nuclear in these cells. In normal lung a similar localization pattern is observed. Scale bar, 100 µm. D. Prostate cancer metastatic nodules in lung show increased proliferation as measured by Ki-67 staining (compare to Figure S2.2 A, Ki-67). Scale bar, 50 µm. E. Myc staining in sham-castrated prostate is comparable to that observed in normal prostate shown in (C) and much weaker than that seen after castration (Figure S2.4 C, Myc) or in lung metastases (Figure S2.5 A). Scale bar, 50µm.

III. Versatility of the RapidCaP system

Introduction

This chapter illustrates the versatility of the RapidCaP model and the conditional spontaneous genetic engineering that can be accomplished in relatively short time period. The applications of RapidCaP include the viral mediated over expression or knock down of targets, viral driven marker expression as well as the simultaneous multiple target delivery with different viruses. The major and unique advantage of RapidCaP is the rapid and high-throughput genetic *in vivo* screening of the cancer candidates, previously identified in human diseases. It has been successfully used to modify multiple targets in a prostate specific manner by delivering several viruses at the same time. In addition, the most remarkable characteristic of RapidCaP,-the high frequency of metastasis- provides a great opportunity to investigate the driver genes promoting disease dissemination.

Results

1. RapidCaP oncogene system(s)

1.1. Exploration of Pten-Myc cooperation

Alterations of chromosome 8, including amplification at 8q24 harboring the *c-MYC* oncogene, have been noted as one of the most common chromosomal abnormalities in prostate cancer (CaP) progression. In addition, human tissue microarrays have found frequent overexpression of *c-MYC* in luminal cells in PIN, as well as in most primary carcinoma and metastatic disease. These results suggested that increased expression of *c-MYC* is a critical oncogenic event, driving prostate cancer initiation and progression. Therefore, c-*Myc* was introduced to murine prostate *via* the RapidCaP system to determine the applicability of RapidCaP for transgene overexpression. To this end, a retroviral construct harboring *c-MYC* and *luciferase* was designed and tested *in vitro* prior to injection (data not shown). It has been previously published that *c-Myc* initiates prostate cancer in cooperation with *Pten* and *Trp53* (Kim et al., 2012). Also the association between PI3K-pathway alteration and *c-MYC*

amplification has been reported in a cohort of primary and metastatic human prostate cancer samples (Jenkins et al., 1997; Sato et al., 1999). Therefore, hypermorphic *Pten* mice (Trotman et al., 2003), mice with 25% reduction of Pten, were selected for the *Myc* trial in order to to test if it accelerates disease progression. In Myc-luciferase retrovirus (RV-Myc-luci., see Supplemental figure 3.1 for the construct map) injected $Pten^{hy/+}$ mice, the luminescence signals were detected and remained until the animals were sacrificed for analysis (Figure 3.1 A). *Post mortem* imaging (54 days post injection) revealed that the viral-injected side of the prostate was positive for luminescence signal (Figure 3.1 B). From the *post mortem* analysis, the majority of *Myc* delivered mice have been found to have secondary signals. These signal spreads were not recognized until *ex vivo* imaging was conducted because the signal spreads were mainly in organs proximal to prostate, such as lymph node and epididymal fat pad. These signal spreads were observed in *Myc* injected Bl6 cohorts also (Figure 3.1 C, marked with green arrows). The obvious visual differences in shape and size were not observed in *Myc* injected prostate compared to the non-injected prostate (data not shown). Compared to control injected animals, the significant signal spreads in *Myc* injected $Pten^{hy/+}$ mice and Bl6 mice are depicted (Figure 3.1 D). Importantly, significantly higher frequencies of secondary signal were observed in *Myc* injected $Pten^{hy/+}$ mice than in Bl6 control mice. These data suggest that cooperation of *Myc* with *Pten*-loss can be modeled in the RapidCaP system to recapitulate human disease progression. The increased *Myc* expression was confirmed by RT-qPCR, demonstrating delivery of the transgene to prostate (Figure 3.1 E). These results demonstrate that RapidCaP is not only able to deliver and stably express oncogenes in prostate, but also that the *Myc* overexpression is sufficient to induce disease dissemination to proximal organs. Moreover, consistent with other studies, over-expressed *Myc* efficiently promoted disease dissemination in cooperation with *Pten*.

2. Tumor suppressor-hairpin systems

The RNAi mediated down-regulation of targets has been broadly accepted as valuable tool for functional studies of target genes. However, the majority of research utilizing RNAi technology has been based on *in vitro* experiments. The increasing demands for the *in vivo* relevance of knocking down targets has forced the development of useful RNAi mouse models, such as inducible RNAi transgenic mice in which target specific shRNA expression is achieved

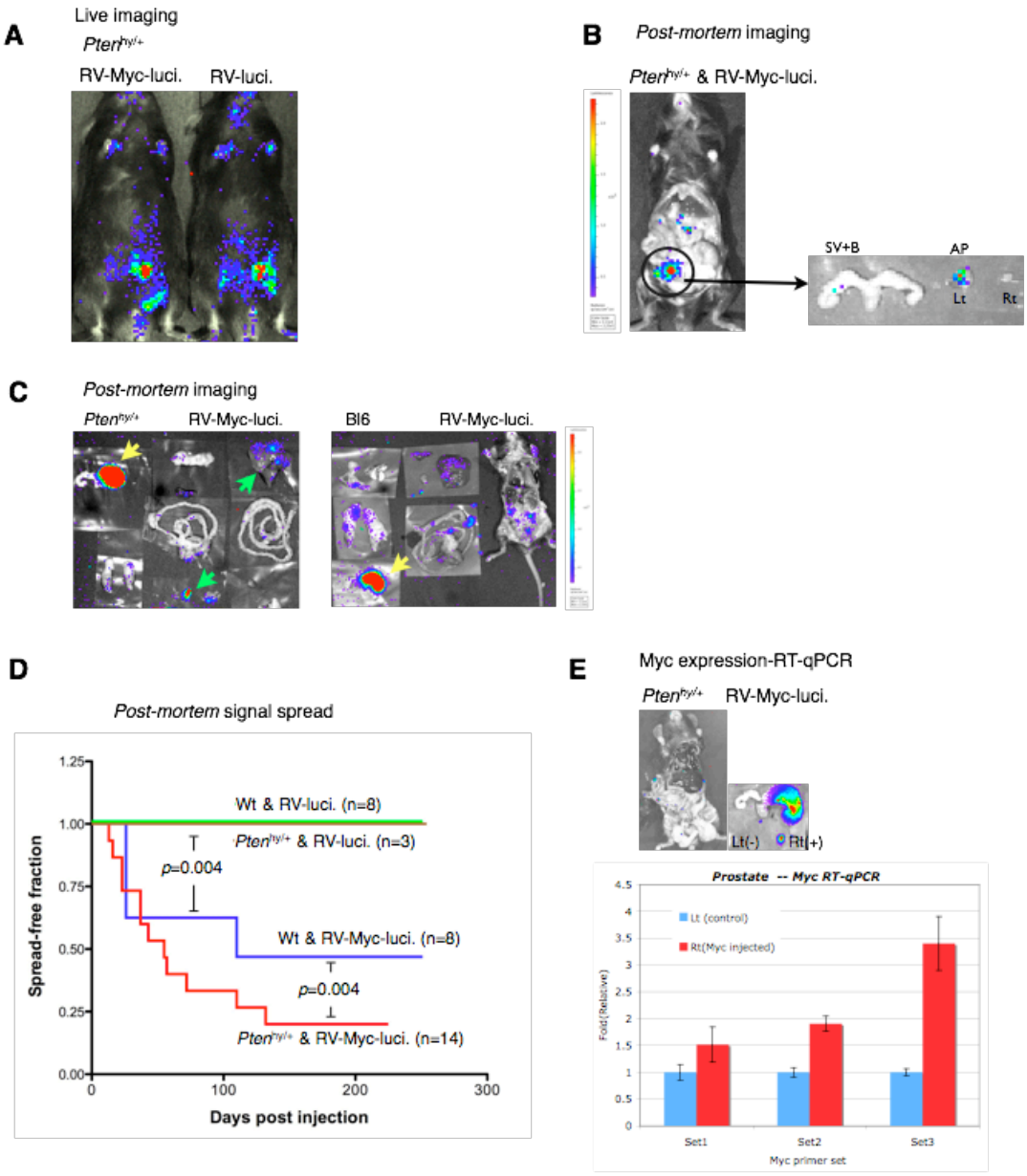

Figure 3.1 Viral injection delivers oncogene, *c-Myc*, to prostate. A. Typical live imaging of *Pten*$^{hy/+}$; RV-Myc-luci /RV-luci injected mice shows lower abdominal signals and absence of distant metastasis. Note that *Pten*$^{hy/+}$ mice express only 75% Pten throughout their body (see: Trotman et al., Pten dose dictates cancer progression in the prostate. PLoS Biol., 2003;1:E59). B. *Post mortem* imaging of RV-Myc-luci injected *Pten*$^{hy/+}$ mouse, harvested in 56 days post viral injection. Note that RV-Myc-luci injected(Lt) anterior prostate (AP) shows luminescence signal. C. Autopsy analysis of Myc-driven RapidCaP models (RV-Myc-Luci into *Pten*$^{hy/+}$ or Bl6 wt mice) unveils local, mostly lower abdominal disease dissemination from prostate (yellow arrows) to secondary sites (green arrows), including local lymph nodes. Note that in contrast, *Pten/Trp53*-deletion generates distant metastasis. D. Kaplan-Meier analysis of disease spread in indicated RapidCaP models reveals that Myc expression can drive local dissemination of prostate cancer and cooperate with *Pten*-suppression, as revealed by RV-Myc-luci injection into *Pten*$^{hy/+}$ mice. Log-rank (Mantel-Cox) testing shows that wt and *Pten*$^{hy/+}$ study arms are significantly different (p=0.004). E. Reverse transcript qPCR analysis of c-MYC reveals over-expression in injected prostate at harvest, 416 days p.i.

by viral mediated delivery to embryonic stem cells (Dow et al., 2012). However, this model is also genetically engineered, the effects of target knock-down are observed only after the time required for engineering of embryos, gestation and development. As RapidCaP can deliver transgenes directly to target organs (Chapter II and above), hairpins were also developed for delivery to prostate with this system. To determine whether the RapidCaP system can be used for studying the biological effects of target knockdown, *Trp53* (LMP, Supplemental figure 3.1, (Dow et al., 2012)) was initially selected and injected into $Pten^{+/-}$ mice for observation of the development of a prostate disease phenotype. Note that loss of *Trp53* alone has not been shown to be sufficient to promote prostate neoplasia in mice (Chen et al., 2011). At 79 days post viral injection, prostate sections were prepared for histological analysis. H&E staining and immunofluorescence with Ki67 antibody demonstrated that frequently Ki67 positive cells were found in GFP positive regions (Figure 3.2 A and B). These data suggested that shRNA driven down-regulation of *Trp53* promoted active cell proliferation, compared to the GFP-negative neighboring regions. To further study the cooperative effect of *Trp53*-loss with *Pten*-loss in prostate disease progression, $Pten^{loxp/loxp}$*;* $Trp53^{loxp/+}$ mice were injected with LV-Cre/luci and RV-shp53-GFP, in parallel to LV-Cre/luci control injections. Prior to performing double injections into mouse prostate, double infection with LV-Cre-Tdtomato and RV-shp53-GFP of MEFs demonstrated that double infection can be achieved (Supplemental figure 3.2, white arrow). Live imaging 50 days post injection of control mice demonstrated the presence of signal restricted to the primary organ (prostate). However the shp53 injected mice consistently revealed dissemination of signal (Figure 3.2 C). Surprisingly, the signal spread from the LV-Cre/luci and RV-shp53-GFP injected $Pten^{loxp/loxp}$*;* $Trp53^{loxp/+}$ cohort was observed in a shorter time post-injection than that from mice in the LV-Cre/luci injected $Pten^{loxp/loxp}$*;* $Trp53^{loxp/loxp}$ cohort (see Chapter II). The *post mortem* analysis of secondary tissues with luminescence signals proved that both virus infections were shown in the same tissues (Figure 3.2 D). Also, the positive correlation of either Ki67 or AKT activation was commonly found in the region where GFP was strongly expressed, based on immunofluorescence (Figure 3.2 E). These data supported the notion that that primary and secondary diseases were caused by simultaneous infection of both viruses in the prostate.

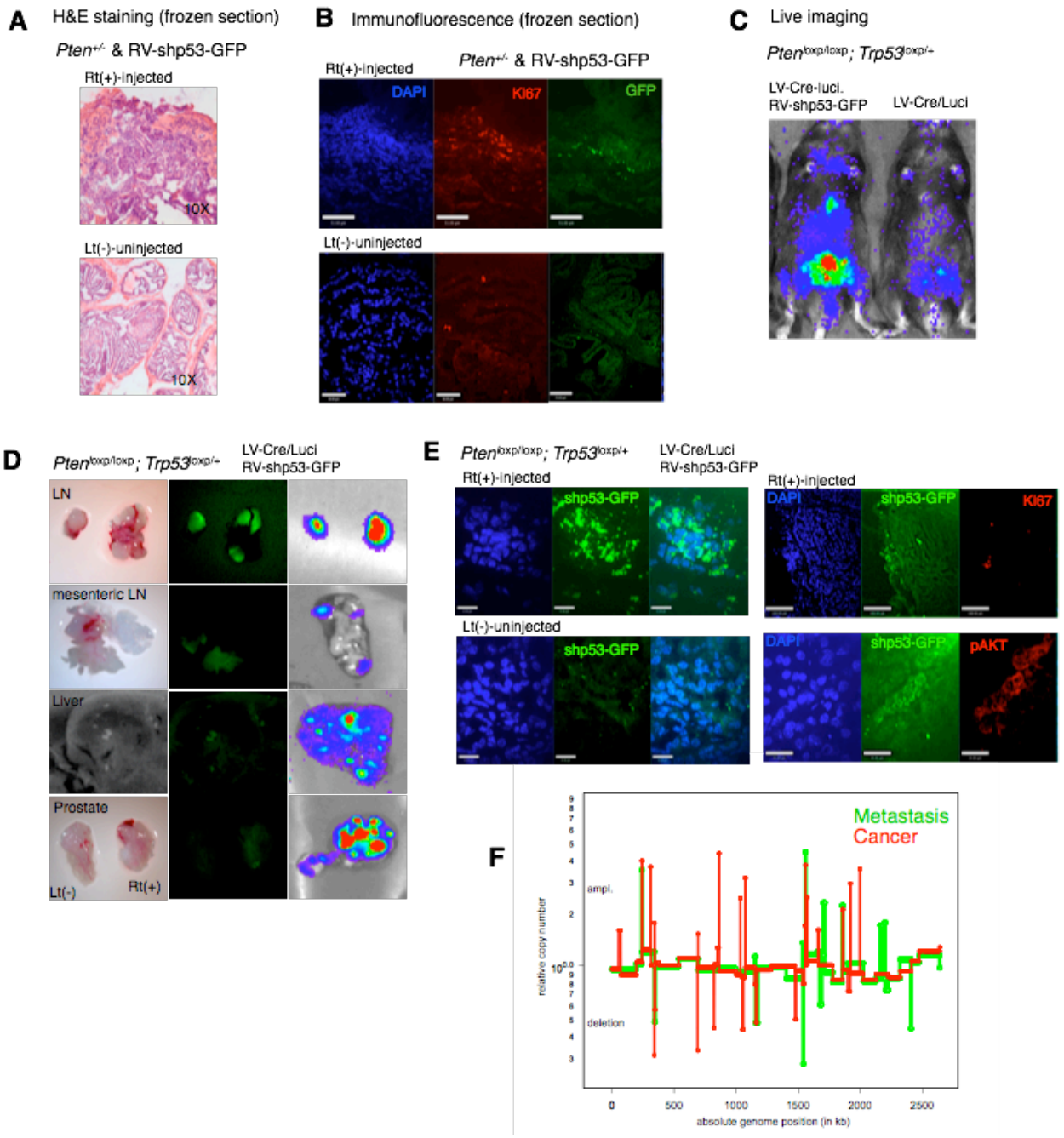

Figure 3.2 Trp53 knockdown cooperates with Pten-loss.

Figure 3.2 Trp53 knockdown cooperates with Pten-loss. A. H&E staining of RV-shp53-GFP injected (Rt) and un-injected (Lt) $Pten^{+/-}$ prostate. The disorganized luminal structure is shown in virus injected prostate (Rt). B. Immunostaining of Ki67. Active cell proliferation is associated with GFP expression in RV-shp53-GFP injected (Rt) $Pten^{+/-}$ prostate. Scale bars, 51 µm (top panel), 38 µm (bottom left and middle), 70 µm (bottom right). C. The representative live imaging of double virus (LV-Cre/Luci and RV-shp53-GFP) (Left) and single virus (LV-Cre/Luci) (Right) injected $Pten^{loxp/loxp}$; $Trp53^{loxp/+}$ mice. High primary and secondary signals are detected only in double injected mouse compared to single virus injected mouse. D. The luminescence/fluorescence imaging of tissues from double virus (LV-Cre/Luci and RV-shp53-GFP) injected $Pten^{loxp/loxp}$; $Trp53^{loxp/+}$ mice. Note that the collected secondary and primary tissues are positive for both markers. E. The immunostaining of LV-Cre/Luci and RV-shp53-GFP injected $Pten^{loxp/loxp}$; $Trp53^{loxp/+}$ prostate. The strong GFP expression is shown in a fixed prostate section (top left panel). Frequent Ki67 (top right panel) and activated Akt (bottom right panel) are correlated with GFP signals. Scale bars, 15 µm (left panel), 100 µm (top right) and 20 µm (bottom right) F. The genome wide analysis of primary and secondary disease. DNA copy number analysis with GFP positive prostate and liver cells reveals several common genomic events (deletions/ampplifications), implying there might be an evolutionary link between primary and secondary disease (see Navin, N., J. Kendall, et al. 2011; Baslan, T., J. Kendall, et al. 2012 for the method)

For further proof of disease dissemination in this model, the GFP positive cells from prostate and liver (Supplemental figure 3.3) were isolated and subjected to whole genome analysis to derive copy number alterations (CNAs) in collaboration with Dr. Jim Hicks. Several common CNA events were found in both the prostate and metastatic cells confirming their common origin. The detailed analyses and identification of specifically altered genomic loci are ongoing (Figure 3.2 F).

3. RapidCaP and tumor suppressor screening - a proof of principle

With current GEM models, it is challenging and time consuming to generate animal models harboring multiple genetic modifications, alone or in combination. This, however, is essential for understanding deletion or amplification of DNA regions during the progression of human disease. The RapidCaP approach can target multiple genes and this trait could be the basis for an *in vivo* screening model for identifying or validating tumor suppressors. To this end, a sensitized genetic background, depicted in Figure 3.2, *Pten* null and *Trp53* heterozygous prostate, which can be generated by injecting LV-Cre/luci *in*to *Pten*$^{loxp/loxp}$*; Trp53*$^{loxp/+}$ mice, was utilized. The three genes, *FOXP1, RYBP* and *SHQ1*, have been described as residing in a focal region (3p14.1-p13) which is frequently deleted in human prostate cancer (Figure 3.3 A) (Taylor et al., 2010), especially in combination with loss of *PTEN* or *TP53*. It has remained unclear if one of them or all together are involved in disease progression. For each candidate, the best shRNAs were selected after Western blotting or competition assays (Figure 3.3 B, note that no functioning SHQ1 antibodies are available commercially (not shown, C. Sawyers & Phil Iaquinta, personal communication). RV-shp53-GFP was tested as positive control for disease. Live imaging demonstrated that all signals disappeared over time except for RV-shp53-GFP, the positive control, and RV-shShq1-GFP injected animals, in which the primary signal was maintained and a signal spread appeared after 60 days post-injection (Figure 3.3 C). As the signal became stronger in the primary and secondary regions, the LV-Cre/luci + RV-shp53-GFP injected mice were terminated for analysis subsequent to 93 days of non-invasive live imaging. The experiments were repeated with more Shq1-targeted animals and cohorts were monitored and are displayed in the Kaplan-Meier plot (Figure 3.3 D). The other genes in the loci or their combination showed no effects and only loss of signal in the mice.

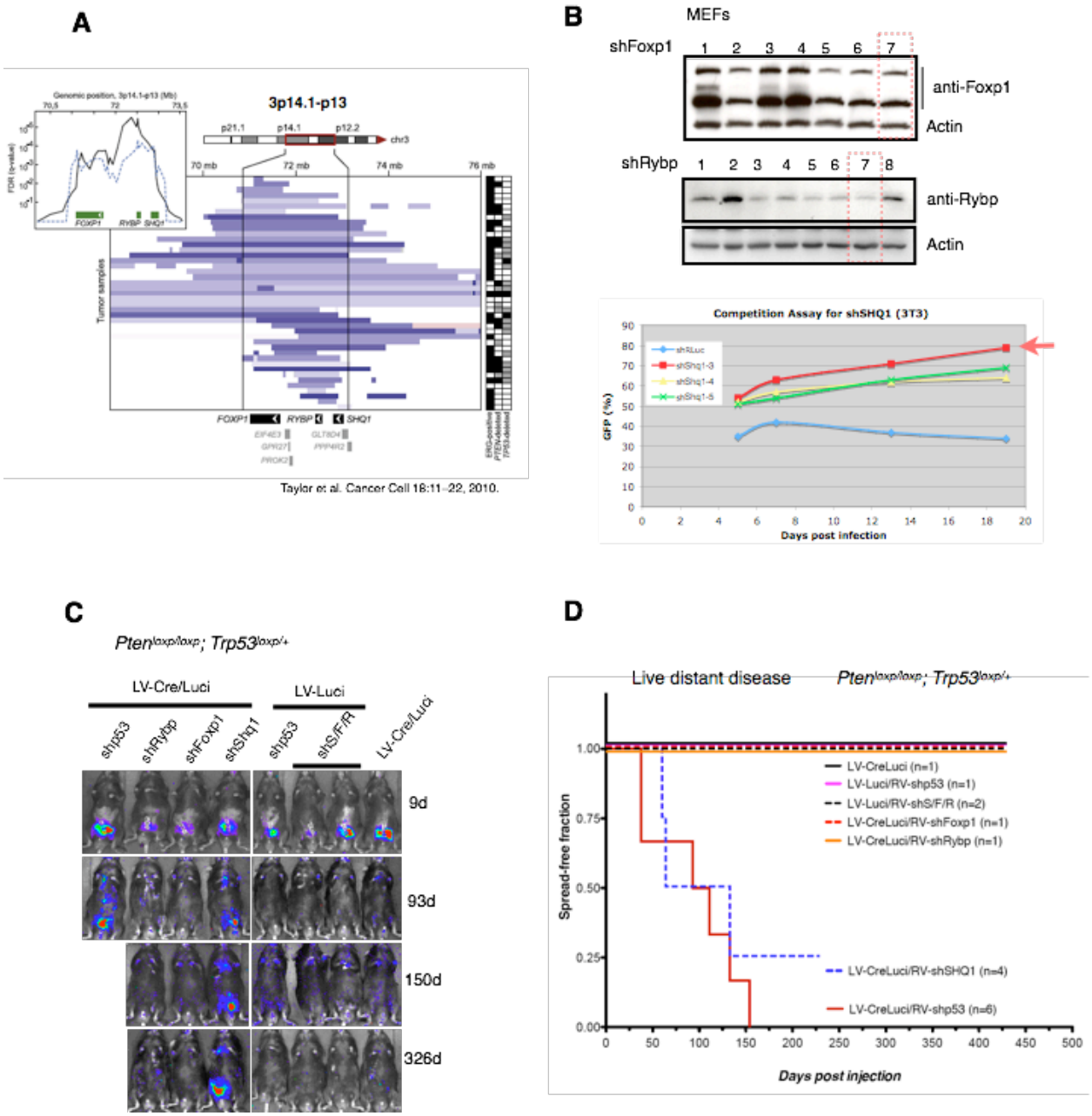

Figure 3.3 RapidCaP and Human genomics validation. A. The frequent focal deleted locus at chromosome 3p14 in human prostate cancer. The region contains 3 potential cooperative tumor suppressors, *FOXP1, RYBP,* and *SHQ1*. (Taylor et al. Cancer Cell, 2010) B. The western blot and competition assay to validate shRNA targeting *FOXP1, RYBP,* and *SHQ1*. For the injection, sh*Foxp1* (lane 7), sh*Rybp1* (lane 7) and *Shq1* (shShq1-3) was selected based on *in vitro* tests. C. Live imaging of LV-Cre/Luci and RV-shRNA-GFP injected mice. Each target shRNA or combined sh (shShq1, shFoxp1 and shRybp or shS/F/R) was injected to *Pten*$^{loxp/loxp}$*; Trp53*$^{loxp/+}$ mice with either LV-Cre/Luci or LV-Luci. Notably, shp53 and shShq1 injected mice maintain the primary signal and developed the secondary signals. D. The Kaplan-Meier curve of the signal spreads. The frequency of signal spreads is high in shp53 and shShq1 injected mice but none of other injections shows the signal spreads.

These results suggested that *SHQ1* deletion may be the driver tumor suppressor of the 3p13 locus, which warrants further detailed analysis of its tumor biology (ongoing collaboration with P. Iaquinta and C. Sawyers, MSKCC).

4. Marker genes in RapidCaP

Cre-loxp dependent expression of fluorescence proteins has been used as a powerful biological tool for cell lineage tracing, fate-mapping, and genetic analysis. Live tissue imaging has significantly improved with the development of far-red fluorescent proteins, with optimized spectral characteristics for *in vivo* applications (Deliolanis et al., 2008). L*ox-stop-lox (LSL)-Tdtomato* (*lsl-Tdtomato*) and *lox-stop-lox (LSL)-Luciferase* (*lsl-Luci*) strains were crossed to generate triple *loxp* mice (*Pten*$^{loxp/loxp}$*; Trp53*$^{loxp/loxp}$*; lsl-Tdtomato, Pten*$^{loxp/loxp}$*; Trp53*$^{loxp/loxp}$*; lsl-Luci*). The triple *loxp* strains should allow labeling of cells with both fluorescence and luminescence markers subsequent to single virus injection (with either LV-Cre/luci or LV-Cre-Tdtomato). As a result of either LV-Cre/luci or LV-Cre-Tdtomato injection, luminescence signals were detected , however no signals were shown by Xenogen fluorescence imaging (Figure 3.4 A and B). This suggests that the Tdtomato fluorescence signal intensity may not be enough for live detection, unlike luminescence signals. The *post mortem* imaging also demonstrated that Tdtomato fluorescence signals are not specific to the target organs as high background signals were shown in both viral injected and un-injected mice, which is dissimilar to the luminescence signal (Figure 3.4 A, B and C). Cell-level analysis for Tdtomato fluorescence protein expression (from *lsl-Tdtomato* mice or from LV-Cre-Tdtomato) revealed expression in fixed LV-Cre/luci injected (Lt) prostate sections. Flow cytometry analysis (Figure 3.5 A and B) revealed that up to 16% of cells were recombined at 197 days post injection, indicating the expansion rate of mutated cells in this experimental cohort.

Discussion

The unique characteristics of RapidCaP allowed us to demonstrate that the various genetic modifications in target tissue are deliverable by a single or combined viral injection. This

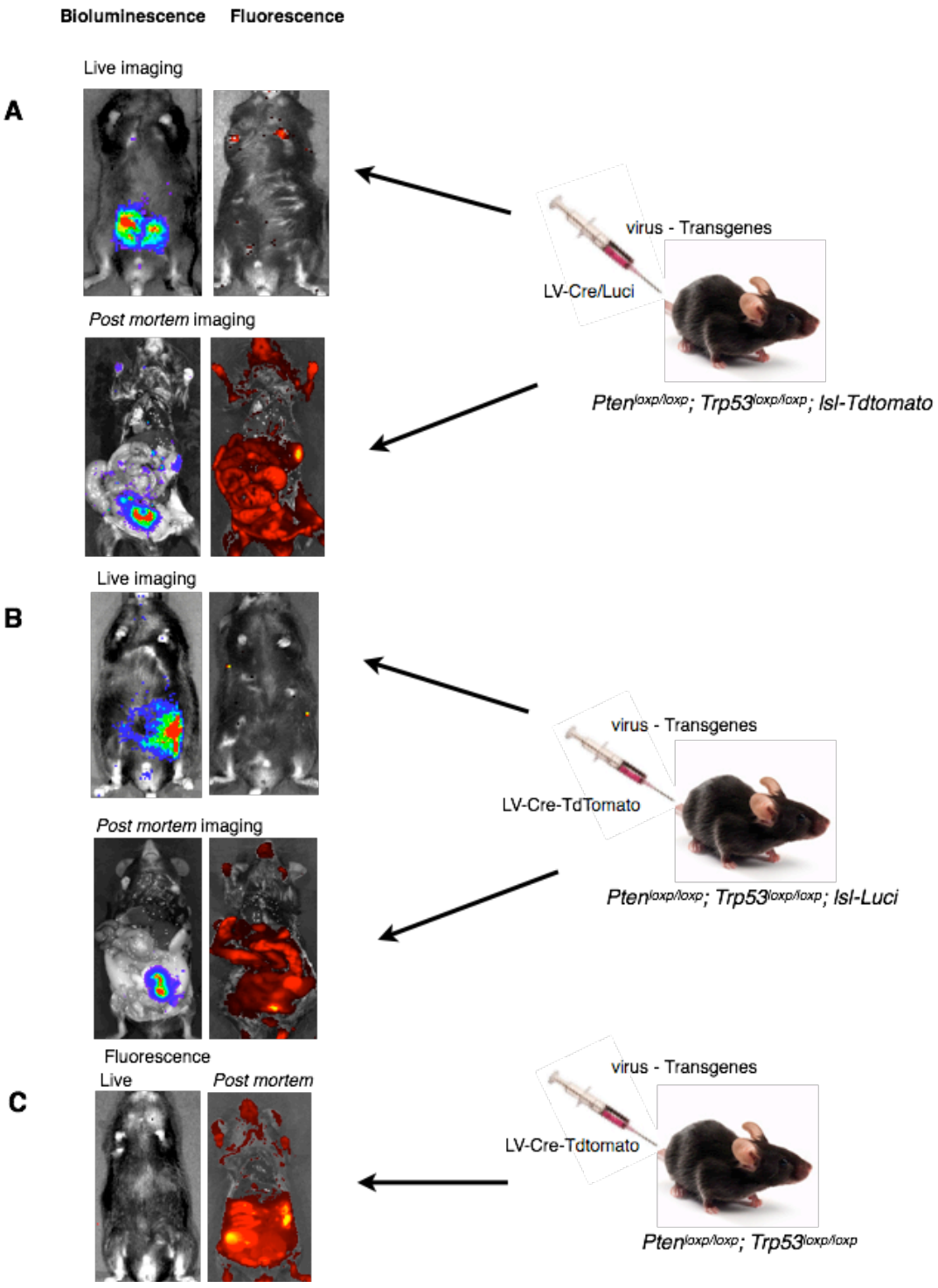

Figure 3.4 Marker delivery for sorting. A-B. Live and *post mortem* luminescence and fluorescence imaging of LV-Cre/Luci injected *Pten*$^{loxp/loxp}$*; Trp53*$^{loxp/loxp}$*; lsl-Tdtomato* mice (A) and LV-Cre/Tdtomato injected *Pten*$^{loxp/loxp}$*; Trp53*$^{loxp/loxp}$*; lsl-Luci* mouse (B). Note only luminescence signal is detected in live imaging and is specific in *post mortem* imaging in both cases (A, B). C. Live and *post mortem* fluorescence imaging of LV-Cre/Tdtomato injected *Pten*$^{loxp/loxp}$*; Trp53*$^{loxp/loxp}$ mice. The fluorescence signal is not detected in live imaging and high background signal is shown in *post mortem* imaging.

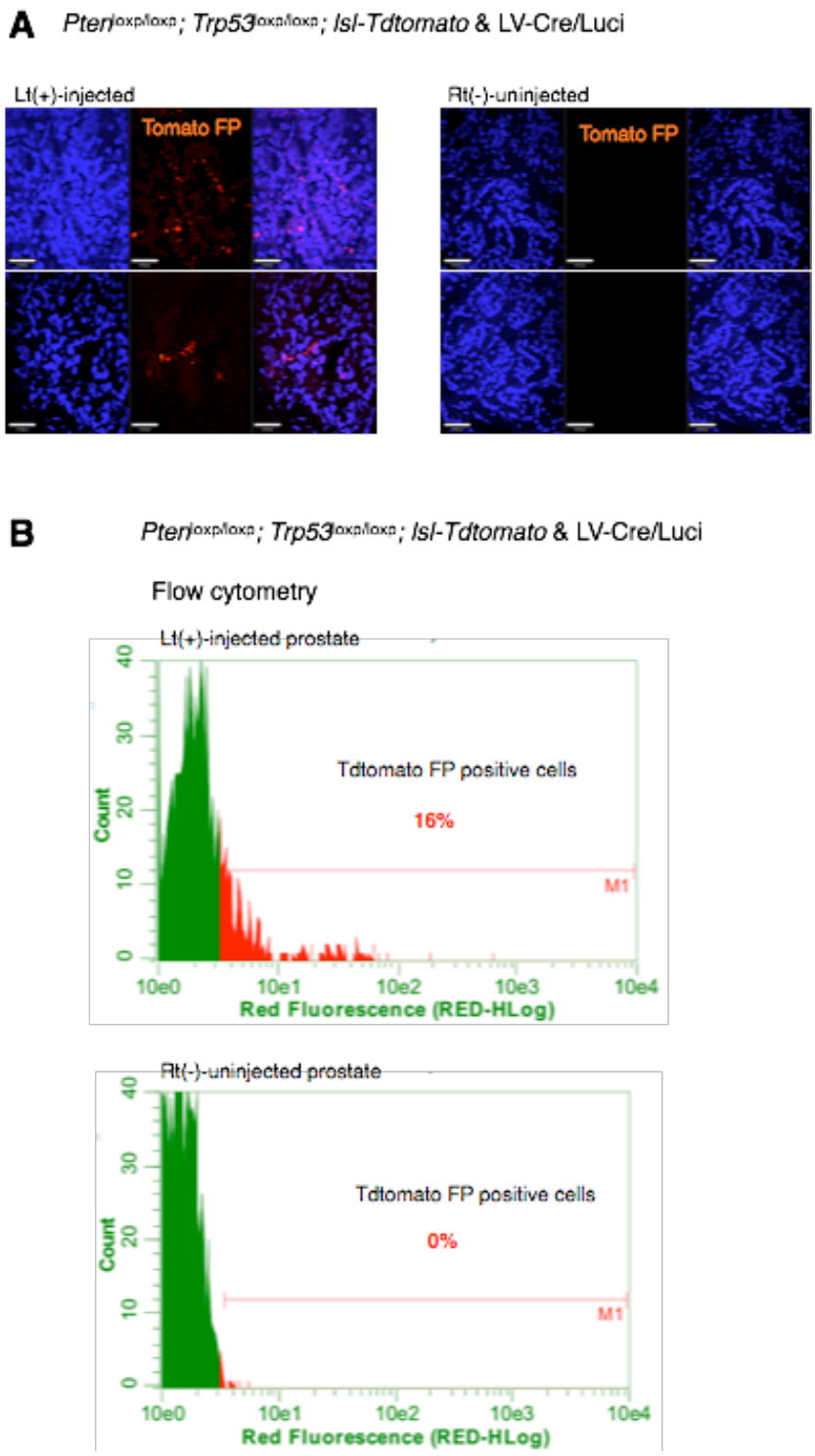

Figure 3.5 Analysis of fluorescence marker expression. A. The expression of Tdtomato fluorescence protein in prostate. LV-Cre/Luci injected *Pten*$^{loxp/loxp}$*; Trp53*$^{loxp/loxp}$*; lsl-Tdtomato* mice was analyzed 198 days post injection. Scale bars, 25 μm (left panel) and 38 μm (right panel). B. The flow cytometry analysis of LV-Cre/Luci injected/uninjected *Pten*$^{loxp/loxp}$*; Trp53*$^{loxp/loxp}$*; lsl-Tdtomato* prostate. The cell suspensions were obtained from the same prostates, shown in A, 16% of cells are positive for Tdtomato fluorescence protein expression in virus injected prostate (Lt(+)-injected).

chapter has focused on the expansion of RapidCaP applications to explore the range of genetic manipulations that can be accomplished without conventional breeding.

Among the most studied oncogenes in prostate cancer is *MYC*. It also has been suggested that the overexpression of *MYC* transformed prostate epithelial cells, is immortalizing cells in a single step that was sufficient to generate tumors with increased proliferative capacity (Hawksworth et al., 2010). The initiation and early progression of prostate cancer has been recapitulated in GEM models with the loss of tumor suppressors and activation of *Myc* (Ellwood-Yen et al., 2003). Interestingly, the RapidCaP trial with *Myc* overexpression revealed cooperation between Myc and Pten-suppression in local metastasis. This finding is supported by recently published research that the cooperation of *Myc* and *Akt* promote the progression to invasion in a murine prostate cancer model (Carver et al., 2011). However, histopathological analysis of secondary tissues derived from *Myc* overexpression-induced primary lesions is still required to confirm the contribution of Myc in these disseminated lesions. Importantly however, the spontaneous activation of Myc has been found in metastatic lung regions in LV-Cre/Luci injected $Pten^{loxp/loxp}$; $Trp53^{loxp/loxp}$ (Supplemental figure 2.5 A).

Unlike with luminescence, live tracking was not possible with the Tdtomato fluorescence protein driven by either viral delivery or Cre-mediated endogenous expression. This trial for fluorescence marker expression suggested that RapidCaP can be used for the *Cre-loxp* based expression of fluorescence/luminescence markers which will be a useful tool for harvesting tumor cells in *post-mortem* analysis.

This chapter highlighted that RapidCaP has great potential as a platform to validate and investigate key genetic events resulting in metastasis by combining the property of rapid disease dissemination with the specific expression of fluorescence markers in primary and secondary disease. By straightforward engineering of multiple targets at the same time, the system enables the distinction of driver from passenger mutations. It will be interesting to see if the process can be adapted to large scale *in vivo* screening of cancer candidate genes identified in human genomics research.

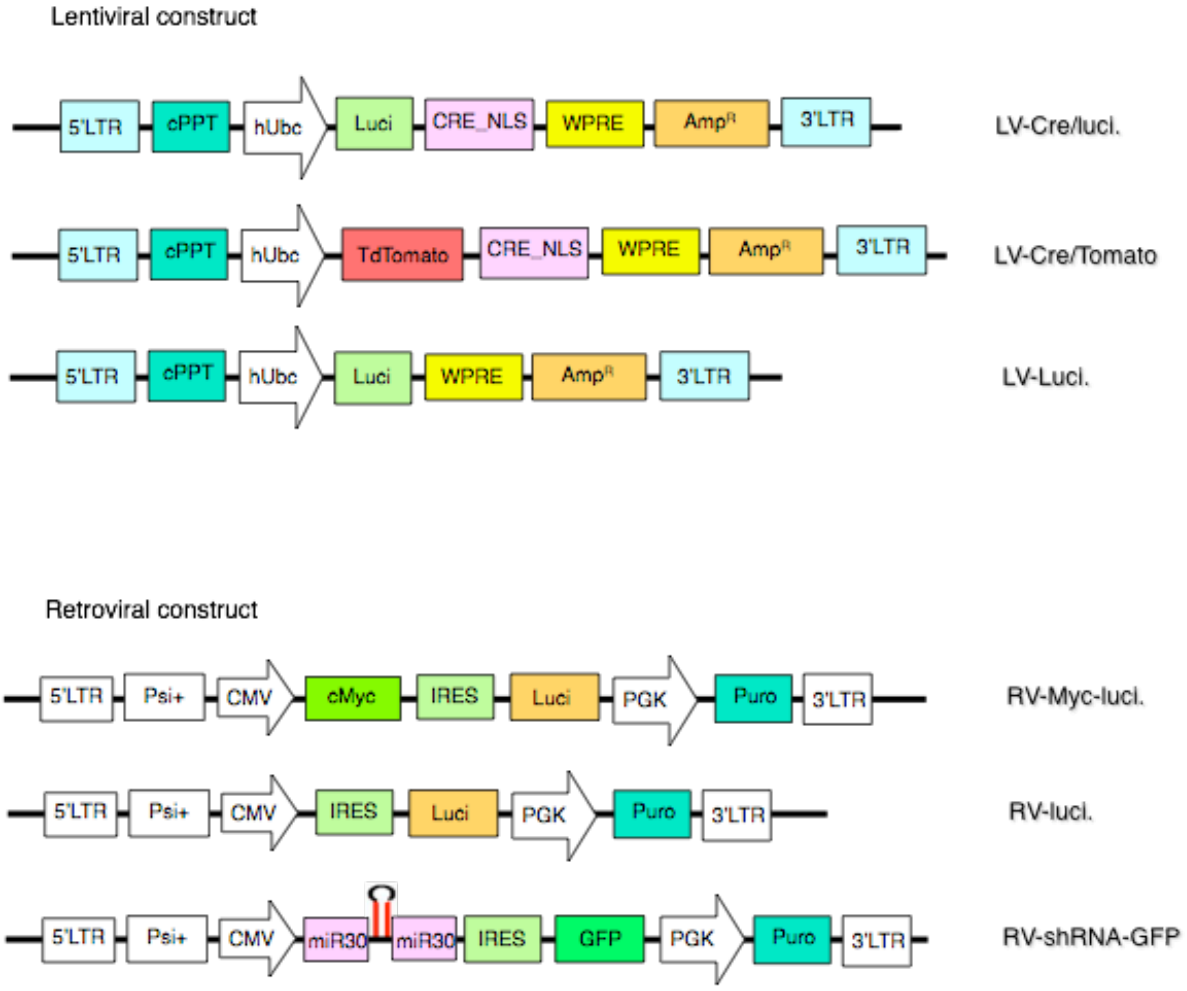

Supplemental figure 3.1 The viral constructs for prostate injection. The lentiviral constructs (LV-Cre/Tomato and LV-Luci) were modified from LV-Cre/Luci, purchased from Addgene (Tyler Jacks, Plasmid 20905: Luc.Cre empty vector). The retroviral constructs (RV-shp53-GFP;LMP and RV-Myc-luci) were gifts from Scott. Lowe laboratory. Other shRNA harboring constructs were made by replacing shp53 with target shRNA.

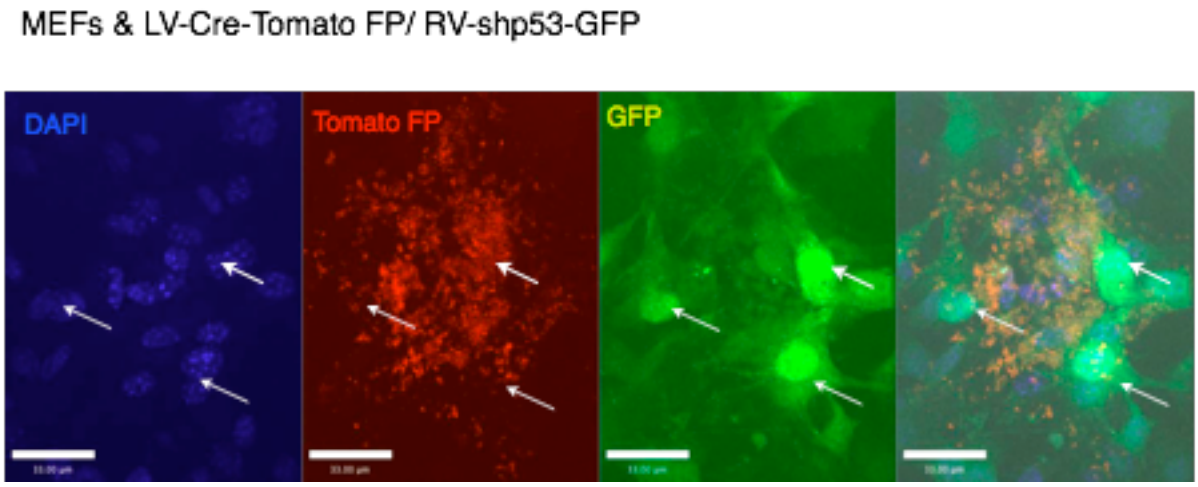

Supplemental figure 3.2 The double virus delivery *in vitro.* The expressions of Tdtomato fluorescence protein and GFP in MEFs. The LV-Cre-Tomato and RV-shp53-GFP were simultaneously infected to MEFs. The image displays the cells express both of fluorescence proteins, indicating both virus can infect the same cells. Scale bar, 33 μm.

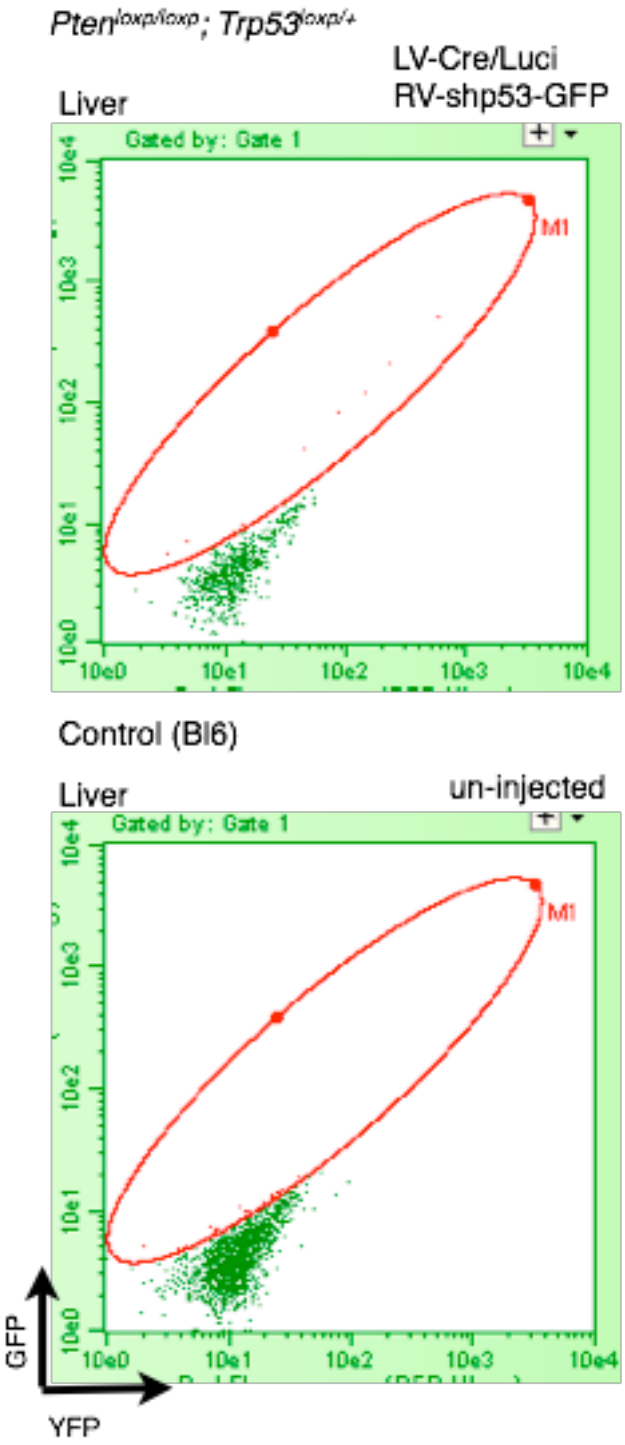

Supplemental figure 3.3 FACS analysis of disseminated cells in liver. The FACS analysis of liver cells from LV-Cre/Luci and RV-shp53-GFP injected *Pten*$^{loxp/loxp}$*; Trp53*$^{loxp/+}$ mouse. These cells were used for whole genome analysis (Figure 3.2 F), no GFP positive cell was shown from control Bl6 liver.

IV. A dual color screening system to identify regulators of PTEN stability

Introduction

The *PTEN* tumor suppressor gene is located on chromosome 10q23. A surprisingly high number of mono-allelic mutations of this locus have been shown to cause 50-80% of sporadic tumors. Complete loss of *PTEN* is frequently observed in advanced cancer and metastases (Salmena et al., 2008; Vivanco and Sawyers, 2002; Yoshimoto et al., 2006). Various mouse models in which *Pten* was deleted developed multiple tumors. It was also shown that loss of one *PTEN* allele in mice promotes the initiation of cancer in conjunction with other genetic insults (Di Cristofano et al., 2001; Trotman et al., 2006). Moreover, a series of *Pten* hypomorphic alleles was used to demonstrate that cellular levels of Pten protein have an inverse correlation with the occurrence of prostate cancer (Trotman et al., 2003). A number of human and mouse studies indicate that PTEN is functionally haploinsufficient and does not conform to the Knudson 'two-hit hypothesis'(Knudson, 1971). The discovery that complete loss of *Pten* triggers a *Trp53*-dependent senescence response finally explained why partial loss might be beneficial and therefore so frequent in early tumors that still have wild type *Trp53*.

Functionally, the PTEN phosphatase antagonizes the phosphatidylinositol-3-kinase (PI 3-K)/ AKT pathway thereby controlling cell growth, proliferation, cell polarity and metabolism by catalyzing the production of phosphatidylinositol 4,5-bisphosphate (PIP_2) from phosphatidylinositol 3,4,5-triphosphate (PIP_3), a second messenger generated by activated PI3-K subsequent to activation by growth stimuli. With *PTEN* loss, PIP_3 is accumulated which in turn allows AKT recruitment to cell membranes where it is activated by PDK1 and subsequently the mTOR kinase complex 2 (mTORC2). Activated phospho-AKT (pAKT) works through direct phosphorylation of a great number of substrates, including GSK3, FOXO3a and p27 as well as through indirect activation of mTORC1, which induces translation of many targets. In many human cancers the PI 3-K/AKT/mTOR pathway is overactive and *PTEN*-loss or alteration is a major underlying cause of prostate, breast, endometrial and colon cancers. In addition, it has been reported that PI 3-K mutation and *PTEN* loss could cooperate in breast, endometrial and colon cancer (Yuan and Cantley, 2008).

Taken together, the *PTEN/ PI 3-K* pathway is a major axis deregulated in cancer and partial PTEN inactivation is a common cause of tumor initiation. This demonstrates the importance of understanding PTEN regulation.

1. Regulation of PTEN levels

PTEN is a target of multiple post-translational modifications including phosphorylation, ubiquitination, acetylation and oxidation (Salmena et al., 2008). In respect to PTEN stability, phosphorylation of PTEN appears to affect turnover indirectly through ubiquitin mediated proteasomal degradation, a common mechanism mediating protein stability.

The first defined PTEN E3 ubiquitin ligase, NEDD4-1, was identified through a biochemical approach: recombinant GST-tagged PTEN, recombinant E1, E2, ubiquitin and ATP were incubated with chromatography-fractionated HeLa cell cytosol and *in vitro* poly-ubiquitinated PTEN was detected by Western blotting. Using this assay the strongest activity-containing fraction was further fractionated through various chromatography and precipitation steps to produce a high activity-containing sample with only few proteins, of which only NEDD4-1 was demonstrated to be a PTEN E3 ligase (Wang et al., 2007).

2. PTEN nuclear import versus degradation

Two major conserved sites (lysine 289 and 13) for PTEN ubiquitination were identified at the same time through mass spectrometry; mono-ubiquitination of either of these two sites was shown to be necessary for nuclear-cytoplasmic translocation of PTEN (Trotman et al., 2007). In addition, recent work from our group showed that double mutants of these sites together are highly stable and unable to enter the nucleus, indicating that both mono- and poly-ubiquitination occur mainly through these two sites.

In patients with esophageal squamous cell carcinoma, colon cancer and pancreatic cancer, lack of nuclear PTEN was often seen to correlate with worse prognosis (Perren et al., 1999; Zhou et al., 2002) and later studies showed that enhanced nuclear expression of PTEN could block anchorage-independent growth in transformation assays (Liu et al., 2005). While such data suggested that nuclear localization of PTEN is important for its tumor suppressive function, no clear mechanisms could be established. Many nuclear functions for PTEN have been proposed (Salmena et al., 2008), however most of these could also be achieved by cytoplasmic PTEN. Trotman *et al*. identified the PTEN K289E patient mutation, which has nuclear import defect but normal phosphatase activity; this allowed the separation of PTEN

nuclear localization from function in the pathway. These studies showed that nuclear PTEN is more stable than cytoplasmic PTEN, presumably due to cytoplasmic localization of NEDD4-1. Therefore, nuclear import of mono-ubiquitin conjugated PTEN could be a way to protect PTEN from proteasomal degradation in the cytoplasm.

3. Studies on PTEN half-life and mechanism of its degradation

PTEN is known as a relatively stable protein even though it contains two PEST motifs, a feature of short-lived proteins that undergo proteasomal degradation (Vazquez et al., 2001). In general, it has been suggested that PTEN is stable in normal cells because the activity of NEDD4-1 is suppressed and degradation occurs only when it is needed (Wang and Jiang, 2008). The high steady-state level of PTEN is key to maintain low PIP_3 levels in normal cells, allowing them to boost PIP3 only transiently after growth stimulation. This is in contrast to the p53-degradation system, where basal levels of p53 in normal cells are low but build up rapidly in response to DNA damage or other stress by suppressing Mdm2-mediated degradation. However, these models cannot explain why PTEN is relatively stable even in cells with high NEDD4-1 levels. Moreover, only very robust over-expression of NEDD4-1 was shown to reduce PTEN levels (Wang et al., 2007) and previously produced Nedd4-1 heterozygous and null MEFs showed hardly any Pten turnover in 12 hours in one report (Fouladkou et al., 2008). In sharp conflict to these results however, subsequent studies including the conditional knockout of Nedd4-1 in brain fully confirmed its role in Pten regulation (DiAntonio, 2010). Previous studies suggest that Nedd4-1 could therefore need to be activated in order to suppress PTEN (Wang and Jiang, 2008). However, our preliminary data suggest an altogether different mechanism of regulating E3 ligase activity, namely the differential subcellular localization of the Ubiquitin-Proteasome System (UPS) system in respect to the PTEN target.

4. Ubiquitin proteasomal degradation

Regulated protein degradation by the UPS affects multiple cellular process such as proliferation, signal transduction and differentiation, as well as many diseases such as autoimmune, neurodegenerative disease and cancer (Cavo, 2006; Schwartz and Ciechanover, 1999). Degradation of a protein *via* the ubiquitin-proteasome pathway is the major pathway of non-lysosomal proteolysis of intracellular proteins and proceeds in two successive steps: 1) conjugation of ubiquitin to the specific substrate and 2) degradation of the tagged protein by the proteasome complex (Hough et al., 1986).

Selective attachment of ubiquitin to the target protein is the initial signal for degradation. The ubiquitination of protein is carried out in three sequential steps involving three enzymes; E1-activating, E2-conjugating enzymes and E3-ligase. There is major E1 in human cells, which activates ubiquitin and transfers it to all E2s. Each E2 works with different E3s to promote modifications of target proteins. The high specificity and selectivity of the UPS relies on E3s that can recognize a specific substrate and only few E2 enzymes (Hershko and Ciechanover, 1998). E3 ligases have been classified into two subfamilies: one contains a homology to the E6AP C-terminus (HECT) domain, the other contains the Really Interesting New Gene (RING) domain. HECT type E3 ligases are monomeric enzymes and have conserved an active cysteine residue, which is required for activity (Scheffner et al., 1993). The family of RING type E3 ligases transfers ubiquitin from E2 to the specific substrate without having enzymatic activity themselves. This subtype can be either single-subunit proteins or multi-subunit complexes (Saurin et al., 1996).

Deubiquitination, the reverse reaction, also regulates the fate and function of ubiquitin-conjugated proteins. Deubiquitinating enzymes (DUBs) catalyze the removal of ubiquitin from specific ubiquitin-conjugated substrates as well as its precursor proteins (Amerik and Hochstrasser, 2004). By doing so, DUBs proofread Ub-modified substrates and also recycle ubiquitin. DUBs occupy the largest family of enzymes in the ubiquitin system, implying their diverse functions in regulation of the ubiquitin-mediated pathways.

In this respect, it is important to note that DUB and Ub function should not be seen as primarily related to *degradation* but as equally important means of protein *regulation*. Mono- and alternative chain linked ubiquitination serves various purposes including transcriptional regulation, membrane trafficking, protein kinase activation, DNA repair, chromatin dynamics (reviewed in (Chen and Sun, 2009)) and nuclear-cytoplasmic shuttling (Plafker et al., 2004; Trotman et al., 2007). Thus, the prevalence of DUBs highlights the role of the UPS as a highly dynamic and reversible modification similar to phosphorylation and de-phosphorylation.

Recently, *USP7* has been suggested as PTEN de-ubiquitinase in the nucleus causing its export by using a candidate approach (Song et al., 2008). Even though the mechanistic basis for de-ubiquitination and nuclear export is entirely lacking, these results illustrate the need for a comprehensive analysis of the interactions between PTEN and the UPS and its role in cancer.

5. The UPS in Cancer therapy

An increasing number of studies suggest that abnormal regulation of E3 ubiquitin ligases is involved in tumor development; major E3 Ub ligases are frequently overexpressed in human cancers. Tp53 levels are mainly regulated by ubiquitin-mediated proteasomal degradation (Brooks and Gu, 2003). The gene amplification and overexpression of *mdm2*, the *Tp53* E3 ligase, has been reported in various tumors (Onel and Cordon-Cardo, 2004; Toledo et al., 2006). Similarly, expression of the cyclin-dependent kinase (CDK) inhibitor, p27 has been found to be decreased in many human cancers, however not through gene mutation (Ponce-Castaneda et al., 1995). Instead, it was shown that E3 ligase SCF^{Skp2} (Skp1/Cul1/F-box protein) uniquitinates p27 for degradation (Carrano et al., 1999). Overexpression of Skp2, the component of SCF, correlated with reduced level of p27 in several tumors. Skp2 can mediate transformation and is up-regulated during oral epithelial carcinogenesis which supports the role of Skp2 as a proto-oncogene in human tumors (Gstaiger et al., 2001). A number of agents that inhibit proteasomal degradation, like Bortezomib, which was approved by the FDA for treatment of relapsed multiple myeloma, have been shown to induce apoptosis, and kill tumor cells (Adams and Kauffman, 2004). However it has been reported that there is a resistance mechanism to Bortezomib, increased expression of heat shock protein-27, the inhibition of which overcomes drug resistance (Chauhan et al., 2003). Since proteasomal inhibitors block broadly functioning and essential molecular targets, the so-called chemotryptic activity of the 20S proteasome, they also show high patient toxicity. Another specific inhibitor of proteasomal degradation, Nutlin, interferes with the interaction between mdm2 and Trp53 (Vassilev, 2004). This shows that there is promise in designing drugs to target an E3/target interaction if we know how they interact each other.

Obviously target specificity is very desirable from a point of view of efficacy and tolerability of a new anticancer drug and hence, inhibiting E3 ligases in particular has great potential. Since many human cancers are caused by decreased but partially retained PTEN, targeting of its regulators could be a promising approach for treatment.

In this chapter, in order to identify the regulators for PTEN stability, major emphasis was placed on establishing a proper screening system with reliable readout reflecting the subtle changes in PTEN stability.

Results

1. Preliminary screen

Prior to testing PTEN stability in target shRNA stable HeLa cell lines, a preliminary experiment, using the *Cre-loxP* system, was conducted to re-confirm if endogenous PTEN is regulated by post-translational degradation as it has been shown (Trotman et al., 2007). To this end, mouse embryonic fibroblasts (MEFs) harboring *loxP* flanked *Pten* (*Pten*$^{loxp/loxp}$) were infected with Adenoviral Cre (Ad-Cre) recombinase and cells were harvested to detect Pten by Western blotting at different time points. In parallel, the same procedure was performed with wild-type (WT) MEFs as a control. In *Pten*$^{loxp/loxp}$ MEFs, a significant decrease in Pten level was seen 38 hrs post Ad-Cre infection whereas no Pten changes were shown in WT MEFs (Figure 4.1 A and B). To investigate whether the decrease of Pten is due to post-translational regulation, 24 hrs post Ad-Cre infection, MG132, a proteasome inhibitor, was added to *Pten*$^{loxp/loxp}$ MEFs and the cells were then harvested to measure Pten by Western blotting. As expected, MG132 (50 μM) prevented Pten degradation and the difference in Pten level with added MG132 was measurable after 4 hrs of MG132 treatment (Figure 4.1 C and D). To further test if Pten regulation is mediated by the proteasome, Pten ubiquitin modification was monitored by immunoprecipitation and immunoblotting after MG132 treatment. With and without Ad-cre infection a significant amount of ubiquitinated PTEN adducts (higher molecular weight intensities above 47 KDa as shown by Western blot) were detected with ubiquitin antibody after *Pten*$^{loxp/loxp}$ MEFs were immunoprecipitated with Pten antibody (Figure 4.1 E and F). These data suggested that endogenous Pten is regulated by proteasomal degradation.

For the pilot screen, the lentiviral pGIPZ construct (from Codex RNAi)(Figure 4.2 A) was utilized to establish single shRNA stable HeLa lines. Based on previous literature, 9 target genes (7 de-ubiquitinases and 2 E2 conjugating enzymes) were selected and 3-13 short hairpins (Table 4.1) against each gene were selected for generating target knockdown cell lines. For

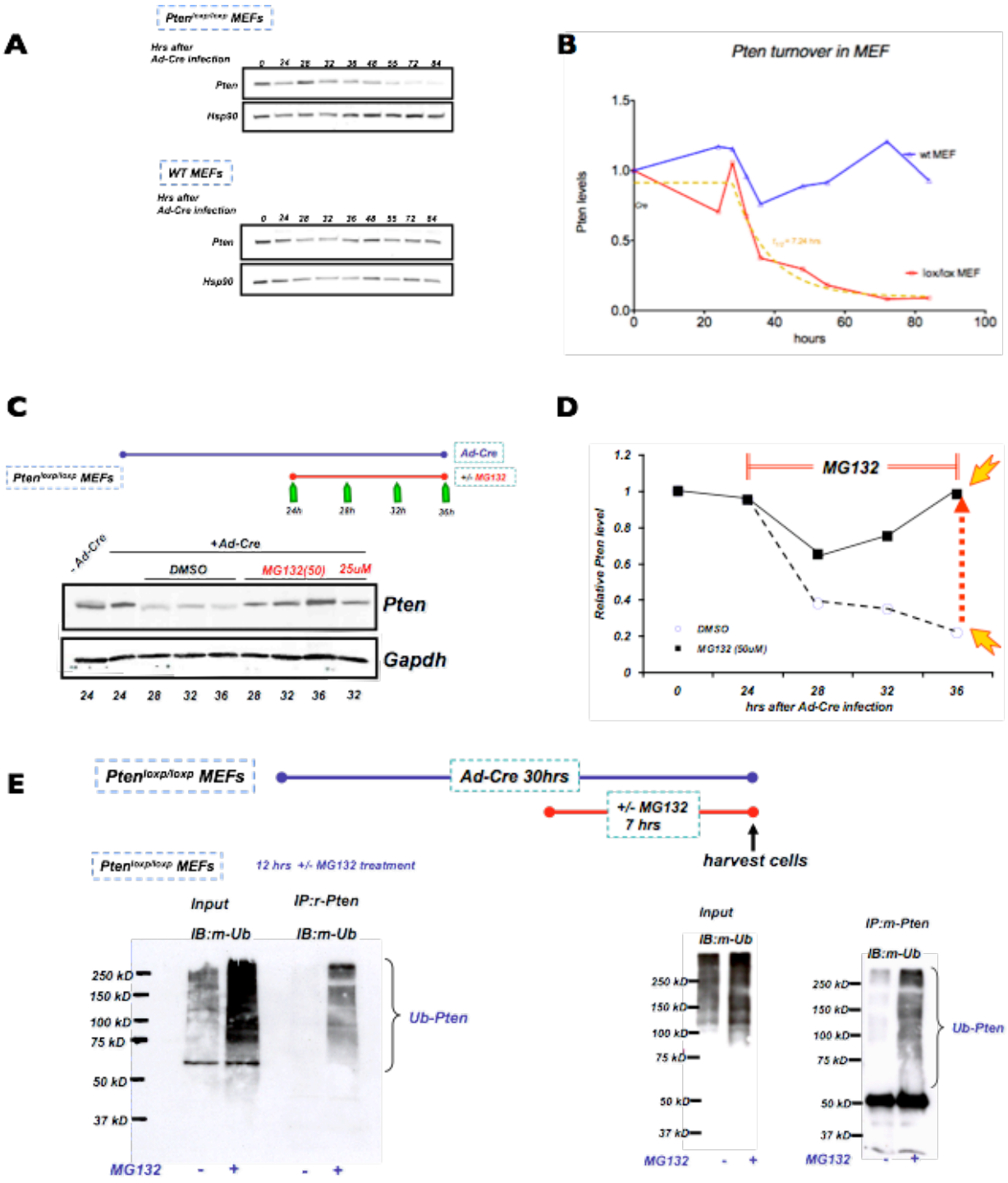

Figure 4.1 Post-translational regulation of Pten stability. A. Reduced Pten stability after Ad-Cre infection into *Pten*$^{loxp/loxp}$ MEFs. B. The quantification of Pten bands. The intensities of Pten bands, shown in A, were measured and the change of Pten levels are shown as relative number. (Virus infection time point set as '0') C. Western blot of Pten with or without MG132 treatment post Ad-Cre infection to *Pten*$^{loxp/loxp}$ MEFs. The hours of MG132 treatment and harvesting time points are shown on top. Note MG132 stabilized Pten compared to DMSO treated control. D. Quantification of Pten intensities shown in C. Pten levels are rescued by MG132 treatment. E. Ubiquitin modification of Pten. MG132 treatment increases ubiquitinated Pten bands.

controls, *NEDD 4-1* (a known *PTEN* E3 ligase), an empty vector, and a hairpin against PTEN itself were included. Given the small target number, Western blotting was used as a readout. First, high knock-down efficiency of each target gene and PTEN stability were confirmed by RT-qPCR and/or Western blotting with specific antibodies (Figure 4.2 C and D). Since there were no significant steady state differences in endogenous PTEN levels, cycloheximide (CHX) was used to block translation and measure PTEN turnover. Using this approach, reproducible differences in PTEN levels were seen after 12 hours of CHX treatment (Figure 4.2 B) that were consistent with earlier published results (Trotman et al., 2007). The change in PTEN stability from each line was then compared with those from the vector control and shPTEN stable line. Since these control experiments generated similar turnover, we went on to rank hairpins according to their effects on PTEN stability. The duplicated results are shown in Figure 4.2 E. It was then possible to confirm that PTEN level differences were due to post-translational regulation by comparing the PTEN Western blot to the PTEN RT-qPCR results (Figure 4.2 C, Primer set in Table 4.2). This ranking approach resulted in confirmation of NEDD 4-1 as an E3 ligase, and suggested that the E2 enzyme, E2E1, is involved in PTEN degradation. On the other hand, it pointed to *USP14* as a PTEN DUB. Since USP14 is associated with the proteasome, this effect could be very broad. Similarly, the E2 effect could be unspecific. However, the closely related E2 enzyme, *E2E2* did not score (Figure 4.2 E) and it is known that E2E1 can work with NEDD 4-1 (Anan et al., 1998). While validating E2E1 effects on PTEN with CHX, it was observed that one form of the E2 enzyme has a very short half-life and almost completely disappears within 6 hrs after drug addition (Figure 4.2 F). If several components of the PTEN-degradation machinery are turned over fast, then CHX will artificially stabilize PTEN. While this might have worked in favor of the E2E1 knockdown experiment, it could greatly bias our screen by introducing an uncontrollable parameter that can amplify or mask results. For this reason, it was decided not to use inhibitors of translation for the screen. Stable expression of PTEN in *PTEN*-null PC3 cells was attempted independently by myself and a lab colleague, which clearly showed that PTEN-levels became undetectable by Western blotting when passaging the cells. This was observed in spite of constant antibiotic selection. RT-qPCR analysis revealed that PTEN protein loss was closely correlated with its mRNA reduction.

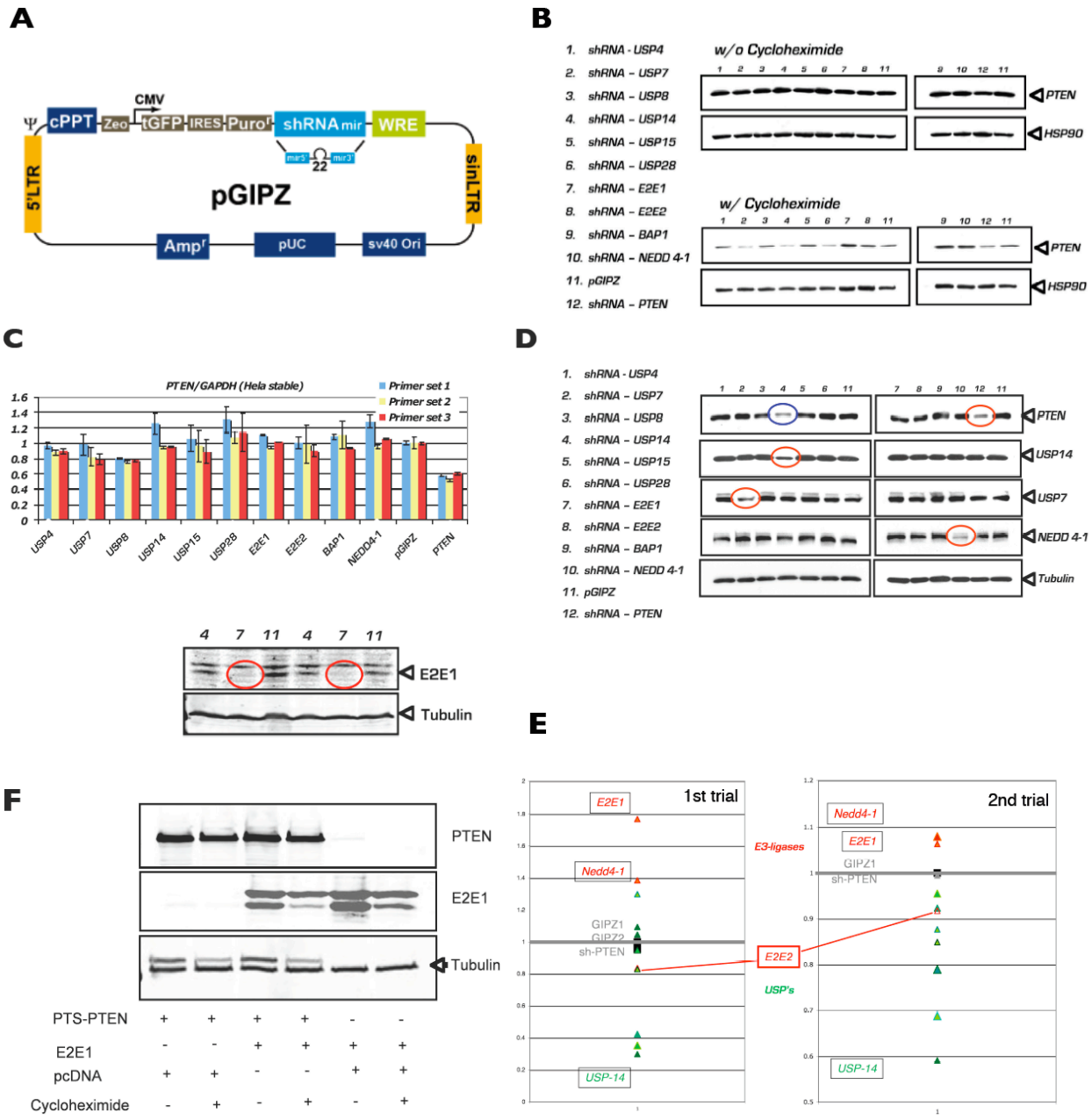

Figure 4.2 Regulation of PTEN stability in stable shRNA HeLa lines. A. pGIPZ lentiviral construct. B. The relative PTEN levels in shRNA stable HeLa lines with cycloheximide treatment. Note that no changes in PTEN levels without cycloheximide. C. PTEN RT-qPCR reveals post transcriptional changes in PTEN levels in stable shRNA HeLa lines. D. Validation of target knock down in sh HeLa stable lines. E. The candidates are ranked based on the PTEN stability in HeLa stable lines. Note the consistent ranking of E2E1 and USP14 in separate trials. F. Rapid degradation of E2E1 after cycloheximide treatment. The stability of potential PTEN regulator, E2E1, is affected rapidly by CHX.

Thus, these stable lines could not be used in our screen. The alternative of using an enzymatically dead *PTEN*-mutant did give stable expression, however it is known that ubiquitination of many substrates is tightly coupled to their activity. Therefore, inactive *PTEN* might not be a suitable replacement for the active form. Based on these findings, an inducible expression approach was taken for the next trial.

2. Construction and validation of reporter systems

2.1. GPS (Global Protein Stability) system

A very elegant way to circumvent pulse/ chase associated complexity in a screen is to evaluate PTEN stability by expressing it from a plasmid that contains a fluorescence protein marker (e.g. DsRed) under an Internal Ribosomal Entry Site (IRES) from the same promotor (e.g. CMV GFP-PTEN-IRES-DsRed). Using this approach, transcriptional effects are largely ruled out by doing GFP to DsRed ratios (Yen and Elledge, 2008; Yen et al., 2008). The principle of this system is that DsRed and GFP-PTEN are expressed at a constant ratio because these two proteins are translated from the same transcript, therefore, the GFP/DsRed ratio measured by FACS at any given time point reveals the degradation rate of GFP-PTEN in a given hairpin cell. An inducible construct harboring GFP-PTEN (Yen et al., 2008) or the non-degradable *PTEN* mutants can be transfected into target knock-down cells, the ratio of GFP/DsRed analyzed when GFP-level is visible by FACS and then high and low expressers can be sorted for sequencing of the hairpin that caused the result. In this screen, DsRed was replaced with mCherry for better separation in FACS analysis (Figure 4.3 A). The screen was performed by infecting and selecting the reporter cell line with virus harboring shRNA, followed by introducing PTEN for FACS analysis.

2.2. Generation of the shRNA library

For the comprehensive screening, a target library was constructed using the Biopred-si algorithm with 412 genes total (Table 4.3); this includes genes involved in the ubiquitin proteasome system (UPS), including 4 controls. Six short hairpins were designed for each gene. In order to increase relevance for cancer and the hit rate, the library size was reduced to contain UPS genes that are highly relevant in prostate cancer. To this end, 186 patient samples from our collaboration on the human Sloan Kettering data set that contains immunohistochemistry on

tumor tissue microarrays and gene copy number, was analyzed (Chen et al., 2011; Taylor et al., 2010). In samples showing normal PTEN copy number but low protein in IHC, DNA copy number changes of UPS genes were investigated. In addition, UPS genes that were frequently deleted or amplified were also considered and a final 35 genes were defined as a priority set (Figure 4.3 B). Using the Biopredsi algorithm (developed by Novatis, http://www.biopredsi.org), 6 siRNAs/gene were designed (Table 4.4) and cloned into the retroviral construct (MSCV) under the guidance of Dr. Johannes Zuber. According to sequence verification, 187 out of total 210 shRNAs were successfully cloned into the target vector (5.3 shRNAs/gene) (Figures 4.3 C and D). Each shRNA was infected into the reporter cell line to establish stable single shRNA expressing lines.

2.3. Construction and validation of a reporter line

2.3.1. Establishing a dual color reporter line for PTEN stability

Results from the previous trial showed that the PTEN stable expression cell lines lost PTEN expression over time. Therefore, it was decided to use an inducible system to obtain a consistent level of PTEN expression by adding doxycycline (Dox) to the cells. An inducible single color reporter line (***GPURIN***) was established by using the designated retroviral construct (GPURIN) harboring TRE promoter-controlled GFP-Pten and rtTA3 (Supplemental figure 4.1 A). PC3 cells were infected with either GPURIN virus or GFP control virus (TRIN) and the initial infection efficiency and induction of PTEN were measured by flow cytometry (Guava easyCyte Flow Cytometers) with or without Dox treatment. As the previous experiment showed, in the GPURIN line, the intensity of GFP was significantly lower than control line within 2 days of Dox treatment, although the percentages of GFP positive cells were comparable in both lines (data not shown). Since the GPURIN line was made as a mixed population and the various intensities of GFP were detected in each cell, clonal selection was performed to obtain a more homogenous system. The top 2% of high GFP-expressing cells were sorted and re-seeded for further clonal selection. About 40 clones from the high GFP population were selected under Dox treatment and expanded without PTEN induction. During the validation of selected clones, to our surprise, PTEN was barely detected by Western blotting in the high GFP expresser (clone 12) however the mediocre GFP expresser (clone 9) retained PTEN expression (Supplemental figure 4.1 B).

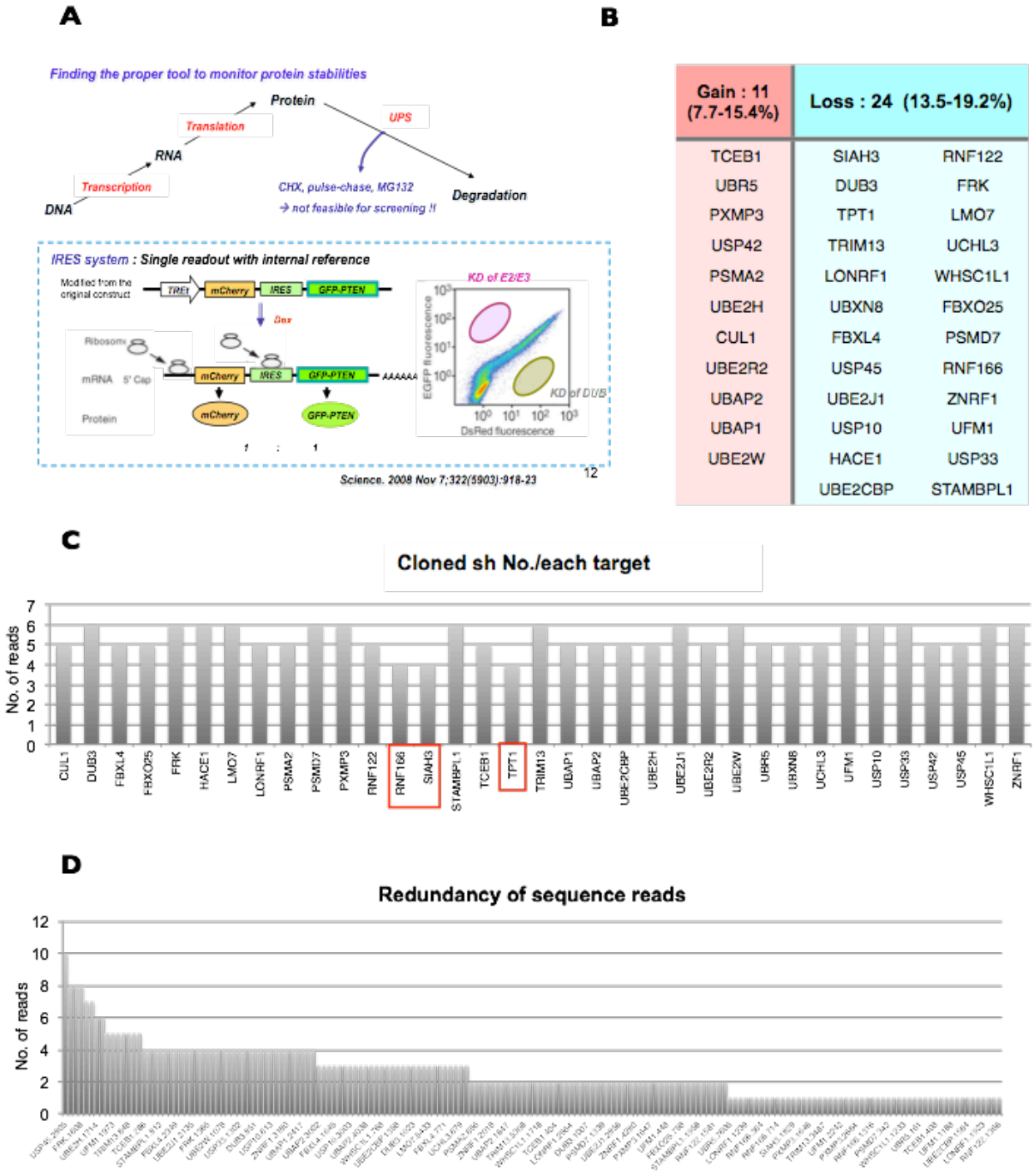

Figure 4.3 Establishing the screening system. A. The GPS system. FACS based screening for protein stability. B. The priority set for the screening. Candidates are selected from prostate cancer genomic analysis. C. The number of cloned shRNA for each candidates. 5-6 shRNA per each target were cloned in the priority shRNA library except for 3 genes (red box). D. Redundancy of shRNA library sequence reads.

These data suggested that even the transiently induced PTEN is toxic to the cells and therefore cells either lost PTEN but kept high GFP expression (clone 12) or maintained low PTEN levels with weak GFP intensity (clone 9). Based on the experiences with the GPURIN system, the PTEN induction was minimized during the establishment of our next reporter system. To improve the reporter system, dual color reporter constructs (GPITCH, VPITCH) were designed based on the GPS system (Supplemental figure 4.1 C). The mCherry and GFP-PTEN expression and their ratio were tested in these reporter lines (Supplemental figure 4.1 D, F), however, the FACS distributions of mCherry and GFP-PTEN were not ideal for performing screening due to the broad range of GFP-PTEN expressions shown (Supplemental figure 4.1 E, marked with red triangle).

In one of the attempts to solve the issue in the dual color system, GFP-PTEN and mCherry were switched to generate a new construct, called **TCHIP** (Supplemental figure 4.2, A). A TCHIP stable line was made with PC3 and the induction of both GFP-PTEN and mCherry was tested. As expected, mCherry was brighter than GFP under microscopic observation (Figure 4.4 A) and a remarkably sharp diagonal cell distribution was shown in flow cytometry analysis (Figure 4.4 C). The TCHIP line appeared to express higher GFP-PTEN and mCherry than those from the previous reporter lines (VPITCH vs. VITCH). The induction of functional PTEN expression was checked by PTEN immunoblotting (Figure 4.4 B). For further validation of the TCHIP system, a control cell line was also made by replacing GFP-PTEN with GFP alone (termed TCHIG) (Supplemental figure 4.2 A). In addition, another control with mCherry alone (2X mCherry) was made to see the distribution of cells in flow cytometry (Supplemental figure 4.2 A) and was later used to gate the mCherry positive population. From these control lines, either single GFP or mCherry alone and TCHIG was induced with Dox and the FACS profiles were made as controls (Figure 4.4 C).

For validation of the TCHIP reporter system, flow cytometry analysis was performed with MG132 treatment after PTEN was induced (FACS profile data not shown). The FACS based ratio of GFP/mCherry was increased in MG132 treated TCHIP but not in TCHIG (Figure 4.5 A), which indicated that the GFP signal faithfully represented the PTEN protein stability in this reporter system. This was confirmed by immunoblotting with PTEN antibody (Figure 4.5 B). with MG132 treatment after PTEN was induced (FACS profile data not shown). The FACS based

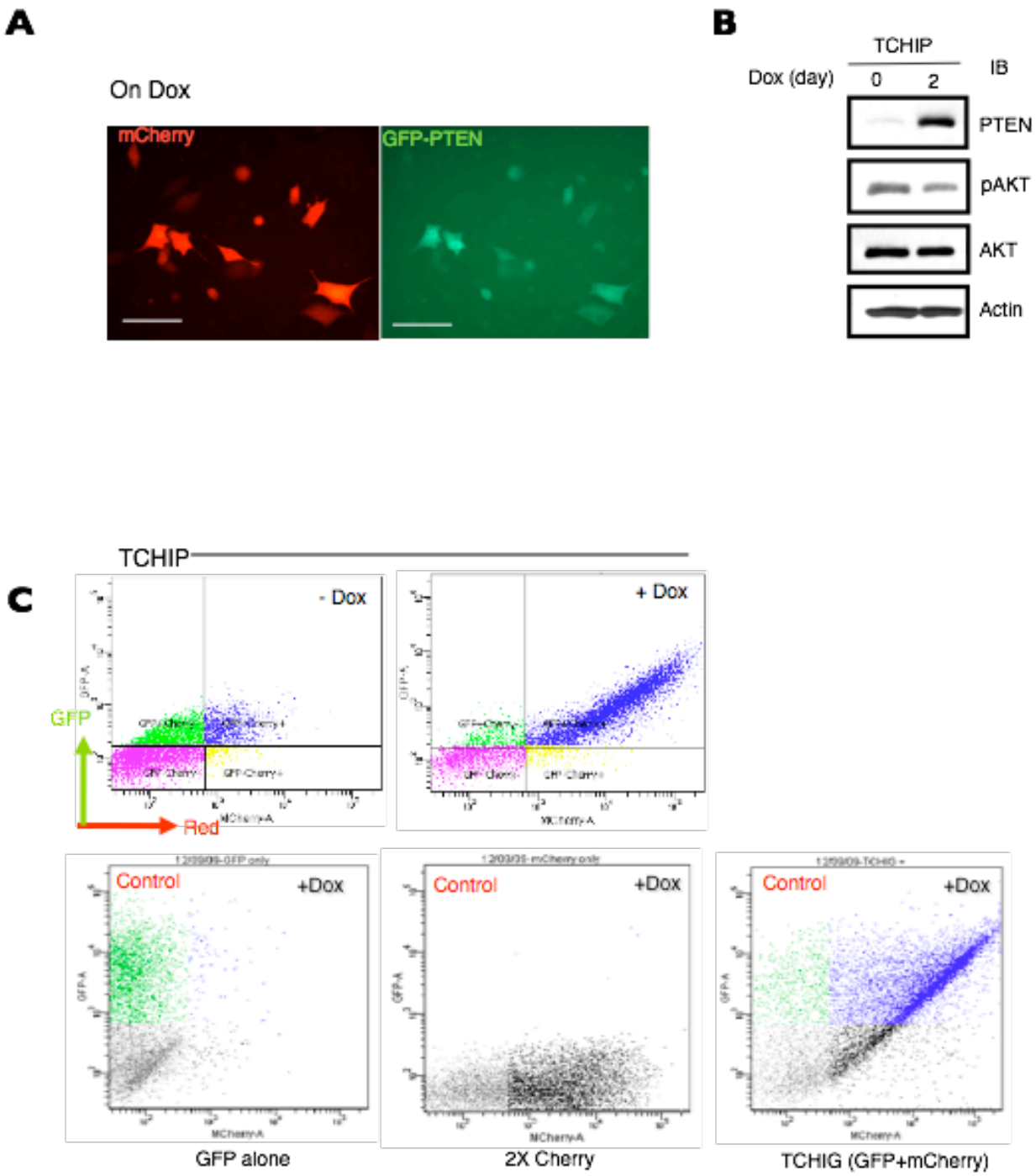

Figure 4.4 FACS based screening system for PTEN stability. A. The dox induced expressions of GFP-PTEN and mCherry in TCHIP reporter line. Scale bar, 50 μm. B. The dox induced expression of PTEN suppresses AKT activation. C. The FACS profile of TCHIP reporter line. The diagonal cell distribution is shown in dox induced TCHIP line.

ratio of GFP/mCherry was increased in MG132 treated TCHIP but not in TCHIG (Figure 4.5 A), which indicated that the GFP signal faithfully represented the PTEN protein stability in this reporter system. This was confirmed by immunoblotting with PTEN antibody (Figure 4.5 B). With MG132 treatment, PTEN was increased (lane 3 compared to lane 2). In contrast, the GFP level in TCHIG as well as mCherry in both TCHIP and TCHIG was not affected. This result supports the notion that PTEN is post-translationally regulated by proteasomal degradation and also that the fluorescence marker proteins used in this system were not influencing PTEN stability.

Next, validation of the TCHIP system was conducted to confirm that the reporter line was suited for introducing shRNA to knock down target genes. For this validation, shPTEN or shRLuc harboring virus was used to infect TCHIP cells and infected cells were selected to establish sh stable lines. With Dox induction, GFP positive cells were barely detected in shPTEN stable TCHIP. However, mCherry single positive cells were still apparent (Figure 4.5 C). These data suggested that shPTEN was targeting PTEN but not affecting mCherry expression. The flow cytometry analysis also determined that there was weaker GFP level and fewer GFP positive cells in the shPTEN stable TCHIP, whereas the expressions of GFP-PTEN and mCherry were not affected in shRLuc expressing TCHIP (Figure 4.5 C). Furthermore, the ratio of GFP/mCherry was measured in each line. Based on the FACS profile, there was obvious loss of the GFP positive population (marked with dotted red circle, compared to solid red circle) in the shPTEN line with Dox induction (Figure 4.5 E) and accordingly clear reduction in ratio was shown in shPTEN TCHIP compared to shRLuc stable TCHIP (shown a relative ratio, 1)(Figure 4.5 D). Immunoblotting re-confirmed the remarkably reduced PTEN level in the shPTEN line after various lengths of Dox induction compared to the shRLuc stable line (Supplemental figure 4.2 B). For further validation of the TCHIP system, PTEN in TCHIP was replaced with the published PTEN K19,289E mutant (PTEN-DK), which is known to be very stable (Wang et al., 2007). Indeed, the GFP/mCherry ratio from TCHIP-DK shifted toward the right compared to WT PTEN expressing TCHIP, demonstrating that the system was sensitive to the stabilization of PTEN (Figure 4.6 A). Also, as expected, MG132 treatment and shPTEN stable TCHIP displayed a striking movement toward the right and shrunk, respectively. However, the TCHIP expressing shNEDD4-1 did not show any obvious change in its FACS profile compared to TCHIP (Figure 4.6 A). From these experiments, TCHIP was validated as a viable reporter system to screen for

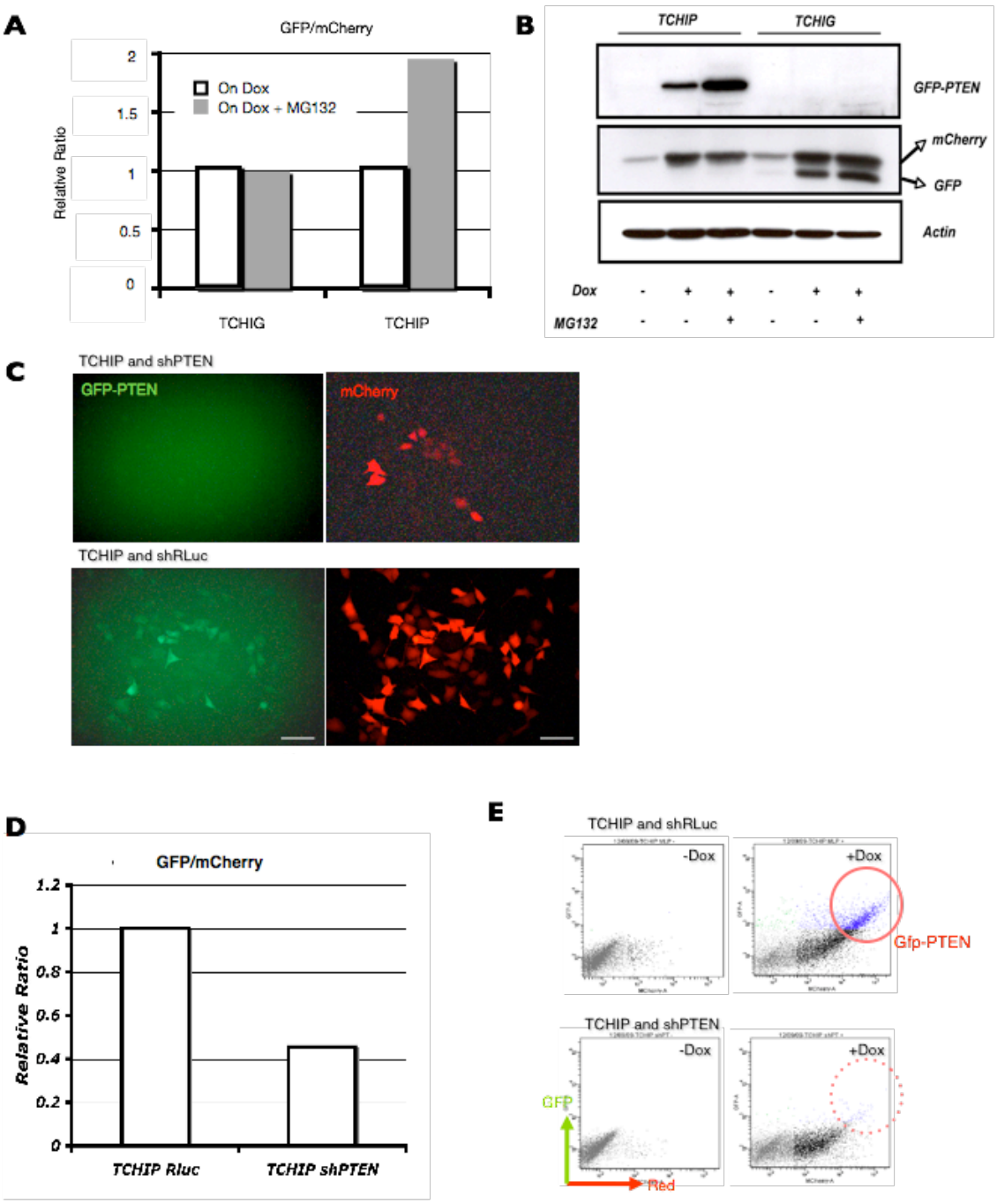

Figure 4.5 Validation of TCHIP. A. MG132 increases GFP/mCherry ratio in TCHIP but not in TCHIG control. The relative GFP/mCherry ratio made out of FACS profiles. B. MG132 stabilizes PTEN in TCHIP. Note stabilities of GFP and mCherry are not affected by MG132. C. The absence of dox induced GFP-PTEN expression in shPTEN. Scale bar, 50 μm. D. The decreased ratio of GFP-PTEN/mCherry in shPTEN reporter line. The relative ratio was measured from FACS profiles with dox treatment. E. The GFP positive population (marked with dotted red circle) in shPTEN reporter line is disappeared.

2.3.2. Screening with the priority set

As mentioned in the previous description (see 2.2. shRNA library), 187 shRNAs from the priority set were successfully cloned (Figure 4.3 B and C) and amplified to produce virus. Each virus was used to infect TCHIP cells leading to the establishment of 187 shRNA expressing cell lines after selection. For each line, PTEN was induced with 2 days of Dox treatment for analysis. As a readout, triplicated FACS analysis every other day for each single sh expressing line and immunoblotting with PTEN antibody using the same materials was performed. Each cell line displayed various cell distribution patterns in FACS analysis (Figure 4.6 B). The biggest issue in interpreting FACS profiles during the screening was the inconsistent patterns shown from the same shRNA stable line in duplicated or triplicated FACS analyses (Figure 4.6 B). The difficulties in analyzing the ratio of GFP-PTEN/mCherry from FACS profiles lead to consideration of an alternative readout option. Western blotting using cell lysates from each shRNA cell line at different passages was adopted to measure and compare the expression level of PTEN and mCherry individually. PTEN and mCherry were detected and quantified using the ImageJ software. The PTEN and mCherry ratios were calculated and the average of ratios from 3 different loadings (shown in Western blotting) was presented as a bar with error rate in this graph (Figure 4.7 A). Data without error bars indicate that they were loaded in only one lane. TCHIP was loaded in each gel as an internal control and the ratio of GFP-PTEN/mCherry from TCHIP was normalized to the relative value 1, shown in the blue dotted box. The ratio from the shPTEN line is located to the far left of the graph (red dotted box). While the Western blotting was performed, PTEN and cherry expression patterns in some shRNA lines changed according to FACS analysis. For example, lysates prepared from different passage of the UBE2J.567 line gave different ratios (marked as red and green cross in graph). This indicated that the Dox-induced PTEN expression in the TCHIP short hairpin stable reporter line was not consistent over time.

The possible reasons for inconsistent results from both trials could be that the repetitive induction of PTEN affects cell viability due to PTEN toxicity. In other words, once the PTEN was induced, cells could be selected against during culture conditions. Thus, only low PTEN expressing cells were measured during the next measurement and these cells were subsequently

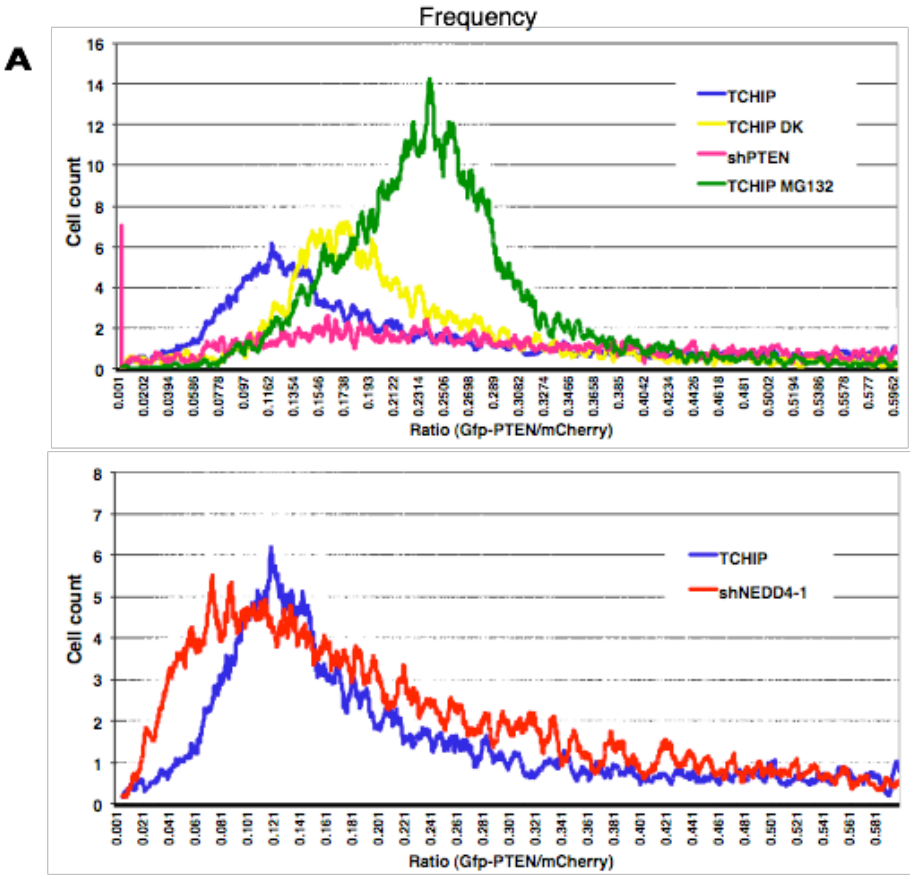

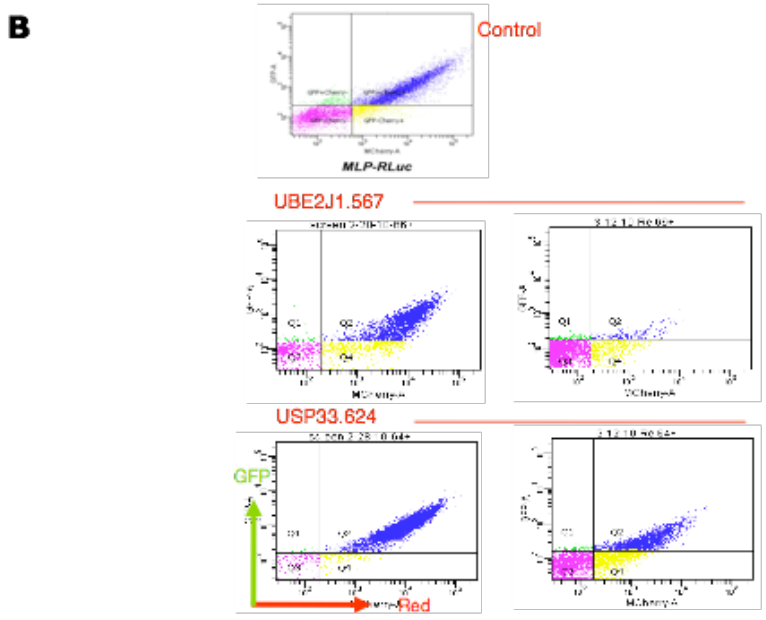

Figure 4.6 Screening - shRNA stable TCHIP. A Validation of TCHIP with known controls. TCHIP responds to controls but not for NEDD4-1 knockdown based on FACS readout. B. The FACS profiles are not consistent in sh stable TCHIP lines. Note the different cell distributions in FACS profiles from the same sh stable TCHIP.

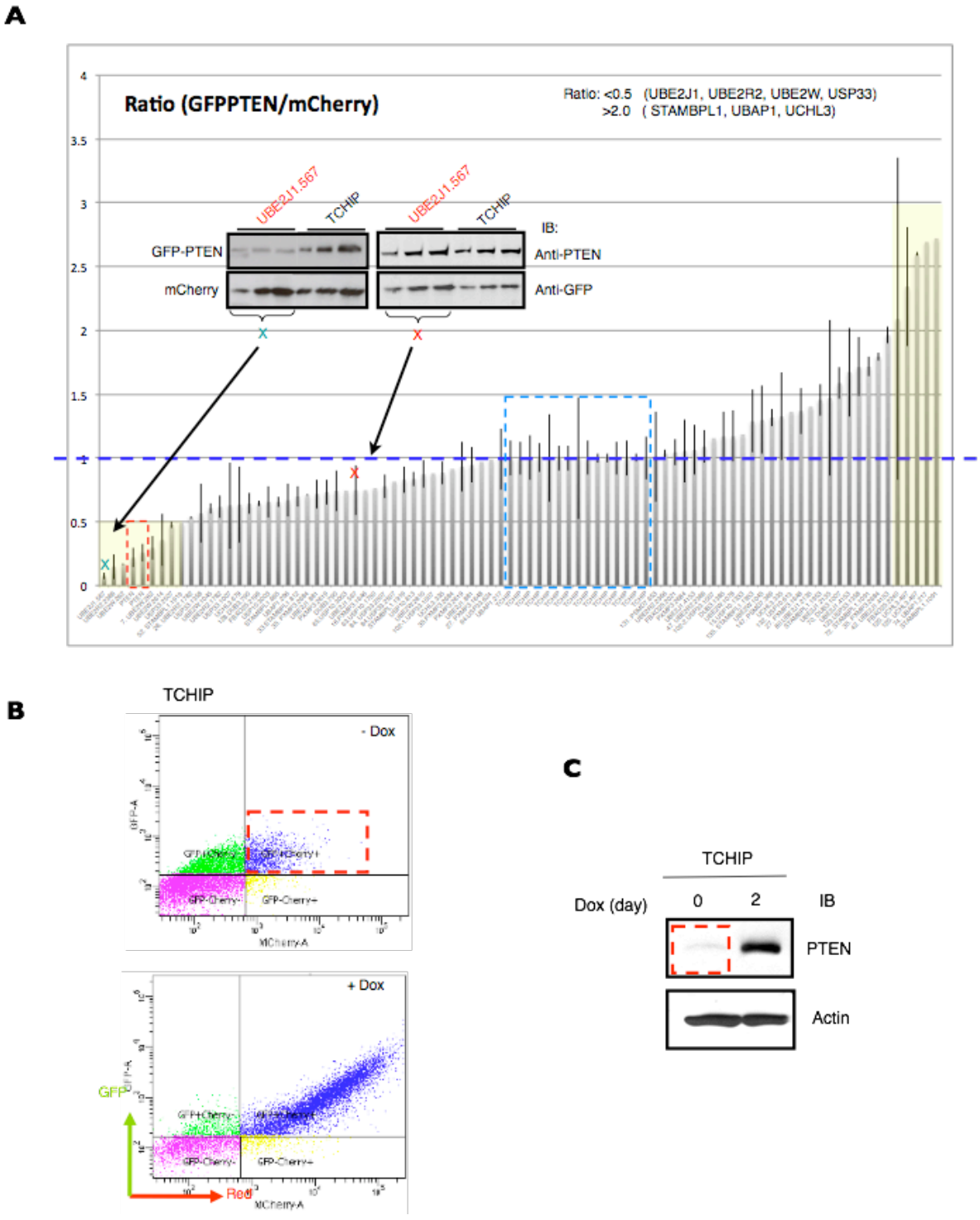

Figure 4.7 TCHIP reporter system only works with direct PTEN affecting controls. A. The western blot readout (GFP-PTEN/mCherry) is not consistent. Note different ranking of ratio from the same sh stableTCHIP line (eg. UBE2J1.567). Controls are marked with dotted boxes (red, shPTEN; blue, TCHIP) B. The leakiness of TCHIP. FACS profile shows the weak expression of GFP-PTEN without dox induction (the population marked with red dotted box). C. Western blot shows the leakiness of TCHIP. PTEN protein is detected without dox treatment (red dotted square).

selected for. Another problem could be leakiness of the TRE promoter, which has been observed previously (Danke, Grunz et al. 2010). Without Dox treatment, PTEN would be constantly expressed at low levels, which has a toxic effect on cells. Therefore, the leaky cells could be selected against during the maintenance period. To support this, cells positive for both GFP and mCherry were detected in FACS analysis even without Dox induction (Figure 4.7 B). Moreover, immunoblotting with PTEN antibody showed also weak expression of PTEN without induction (Figure 4.7 C).

Discussion

This chapter was dedicated to constructing a screen for identifying the regulators of PTEN stability. The major hurdle in the search for PTEN regulators is in the construction of an efficient readout that can reflect small changes in PTEN in a screening system. The conventional way of demonstrating protein stability is to measure protein levels by immunoblotting after inhibiting translation by adding reagents such as cycloheximide (CHX), which is a commonly used reagent to prove the post-translational regulation of protein. There is a CHX-independent assay that is used for this reason, the pulse chase assay, however, this is not feasible for screening purpose. From our preliminary data, the CHX approach was shown to be inadequate when applied to specific proteins with long half-lives, such as PTEN, since certain proteins in the ubiquitination pathway, E2 ubiquitin conjugating enzymes, and NDFIP1, co-operating component in E3 complex (Howitt, Lackovic et al. 2012), are rapidly downregulated due to their short half-life when translation is blocked. Thus, PTEN is likely to lose its degradation machinery soon after translation is blocked, possibly making PTEN more stable. In addition, it is critical to circumvent the introduction of any gross effects on the ubiquitination system itself in a protein stability screen.

In this regard, the global protein stability (GPS) (Yen and Elledge 2008) system was adapted and improved to achieve a suitable tool for PTEN analysis. The major advantages of the GPS were to that it utilized a sensitive fluorescence protein readout for stability and employed an internal control translated from the same construct from which the target is expressed. The problems were noticed immediately after the system started to express PTEN; it was observed time after time that it is not possible to express PTEN stably and reliably in the PC3 cell line

(*PTEN*/*Tp53* null human prostate cancer cell line). Either cells were not viable, or retained a small amount of PTEN expression but did not survive in the long run. To remedy this, an inducible promoter was used, but the expression level of PTEN was not consistent in repeated inductions even from a selected clone, again demonstrating the relationship between PTEN biology and PTEN toxicity. A third major problem for setting up the PTEN stability screen was the absence of any well-established positive or negative PTEN regulators, which could be used as control targets to determine the screening window or practically validate the screening system. One repeated technical issue in most reporter systems that were attempted was that the expression of the internal fluorescence control was not fully comparable to the expression of the target. This was presumably due to the lower efficiency of IRES driven translation (Technical pitfall 1). The other obstacle was that the leakiness of the TRE promoter allowed the for constant, low-level expression of PTEN without induction, which drives negative selection for those cells (Technical pitfall 2). These issues resulted in the inconsistency of FACS profiles and Western blot analyses from the same shRNA line in repeated analyses, which created misleading data that was difficult to draw conclusions from.

Despite these pitfalls, the reporter system responded to all UPS derived controls in a very reliable way. Therefore, this reporter system may be readily modified for the screening of regulators of stability of more amenable protein targets.

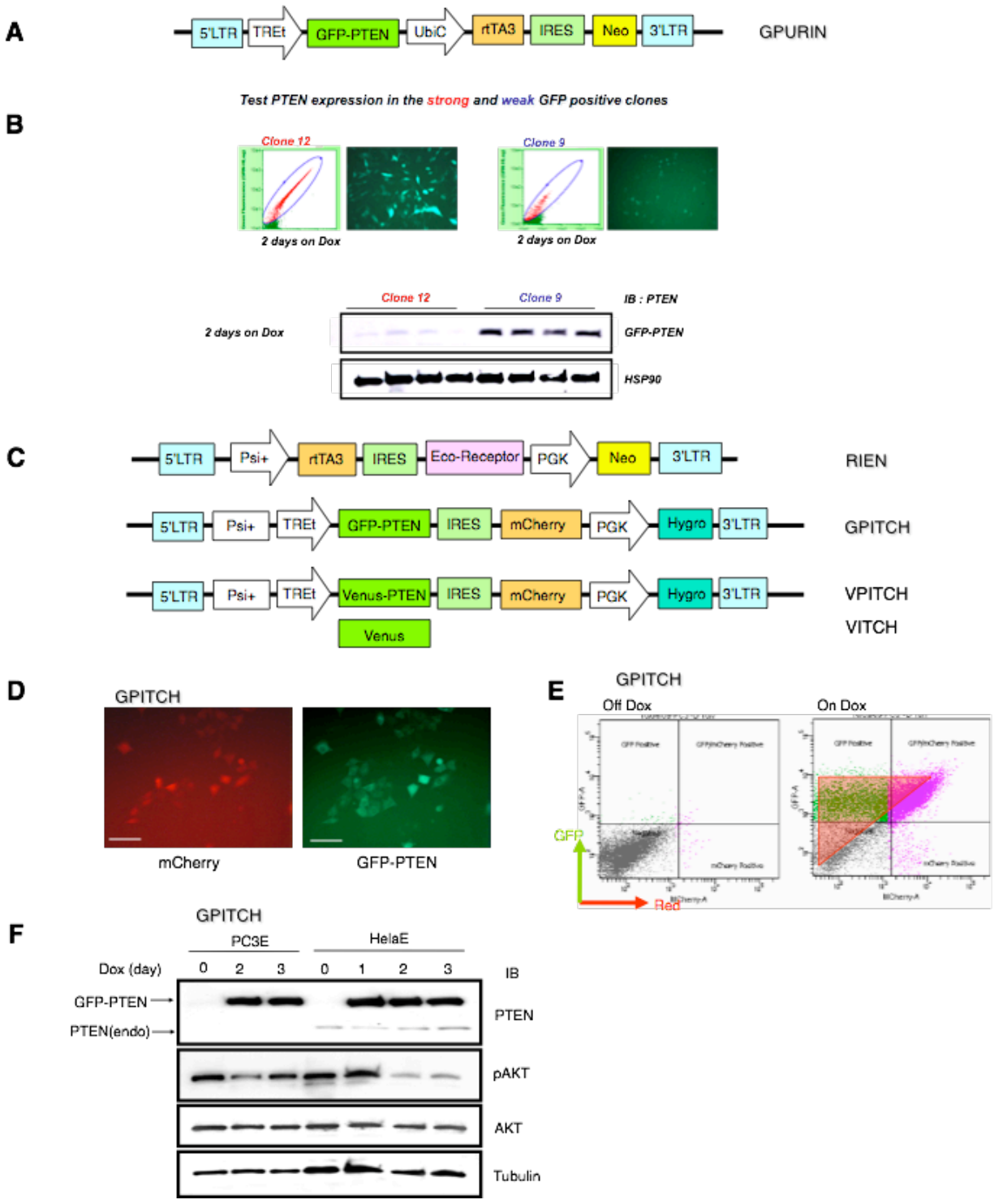

Supplemental figure 4.1 The examination of diverse reporter systems. A. GPURIN reporter construct. B. The clonal selected GPURIN line showed clones either GFP^{hi} ; $PTEN^{low}$ (clone 12) or GFP^{low} ; $PTEN^{hi}$ (clone 9). C. The dual color reporter constructs. D. The expressions of GFP-PTEN and mCherry in GPITCH reporter line. Note the weaker mCherry expression. Scale bar, 50 μm. E. The FACS profile of GPITCH. The stronger expression of GFP-PTEN in GPITCH reporter line (marked with red triangle). F. PTEN expression in GPITCH reporter lines (PC3 and HeLa). Dox induced PTEN suppresses AKT activation.

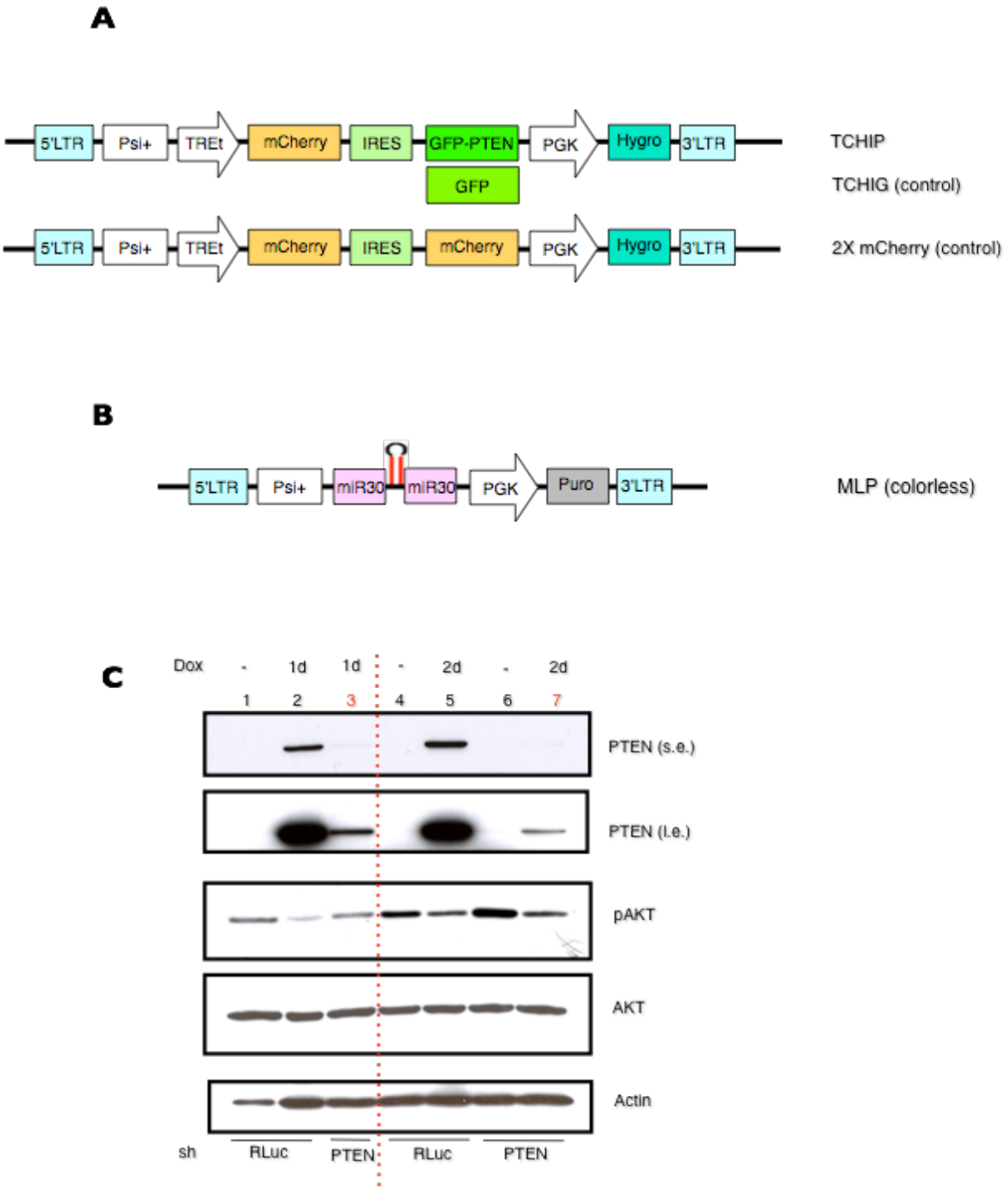

Supplemental figure 4.2 The reporter system-TCHIP. A. The maps of TCHIP and control constructs. B. The colorless retroviral construct for shRNA library. C. The PTEN knockdown is shown in shPTEN stable TCHIP

V. Conclusions and Future Perspectives

Mouse models have remarkably contributed to the understanding of the molecular and pathological features of prostate cancer initiation and progression. Especially, transgenic mouse models based on multiple genetic alterations can reveal unexpected mechanisms of prostate cancer initiation and disease progression. They can be used to validate new therapies as well. New cancer treatments mainly rely on testing in preclinical cancer models. However, significant obstacles have been evident in past and current preclinical mouse models. For instance, subcutaneously implanted tumor cell lines are known to grow much more rapidly than most human cancers; therefore, a transplanted tumor is generally more sensitive to most chemotherapy drugs, which target dividing cells and have easy access to the foreign cancer cells that are not naturally embedded. Moreover, the tumor harboring mice are treated with drug doses that cannot be applied to humans. In addition, contrary to the many Phase I and Phase II clinical trials where most of the patients have already failed other therapies at least once prior to a new therapeutic test, the cancer cells in most preclinical mouse models have not been similarly exposed and selected. These are among the major concerns and may be the reason why many clinical trials have failed in Phase I, II and III, even though the therapy had been successful in pre-clinical mouse models.

Success and problems with genetically engineered spontaneous cancer progression models

Based on the above, a more scientifically feasible pre-clinical trial approach is to use models with endogenous gene alterations that will eventually lead to spontaneous progression. These include some instances of prostate metastasis (Ding et al., 2011) that may better resemble human disease sthan a traditional xenograft model. In prostate cancer research, this approach has indeed been used to successfully derive therapies and signatures of aggressive disease (Carver et al., 2011; Ding et al., 2011). However, these spontaneous metastasis models tend to grow the primary tumor to unnatural sizes (filling the entire lower abdominal space). These tumors are also impacting surrounding tissues, leading to death through bladder obstruction. Such hindrances limit the most successful GEM prostate cancer models to analysis and therapy of tumor development, which can be tracked by MRI and ultrasound. In contrast, the rare instances of metastasis in these models cannot be readily detected by imaging modalities; therefore, they have not been used for pre-clinical trials on advanced disease. Another drawback of widespread

use for pre-clinical disease studies of the Probasin-Cre driven models lies in the complicated breeding scheme that would be required. Taken together, in spite of great advances in the understanding of tumor development, the above approach has only gained traction in the academic setting and is unfortunately not used by industry.

RapidCaP and pre-clinical trials

Due to the above limitations of germline conditional prostate knockout models, it has remained unclear if metastasis is not detected for a) technical, b) genetic or c) mouse-specific biological reasons. This ambiguity became obvious when analysis of human metastatic prostate cancer genomes revealed the critical role of *PTEN/Tp53* co-deletion, and thus suggested that the *PbCre*-conditional *Pten/ Trp53* double-null prostate, at least on paper, fulfilled the basic genetic requirements for metastasis, assuming that *Trp53*-loss after *Pten*-loss would present a natural bottleneck for spontaneous further tumor evolution (Chen et al., 2011).

The work presented in chapter 2 has addressed this discrepancy by showing that the genetic setting of *Pten/ Trp53*-loss is sufficient for metastasis (while *Pten*-loss and *Trp53* heterozygosity was not). Thus, the lack of metastasis in the germline model is unlikely due to mouse-specific or genetic deficiencies, but rather caused by technical differences between the RapidCaP and germline approaches. While the verdict is not yet out, it will be interesting to see which feature marks the difference to allow cells of the same genotype to metastasize early and frequently only in the RapidCaP model.

Another major insight afforded by the new model is that metastasis and changes in disease burden can be tracked by luciferase imaging. This is among the most beneficial aspects over the germline prostate models, and makes preclinical studies possible without dedicated, hi-tech imaging staff and technology. Standard of care methods, such as MRI, ultrasound and CT, are unfortunately still cost-inefficient and too complicated to conduct frequently for a bulky cohort, at least outside of a research hospital setting. Bioluminescence-based imaging technology greatly facilitates routine preclinical approaches. First, with live imaging, the researcher can easily identify experimental cohorts with disseminated disease (currently 56% at 4 months) for therapy studies. Moreover, these ‘future patients’ can be more closely monitored at little cost as

metastasis evolves further to create experimental baselines of progression. The RapidCaP animals can also be castrated to allow studying the biology of relapse and second/ third-lane therapy approaches. Most currently used GEM models for pre-clinical studies are ideal for first-line trials (Singh and Johnson, 2006). In contrast, our results show that first-line resistance is easily achieved in RapidCaP and a window for treatment with second- or third-line therapy clearly exists. This is critical, especially in prostate cancer, because first-line hormone ablation therapy is very consistently used in humans and invariably fails. Thus, studies to test if RapidCaP resistance biology indeed reflects changes in human are critical to establish it as a new platform for lethal prostate cancer therapy.

Detecting metastatic drivers in RapidCaP

While chapter 2 showed the potential for gaining new insights into prostate cancer metastasis, in chapter 3, we are addressing how RapidCaP can be used to find and validate genes of interest. Among these applications, the most intriguing result was observed when the three short hairpins targeting the known genes (*FOXP1, RYBP, SHQ1*) inside the common human chr. 3p14.1-p13 deletion of advanced metastatic prostate cancer (Taylor et al., 2010). This locus is commonly co-deleted with *PTEN* and *TP53,* and RapidCaP results suggested that the *Shq1* loss cooperates with deletion of the two tumor suppressors. Strikingly, independent analysis by the team of Dr. Charles Sawyers at MSKCC using renal capsule grafts of *Pten*-deficient mouse prostate cells infected with the Shq1 hairpin have confirmed this cooperation (C. Saywers/ P. Iaquinta, ongoing collaboration). If validated, by molecular pathology analysis of the metastatic lesions, these findings would suggest that RapidCaP could be used for high-throughput *in vivo* validation of candidate metastasis drivers.

Finally, the preliminary work on incorporation of fluorescent protein expression for enrichment and separation of mutant cells by FACS analysis suggests that several avenues can be taken to isolate mutant cells. In a proof-of-principle approach, whole genome copy number changes have been determined by bulk analysis and have revealed the common origin of primary and metastatic cells. Now, two general approaches can be further explored. The comparison of genomes from cells in different primary and metastatic loci will help elucidate the nature of disease progression and metastasis. On the other hand, comparison of primary and metastatic

genomes from treated/ relapsed animals with those of untreated animals will answer the important question of whether or not mouse resistance genetics are related to those observed in human.

Taken together, my work has introduced a novel approach for prostate cancer mouse modeling. The hallmarks of this system are speed, flexibility and metastasis.
This combination allowed me to improve the technology and study the biology at the same time.

During the investigation of prostatic metastasis on the molecular level, we found defined activation of Myc and absence of Akt activation in metastatic regions resulting from *Pten*/*Trp53* loss in RapidCaP. In subsequent trials to suppress Myc, the metastatic disease responded to JQ1 (collaboration with Jay Bradner and Chris Vakoc)(Filippakopoulos et al., 2010), a Brd4 inhibitor that epigenetically suppresses Myc transcription. This confirmed the significance of Myc activation in metastasis. Further analysis of the mechanism of Myc up-regulation will highlight traits of the metastatic disease. For example, it will be important to test if Myc activation with p53 loss will develop the same phenotype as *Pten*/*Trp53* null mice. This can be readily achieved by co-injecting the Myc and Cre viruses into *Trp53*$^{lox/lox}$ mice.

My results also showed that Myc might promote castration resistance. To test this hypothesis, Myc injected mice can be castrated to test if the disease in these mice still responds to castration. Furthermore, *Pten*/*Trp53* null mice with Myc overexpression are expected to be refractory to castration.

I also found that Shq1 plays an important role in metastasis progression. SHQ1 is an essential factor for H/ACA ribonucleoproteins (RNPs) required for ribosome biogenesis, pre-mRNA splicing, and telomere maintenance. Specifically, SHQ1 interacts with dyskerin/NAP57, the catalytic subunit of human H/ACA RNPs (Walbott et al., 2011). Importantly, dyskerin (Dkc1) has previously been linked to tumorigenesis (ruggero et al. 2003) and it will be interesting to see if SHQ1 cooperates with DKC1 in prostate cancer suppression. Intriguingly, studies in the lab of Dr. Charles Sawyers also confirmed the cooperation of Shq1 with Pten. We are now collaborating to publish these results.

Future optimization of the RapidCaP system

Despite extensive studies, we have not been able to identify extensive prostate

adenocarcinoma in *Pten*/*Trp53* null RapidCaP; however, prostatic metastasis was observed at high penetrance. This property is surprising and evident only in the RapidCaP system. In fact, it is actually the reverse of other prostate models, even those with identical genetic insults, where cancers are very large but metastasis is not found. This may be the consequence of focally engineered prostate cells having acquired enough genetic events to undergo dissemination, allowing spread of disease to occur even before the tumor has formed a large mass in the primary region. In addition, I found that RapidCaP-mediated loss of *Pten*/*Trp53* in prostate does not trigger the stromal expansion response, which in contrast, is always taking place in the genetically engineered Pten/p53 mouse models (Dawid Nowak, unpublished results). Thickened stroma, and also the observed sarcoma in the GEM model might act as a barrier against disseminating the disease from the primary cancer to secondary organs. This observation could thus explain why metastasis has not been found, precisely when large primary tumors are reported in the Probasin-Cre driven GEM models.

I would conclude here by stating that therefore, the RapidCaP model appears ideal for studying metastasis, rather than primary disease.

VI. Materials and Methods

Mice

Pten$^{loxp/loxp}$*; Trp53*$^{loxp/loxp}$, *Pten*$^{hy/+}$, *Pten*$^{loxp/loxp}$*; Trp53*$^{loxp/loxp}$ *; lsl-Tdtomato*, *Pten*$^{loxp/loxp}$*; Trp53*$^{loxp/loxp}$*; lsl-Luci* transgenic mice and C57BL/6 were used in this study. All protocols for mouse experiments were in accordance with institutional guidelines and were approved by the Institutional Animal Care and Use Committee (IACUC). *Pten*$^{loxp/loxp}$*; Trp53*$^{loxp/loxp}$ transgenic mice were generated by crossing *Pten*$^{loxp/loxp}$ with *Trp53*$^{loxp/loxp}$ (From Scott W. Lowe laboratory). For genotyping, tail DNA was subjected to polymerase chain reaction analysis with the following primers. For *Pten*$^{loxp/loxp}$, primer 1 (5′ -TGTTTTTGACCAATTAAAGTAGGCTGTG-3′) and primer 2 (5′ -AAAAGTTCCCCTGCTGATGATTTGT-3′) were used. For *Trp53*$^{loxp/loxp}$, primer 1 (5′ -CACAAAAACAGGTTAAACCCAG-3′) and primer 2 (5′ -AGCACATAGGAGGCAGAGA C-3′) were used. The homozygous reporter allele *Rosa-LSL-Tdtomato* (no. 007905) and *Rosa26-LSL-Luciferase* transgenic mice (FVB background, no. 005125) were obtained *via* Jackson Laboratories and crossed with *Pten*$^{loxp/loxp}$*; Trp53*$^{loxp/loxp}$ transgenic mice to generate triple *loxp* mice (*Pten*$^{loxp/loxp}$*; Trp53*$^{loxp/loxp}$ *; lslTdtomato*, *Pten*$^{loxp/loxp}$*; Trp53*$^{loxp/loxp}$ *; lslLuci)*.

Viral constructs

Lentiviral constructs - The Luc.Cre lentiviral plasmid (Taylor Jacks, Addgene plasmid 20905), pMD2.G and psPAX2 were purchased. The luciferase lentiviral plasmid was generated by eliminating CreNLS from above construct. Lentiviral Cre-Tomato construct was cloned by replacing luciferase with TdTomato from the Luc.Cre construct. Retroviral Myc-luciferase, shp53, shRLuc constructs were received from the Scott W. Lowe laboratory. For generating other short hairpin harboring retroviral constructs, 5 siRNAs were selected for each gene using the RNAi Codex algorithm and cloned to a retroviral GFP expressing construct (LMP)(Dickins, Hemann et al. 2005) for the further validation.

Retrovirus productions and infections

Retrovirus was produced by calcium phosphate transfection, $6X10^6$ phoenix cells were plated in 10 cm plates 6 to 12 hours prior to transfection with 15 μg of target construct and 5 μg of

ecotropic helper plasmid. Fresh media was added 12 hours after transfection and viral supernatant was collected four times at 24, 36, 48 and 60 hours post-transfection. Viral supernatant was filtered through a 0.45 μm filter, then supplemented with polybrene (4 μg/mL final concentration) for infection of target cells. Target cells (PC3, HeLa) were split 1:3 from confluent plates 12-24 hours prior to virus collection. To establish each reporter line, cells were treated with the antibiotics (puromycin, hygromycin and neomycin, Invitrogen) for selection. To establish reporter cell lines, PC3 cells were infected with RIEN virus to introduce rtTA and Ecotropic receptor, cells were then selected with neomycin (500 μg/ml). The second infection with each of three *PTEN* harboring target constructs (GPITCH, VPITCH and TCHIP) was conducted to the RIEN stable line (referred to as PC3E). Then the infected cells were selected with hygromycin (200 μg/ml). The Guava flow cytometer (Millipore, Billerica, MA) was used to determine the infection rate and expression level of GFP-PTEN. To measure the fluorescence ratio of GFP/mCherry, the LSRII flow cytometer (BD) was used. The each shRNA was transfected to packaging cells and generated virus was infected to the stable reporter line individually.

Lentivirus productions, infections and injections

Lentiviruses were produced by calcium phosphate transfection. 293T cells were plated for transfection density $8X10^6$ cells per 10 cm plate. 10 μg of target plasmid was combined with helper constructs, 8.5 μg of pMD2.G and 3.5 μg of psPAX2, for transfection. Lentiviruses were harvested at 24, 36, 48 and 60 h post-transfection and centrifuged (4500 rpm, 15 min) prior to filtering through 0.45-μm-pore cellulose acetate filters. Viral supernatant was concentrated by ultracentrifugation (2 h at 20,000 × *g*). For the viral injection to prostate, the filtered virus was concentrated by ultracentrifugation (2 hours at 50,000 x g), and then an *in vitro* infection test for each batch of virus was conducted in advance.

Intra-prostate injection

After exposure to anesthesia (Isoflurane, 2%), the lower half of the abdomen was shaved and mouse was placed in surgery hood. The mouse was constantly exposed to Isoflurane *via* a nose cone for the entire duration of the 10-minute surgery. The shaved region was cleaned with betadine followed by sterile PBS 3 times. A 0.5 inch long incision in both the skin and

peritoneum was made along the lower abdominal midline, 5 to 8 mm above the external genetalia. The right seminal vesicle was pulled out through incision and placed on sterile gauze in order to position the anterior prostate for injection. 30 µl of concentrated virus was taken up with 31G needle and bubbles were carefully removed from the syringe. Virus was injected to prostate, which inflates as virus is successfully injected. The seminal vesicle was then returned to the abdomen and repositioned. The incision in the peritoneum was then sutured with a size 4-0 suture. The skin was then stapled shut using 2 to 3 stainless steel EZ Clip wound closures. After animals were observed for complete recovery from anesthesia, they were warmed under a heating lamp to regain the ability to maintain sternal recumbence and given DietGel. The mice were then returned to their respective cages and to the biohazard mouse room.

Surgical castration

An anesthetized and surgically prepared animal was placed in dorsal recumbency. Both testes were then pushed down into the scrotal sacs by gently applying pressure to the abdomen. A 1-2 cm ventral midline incision was made in the scrotum and the skin was retracted to expose the tunica. The tunica was pierced and the testes were pushed out one at a time. The testes were then raised to expose the underlying blood vessels and tubules. The fat pad, which adheres to testis, was then grasped with blunt forceps to locate the vas deferens with the prominent blood vessel running along it. The testis is then dissected away from the fat pad and removed. The fat pad is then pushed back into the scrotal sac. All deferential vessels and ducts were replaced back into the tunica. Skin incisions were closed with stainless steel wound closures and removed 7-10 days post-operation.

Bioluminescence Imaging and Fluorescence Imaging

In vitro, in vivo and *ex vivo* Bioluminescence and fluorescence imaging was performed using an Xenogen IVIS Spectrum imager, which utilizes a highly sensitive, cooled CCD camera mounted in a light-tight camera box.

For *in vitro* imaging, MEFs (1X 10^5 cells/well) were seeded in 12-well plate and infected with serial volume of virus. At 24 hrs post infection, the medium was replaced with fresh medium and infection efficiency was measured by bioluminescence imaging 5 days post infection. For *in vitro* imaging, luciferin (D-luciferin, Potassium Salt, Gold Biotechnology) was added to each

well at 150 mg/ml of final concentration in PBS and photons were collected for 3 min. For *in vivo* imaging, animals received luciferin at 200 mg/kg by intra-peritoneal injection 5 min prior to imaging. The animals were then anesthetized using 2% isoflurane and placed onto the warmed stage inside the camera box. The animals received continuous exposure to 2% isoflurane to sustain sedation for 3 min of imaging. For the quantification, regions of interest (ROI) were measured with standardized rectangular regions covering the mouse trunk and extremities. The measured signal was quantified as photons/second (ph/sec) using the Living Image software v.4.2 (Xenogen). Background bioluminescence *in vivo* was in the range 3~6X10^4 ph/sec.
For *ex vivo* imaging, animals were humanely euthanized, tissues of interest excised, and placed individually on paraffin film and imaged for 3 min after 3 mg of D-luciferin (200 ul of 15 mg/ml in PBS) were dropped in each organ. Tissues were subsequently fixed in 10% neutral-buffered formalin (Sigma) overnight and prepared for standard histopathology evaluation.

Dissociation of cells from tissue

For flow cytometry analysis, isolated mouse tissues were minced with a sterile scalpel and washed 3 times with Hanks' Balanced Salt Solution (HBSS). Then collagenase was added at 100 units/ml and tissues were incubated at 37 °C for 4 hours. The cell suspension was filtered through a sterile mesh to separate the dispersed cells and tissue fragments from the larger pieces. The cell suspension was then washed 3 times with HBSS.

PCR analysis to confirm injection

PCR analysis of Cre-mediated recombination in *Pten$^{loxp/loxp}$; Trp53$^{loxp/loxp}$* transgenic mice was performed on genomic DNA extracted from Cre virus injected or non-injected prostates. For *Pten* recombination, primer 2 (5′ -AAAAGTTCCCCTGCTGATGATTTGT-3′) and primer 3 (5′ -CCCCCAAGTCAATTGTTAGGTCTGT-3′)(Trotman et al., 2003) were used. For *Trp53* recombination, primer 1 (5′ -CACAAAAACAGGTTAAACCCAG-3′) and primer 3 (5′ -GAAG ACAGAAAAGGGGAGGG-3′)(Marino et al., 2000) were used. For detecting luciferase, primer 1 (5′ -GAGGTTCCATCTGCCAGGTA-3′) and primer 2 (5′ -CACACAGTTCGCCTCTT TGA-3′) were used.

Histology and Immunohistochemistry analysis

Tissues were fixed in 10% buffered formalin for 24 hrs, followed by gentle wash and transfer to PBS. Then, paraffin-embedded tissues were sectioned 6 μm thick, placed on charged glass slides and stained with hematoxylin & eosin, or the appropriate immunohistochemical stains.

Antigen retrieval was performed by incubating the slides in 0.01 M citric acid buffer (pH 6.0) at 95°C for 15 min. Slides were then allowed to cool to room temperature for 20 min in a citric acid buffer. After washing with deionized water, the slides were transferred to TBS (pH 7.4) for 5 min. The following detection and visualization procedures were performed according to manufacturer's protocol. Slides were counterstained in Mayer's hematoxylin, dehydrated, cleared, and cover slipped. Negative control slides were run without primary antibody. Control slides known to be positive for each antibody were incorporated.

For androgen receptor (AR;D6F11, 1:500, Cell Signaling) and cytokeratin 8 (CK8; EP1628Y, 1:250, Novus Biologicals), cytokeratin 5 (CK5; AF138; 1:4000; Covance), luciferase (NB100-1677; 1:500; Novus Biologicals), pAKT(S473) (D9E; 1:50; Cell Signaling), pAKT(Thr308) (9275; 1:100; Cell Signaling), PTEN (138G6; 1:50; Cell Signaling), Pan-CK (sc-15367; 1:1000; Santa Cruz Biotechnology), Ki67(VP-K452; 1:2000; Vector Laboratories) , cMyc (1472-1; 1:50; Epitomics), CD3 (ab5690; 1:1000; Abcam) staining, pretreated sections were first blocked with 5% normal horse serum and 1% BSA (in TBS) for 1 hour at room temperature. Then the primary antibodies were diluted, as suggested by the manufacturer, and incubated overnight at 4°C. Following three 10 min. washes with TBS, sections were incubated with biotinylated secondary antibody for 30 min. at room temperature and rinsed with TBS three times for 10 min. Finally, the sections were treated with diaminobenzidine for 3 min and rinsed with distilled water to end the reaction, mounted on gelatin-coated slides, air-dried, dehydrated with 70%–100% alcohol, cleared with xylene and cover-slipped for microscopic observation. After examination of all immunohistochemical and special stains, stained slides were digitally scanned using the Aperio ScanScope software (Vista, California).

Double immunofluorescence staining was done with rabbit monoclonal cytokeratin 8 (CK8; EP1628Y, 1:250, Novus Biologicals) and mouse monoclonal PTEN antibody (138G6; 1:50, Cell Signaling), followed by incubation with Alexa Fluor 488 donkey anti-rabbit (1:500, Life

Technologies) and Alexa Fluor 546 goat anti-mouse (1:500, Life Technologies) antibodies for 1 hour at room temperature for visualization. To stain cell nuclei, sections were incubated with a 10 μg/mL solution of 4',6-diamidino-2-phenylindole (DAPI) for 1 hour at room temperature. Sections were rinsed in TBS and distilled water serially, and finally mounted with Mounting Medium (H-1000, Vector Laboratories, Burlingame, CA). Stained slides were imaged and analyzed using both the Ultraview VoX Spinning disk confocal microscope (PerkinElmer) and the Aperio ScanScope software (Vista, California).

Doxycycline treatment

Doxycycline-contained media was prepared at concentration of 1 μg/ml (Sigma-Aldrich, St. Louis, MO).

Adenoviral Cre

Adenoviral Cre virus was purchased commercially from the Gene Transfer Vector Core of the University of Iowa. For *in vitro* infection, 3 μl of adeno-Cre was added to MEFs ($2X10^5$) at a dose of 10^9 pfu for 24 hrs.

Building HeLa shRNA stable lines for pilot screening

Each shRNA stable HeLa line was established by infecting with pooled shRNA harboring lentivirus (2-8 shRNA/each gene) (Table. 4.1). Lentiviruses were produced by calcium phosphate transfection, and 293T cells were plated for transfection density $8X10^6$ cells per 10 cm plate. 10 μg target plasmid was combined with helper constructs, 8.5 μg of pMD2.G and 3.5 μg of psPAX2 for transfection. Lentiviruses were harvested at 24, 36, 48 and 60 h post-transfection and filtered through 0.45-μm-pore cellulose acetate filters prior to infection. shRNA-infected HeLa cells were selected with exposure to puromycin (2 μg/ml) for 2 days.

Immunoprecipitation

Immunoprecipitations were carried out by scraping cells off a 10 cm dish with lysis buffer (1% Triton X-100, 1% Na-Deoxycholate in PBS, containing PMSF, Leupeptin, Aprotinin, Pepstatin protease inhibitors and phosphatase inhibitors, Calbiochem set I) and brief sonication at 4 °C. The cell lysates were collected after centrifugation at 13,000 rpm for 30 min at 4 °C and then the

supernatants were pre-cleared with Protein-G Sepharose beads (Amersham) for 1 hr. Polyclonal rabbit anti-Ub antibody was added for 4 hour incubation at 4 °C, followed by Protein-G Sepharose co-precipitation and 3 consecutive washes.

Western Blotting

For Western blotting analysis, cells were treated as indicated and total lysates were produced by addition of modified RIPA buffer (20 mM Tris pH7.5, 100mM NaCl, 1 mM EDTA, 0.1% NP-40, 0.1% SDS with fresh β-mercaptoethanol). Protein concentration was determined using the Bio-rad DC Protein Assay. 50 μg per sample were subjected to SDS-Polyacrylamide Gel electrophoresis (SDS-PAGE) and transferred to a nylon membrane. The following antibodies were used for further immunoblotting: Rabbit polyclonal antibodies used were: pAKT (Ser 473)(Cell Signaling, #9271), AKT (Cell Signaling, #9272), anti-ubiquitin (Cell Signaling, #3933). Monoclonal antibodies were: anti-PTEN (Cascade Biosciences 6H2.1, #ABM2052), anti-GFP (Clonech, #632381), anti-mCherry (Clontech, #632543), anti-α-Tubulin (Sigma, #T5168), anti-β Actin (Sigma, #A5316). Detection was performed using horseradish peroxidise-conjugated anti-rabbit-IgG (NA943V; GE Healthcare) and anti-mouse-IgG (NA931V; GE Healthcare) secondary antibodies with ECL Plus detection reagent and ECL-Hyperfilm (GE Healthcare). The density of bands was quantified by ImageJ software. For protein stability, cells were treated with 30 μg/ml cycloheximide for the designated amount of time.

RNA Extraction, Reverse Transcription, and Quantitative Polymerase Chain Reaction (RT-qPCR)

Total RNA was extracted from cell lines and tissue samples using the RNeasy kit (Qiagen) (follow the manufacturer's instruction). 2 μg of RNA were used for first strand synthesis and production of cDNA using random primer and SuperScript II (Invitrogen). RNA expression was measured by real-time quantitative reverse transcription-PCR, using the Roche LightCycler 480 (Roche Applied Science) based on the SYBR Green method. Each assay was done in triplicate and the expression of each gene was calculated relative to expression of β-actin. Quantification was based on a standard curve obtained by serial dilution of the indicated control RT reaction. Primer sequences are reported in Table 4.2.

shRNA library production

BIOPREDsi small interfering RNA predictions were used to design siRNA sequences. 125-bp oligonucleotides encompassing the whole stem-loop miR-30 shRNA precursor, flanked by EcoRI and XhoI cloning sites were ordered from Agilent (Santa Clara, CA) and amplified with a library-specific reverse primer (for the priority set : CTCAGCTGCTGTCTAAGGCACAGG) and a common forward primer (miRXhoF : TACAATACTCGAGAAGGTATATTGCTGTTG ACAGTGAGCG). Pooled cloning was conducted with the Platinum Pfx kit (Invitrogen) using the following conditions: a 50 µl reaction containing 0.05 ng oligonucleotide template, 1× Pfx buffer, 1 mM $MgSO_4$, 0.3 mM of each dNTP, 0.8 µM of each primer, and 1.25 U Pfx polymerase; cycling: 94 °C for 2 min; 33 cycles of 94 °C for 15 s; 54 °C for 30 s and 68 °C for 25 s; 68 °C for 5 min. To avoid the introduction of oligonucleotides with synthesis errors such as mutations introduced during PCR amplification steps or concatamerization of inserts during vector ligation, each unique shRNA vector was verified by sequencing before inclusion in the resulting library. Clones were mini prepped and sequenced in 96-well format.

VII. References

Abate-Shen, C., and Shen, M.M. (2002). Mouse models of prostate carcinogenesis. Trends Genet *18*, S1-5.

Abdulkadir, S.A., Magee, J.A., Peters, T.J., Kaleem, Z., Naughton, C.K., Humphrey, P.A., and Milbrandt, J. (2002). Conditional loss of Nkx3.1 in adult mice induces prostatic intraepithelial neoplasia. Mol Cell Biol *22*, 1495-1503.

Adams, J. (1853). The case of scirrhous of the prostate gland with corresponding affliction of the lymphatic glands in the lumbar region and in the pelvis. . Lancet, 1.

Adams, J., and Kauffman, M. (2004). Development of the proteasome inhibitor Velcade (Bortezomib). Cancer Invest *22*, 304-311.

Alimonti, A., Carracedo, A., Clohessy, J.G., Trotman, L.C., Nardella, C., Egia, A., Salmena, L., Sampieri, K., Haveman, W.J., Brogi, E., *et al*. (2010). Subtle variations in Pten dose determine cancer susceptibility. Nat Genet *42*, 454-458.

Alvarez-Cubero, M.J., Saiz, M., Martinez-Gonzalez, L.J., Alvarez, J.C., Lorente, J.A., and Cozar, J.M. (2012). Genetic analysis of the principal genes related to prostate cancer: A review. Urologic oncology.

Amerik, A.Y., and Hochstrasser, M. (2004). Mechanism and function of deubiquitinating enzymes. Biochim Biophys Acta *1695*, 189-207.

Amodio, N., Scrima, M., Palaia, L., Salman, A.N., Quintiero, A., Franco, R., Botti, G., Pirozzi, P., Rocco, G., De Rosa, N., *et al*. (2010). Oncogenic role of the E3 ubiquitin ligase NEDD4-1, a PTEN negative regulator, in non-small-cell lung carcinomas. The American journal of pathology *177*, 2622-2634.

Anan, T., Nagata, Y., Koga, H., Honda, Y., Yabuki, N., Miyamoto, C., Kuwano, A., Matsuda, I., Endo, F., Saya, H., *et al*. (1998). Human ubiquitin-protein ligase Nedd4: expression, subcellular localization and selective interaction with ubiquitin-conjugating enzymes. Genes Cells *3*, 751-763.

Aus, G., Damber, J.E., Khatami, A., Lilja, H., Stranne, J., and Hugosson, J. (2005). Individualized screening interval for prostate cancer based on prostate-specific antigen level: results of a prospective, randomized, population-based study. Arch Intern Med *165*, 1857-1861.

Baca, S.C., Prandi, D., Lawrence, M.S., Mosquera, J.M., Romanel, A., Drier, Y., Park, K., Kitabayashi, N., Macdonald, T.Y., Ghandi, M., *et al*. (2013). Punctuated evolution of prostate cancer genomes. Cell *153*, 666-677.

Banez, L.L., Hamilton, R.J., Partin, A.W., Vollmer, R.T., Sun, L., Rodriguez, C., Wang, Y., Terris, M.K., Aronson, W.J., Presti, J.C., Jr., *et al*. (2007). Obesity-related plasma hemodilution and PSA concentration among men with prostate cancer. Jama *298*, 2275-2280.

Becher, O.J., and Holland, E.C. (2006). Genetically engineered models have advantages over xenografts for preclinical studies. Cancer Res *66*, 3355-3358, discussion 3358-3359.

Bhatia-Gaur, R., Donjacour, A.A., Sciavolino, P.J., Kim, M., Desai, N., Young, P., Norton, C.R., Gridley, T., Cardiff, R.D., Cunha, G.R., *et al*. (1999). Roles for Nkx3.1 in prostate development and cancer. Genes Dev *13*, 966-977.

Bookstein, R., Rio, P., Madreperla, S.A., Hong, F., Allred, C., Grizzle, W.E., and Lee, W.H. (1990). Promoter deletion and loss of retinoblastoma gene expression in human prostate carcinoma. Proc Natl Acad Sci U S A *87*, 7762-7766.

Borno, S.T., Fischer, A., Kerick, M., Falth, M., Laible, M., Brase, J.C., Kuner, R., Dahl, A., Grimm, C., Sayanjali, B., *et al*. (2012). Genome-wide DNA methylation events in TMPRSS2-ERG fusion-negative prostate cancers implicate an EZH2-dependent mechanism with miR-26a hypermethylation. Cancer discovery *2*, 1024-1035.

Bosma, M.J., and Carroll, A.M. (1991). The SCID mouse mutant: definition, characterization, and potential uses. Annu Rev Immunol *9*, 323-350.

Brooke, G.N., and Bevan, C.L. (2009). The role of androgen receptor mutations in prostate cancer progression. Curr Genomics *10*, 18-25.

Brooks, C.L., and Gu, W. (2003). Ubiquitination, phosphorylation and acetylation: the molecular basis for p53 regulation. Curr Opin Cell Biol *15*, 164-171.

Brooks, J.D., Bova, G.S., and Isaacs, W.B. (1995). Allelic loss of the retinoblastoma gene in primary human prostatic adenocarcinomas. Prostate *26*, 35-39.

Bubendorf, L., Schopfer, A., Wagner, U., Sauter, G., Moch, H., Willi, N., Gasser, T.C., and Mihatsch, M.J. (2000). Metastatic patterns of prostate cancer: an autopsy study of 1,589 patients. Hum Pathol *31*, 578-583.

Buijs, J.T., and van der Pluijm, G. (2009). Osteotropic cancers: from primary tumor to bone. Cancer Lett *273*, 177-193.

Cai, C., Wang, H., Xu, Y., Chen, S., and Balk, S.P. (2009). Reactivation of androgen receptor-regulated TMPRSS2:ERG gene expression in castration-resistant prostate cancer. Cancer Res *69*, 6027-6032.

Calvo, A., Perez-Stable, C., Segura, V., Catena, R., Guruceaga, E., Nguewa, P., Blanco, D., Parada, L., Reiner, T., and Green, J.E. (2010). Molecular characterization of the Ggamma-globin-Tag transgenic mouse model of hormone refractory prostate cancer: comparison to human prostate cancer. Prostate *70*, 630-645.

Cao, X., Shores, E.W., Hu-Li, J., Anver, M.R., Kelsall, B.L., Russell, S.M., Drago, J., Noguchi, M., Grinberg, A., Bloom, E.T., *et al*. (1995). Defective lymphoid development in mice lacking expression of the common cytokine receptor gamma chain. Immunity *2*, 223-238.

Capecchi, M.R. (1989). Altering the genome by homologous recombination. Science *244*, 1288-1292.

Carpten, J., Nupponen, N., Isaacs, S., Sood, R., Robbins, C., Xu, J., Faruque, M., Moses, T., Ewing, C., Gillanders, E., *et al*. (2002). Germline mutations in the ribonuclease L gene in families showing linkage with HPC1. Nature genetics *30*, 181-184.

Carrano, A.C., Eytan, E., Hershko, A., and Pagano, M. (1999). SKP2 is required for ubiquitin-mediated degradation of the CDK inhibitor p27. Nat Cell Biol *1*, 193-199.

Carver, B.S., Chapinski, C., Wongvipat, J., Hieronymus, H., Chen, Y., Chandarlapaty, S., Arora, V.K., Le, C., Koutcher, J., Scher, H., *et al*. (2011). Reciprocal feedback regulation of PI3K and androgen receptor signaling in PTEN-deficient prostate cancer. Cancer Cell *19*, 575-586.

Carver, B.S., Tran, J., Gopalan, A., Chen, Z., Shaikh, S., Carracedo, A., Alimonti, A., Nardella, C., Varmeh, S., Scardino, P.T., *et al*. (2009). Aberrant ERG expression cooperates with loss of PTEN to promote cancer progression in the prostate. Nat Genet *41*, 619-624.

Casey, G., Neville, P.J., Plummer, S.J., Xiang, Y., Krumroy, L.M., Klein, E.A., Catalona, W.J., Nupponen, N., Carpten, J.D., Trent, J.M., *et al*. (2002). RNASEL Arg462Gln variant is implicated in up to 13% of prostate cancer cases. Nat Genet *32*, 581-583.

Cavo, M. (2006). Proteasome inhibitor bortezomib for the treatment of multiple myeloma. Leukemia *20*, 1341-1352.

Chada, K., Magram, J., and Costantini, F. (1986). An embryonic pattern of expression of a human fetal globin gene in transgenic mice. Nature *319*, 685-689.

Chambers, A.F., Groom, A.C., and MacDonald, I.C. (2002). Dissemination and growth of cancer cells in metastatic sites. Nat Rev Cancer *2*, 563-572.

Chauhan, D., Li, G., Shringarpure, R., Podar, K., Ohtake, Y., Hideshima, T., and Anderson, K.C. (2003). Blockade of Hsp27 overcomes Bortezomib/proteasome inhibitor PS-341 resistance in lymphoma cells. Cancer Res *63*, 6174-6177.

Chen, C.D., Welsbie, D.S., Tran, C., Baek, S.H., Chen, R., Vessella, R., Rosenfeld, M.G., and Sawyers, C.L. (2004). Molecular determinants of resistance to antiandrogen therapy. Nature medicine *10*, 33-39.

Chen, H., Nandi, A.K., Li, X., and Bieberich, C.J. (2002). NKX-3.1 interacts with prostate-derived Ets factor and regulates the activity of the PSA promoter. Cancer Res *62*, 338-340.

Chen, M., Pratt, C.P., Zeeman, M.E., Schultz, N., Taylor, B.S., O'Neill, A., Castillo-Martin, M., Nowak, D.G., Naguib, A., Grace, D.M., *et al*. (2011). Identification of PHLPP1 as a tumor suppressor reveals the role of feedback activation in PTEN-mutant prostate cancer progression. Cancer Cell *20*, 173-186.

Chen, Y., Sawyers, C.L., and Scher, H.I. (2008). Targeting the androgen receptor pathway in prostate cancer. Curr Opin Pharmacol *8*, 440-448.

Chen, Z., Trotman, L.C., Shaffer, D., Lin, H.K., Dotan, Z.A., Niki, M., Koutcher, J.A., Scher, H.I., Ludwig, T., Gerald, W., *et al*. (2005). Crucial role of p53-dependent cellular senescence in suppression of Pten-deficient tumorigenesis. Nature *436*, 725-730.

Chen, Z.J., and Sun, L.J. (2009). Nonproteolytic Functions of Ubiquitin in Cell Signaling. Mol Cell *33*, 275-286.

Chiaverotti, T., Couto, S.S., Donjacour, A., Mao, J.H., Nagase, H., Cardiff, R.D., Cunha, G.R., and Balmain, A. (2008). Dissociation of epithelial and neuroendocrine carcinoma lineages in the transgenic adenocarcinoma of mouse prostate model of prostate cancer. Am J Pathol *172*, 236-246.

Cordon-Cardo, C., Koff, A., Drobnjak, M., Capodieci, P., Osman, I., Millard, S.S., Gaudin, P.B., Fazzari, M., Zhang, Z.F., Massague, J., *et al*. (1998). Distinct altered patterns of p27KIP1 gene expression in benign prostatic hyperplasia and prostatic carcinoma. J Natl Cancer Inst *90*, 1284-1291.

Craft, N., Shostak, Y., Carey, M., and Sawyers, C.L. (1999). A mechanism for hormone-independent prostate cancer through modulation of androgen receptor signaling by the HER-2/neu tyrosine kinase. Nat Med *5*, 280-285.

de Bono, J.S., Logothetis, C.J., Molina, A., Fizazi, K., North, S., Chu, L., Chi, K.N., Jones, R.J., Goodman, O.B., Jr., Saad, F., *et al*. (2011). Abiraterone and increased survival in metastatic prostate cancer. N Engl J Med *364*, 1995-2005.

de Jong, M., and Maina, T. (2010). Of mice and humans: are they the same?--Implications in cancer translational research. J Nucl Med *51*, 501-504.

Deliolanis, N.C., Kasmieh, R., Wurdinger, T., Tannous, B.A., Shah, K., and Ntziachristos, V. (2008). Performance of the red-shifted fluorescent proteins in deep-tissue molecular imaging applications. J Biomed Opt *13*, 044008.

Di Cristofano, A., De Acetis, M., Koff, A., Cordon-Cardo, C., and Pandolfi, P.P. (2001). Pten and p27KIP1 cooperate in prostate cancer tumor suppression in the mouse. Nat Genet *27*, 222-224.

Di Cristofano, A., Pesce, B., Cordon-Cardo, C., and Pandolfi, P.P. (1998). Pten is essential for embryonic development and tumour suppression. Nat Genet *19*, 348-355.

DiAntonio, A. (2010). Nedd4 branches out. Neuron *65*, 293-294.

Ding, Z., Wu, C.J., Chu, G.C., Xiao, Y., Ho, D., Zhang, J., Perry, S.R., Labrot, E.S., Wu, X., Lis, R., *et al*. (2011). SMAD4-dependent barrier constrains prostate cancer growth and metastatic progression. Nature *470*, 269-273.

Dong, J.T. (2006). Prevalent mutations in prostate cancer. Journal of cellular biochemistry *97*, 433-447.

Dow, L.E., Premsrirut, P.K., Zuber, J., Fellmann, C., McJunkin, K., Miething, C., Park, Y., Dickins, R.A., Hannon, G.J., and Lowe, S.W. (2012). A pipeline for the generation of shRNA transgenic mice. Nat Protoc *7*, 374-393.

Egevad, L., Granfors, T., Karlberg, L., Bergh, A., and Stattin, P. (2002). Prognostic value of the Gleason score in prostate cancer. BJU Int *89*, 538-542.

Ellwood-Yen, K., Graeber, T.G., Wongvipat, J., Iruela-Arispe, M.L., Zhang, J., Matusik, R., Thomas, G.V., and Sawyers, C.L. (2003). Myc-driven murine prostate cancer shares molecular features with human prostate tumors. Cancer Cell *4*, 223-238.

Ellwood-Yen, K., Wongvipat, J., and Sawyers, C. (2006). Transgenic mouse model for rapid pharmacodynamic evaluation of antiandrogens. Cancer Res *66*, 10513-10516.
Elo, J.P., and Visakorpi, T. (2001). Molecular genetics of prostate cancer. Ann Med *33*, 130-141.
Emmert-Buck, M.R., Vocke, C.D., Pozzatti, R.O., Duray, P.H., Jennings, S.B., Florence, C.D., Zhuang, Z., Bostwick, D.G., Liotta, L.A., and Linehan, W.M. (1995). Allelic loss on chromosome 8p12-21 in microdissected prostatic intraepithelial neoplasia. Cancer Res *55*, 2959-2962.
Eshhar, Z., Waks, T., and Pinthus, J. (2005). Redirecting immune cells against bone metastases: Immunotherapy of prostate cancer metastases using genetically programmed immune effector cells. Discov Med *5*, 259-264.
Eyles, J., Puaux, A.L., Wang, X., Toh, B., Prakash, C., Hong, M., Tan, T.G., Zheng, L., Ong, L.C., Jin, Y., *et al*. (2010). Tumor cells disseminate early, but immunosurveillance limits metastatic outgrowth, in a mouse model of melanoma. The Journal of clinical investigation *120*, 2030-2039.
Fouladkou, F., Landry, T., Kawabe, H., Neeb, A., Lu, C., Brose, N., Stambolic, V., and Rotin, D. (2008). The ubiquitin ligase Nedd4-1 is dispensable for the regulation of PTEN stability and localization. Proc Natl Acad Sci U S A *105*, 8585-8590.
Freeman, D.J., Li, A.G., Wei, G., Li, H.H., Kertesz, N., Lesche, R., Whale, A.D., Martinez-Diaz, H., Rozengurt, N., Cardiff, R.D., *et al*. (2003). PTEN tumor suppressor regulates p53 protein levels and activity through phosphatase-dependent and -independent mechanisms. Cancer Cell *3*, 117-130.
Frese, K.K., and Tuveson, D.A. (2007). Maximizing mouse cancer models. Nat Rev Cancer *7*, 645-658.
Gann, P.H., Hennekens, C.H., and Stampfer, M.J. (1995). A prospective evaluation of plasma prostate-specific antigen for detection of prostatic cancer. Jama *273*, 289-294.
Garabedian, E.M., Humphrey, P.A., and Gordon, J.I. (1998). A transgenic mouse model of metastatic prostate cancer originating from neuroendocrine cells. Proc Natl Acad Sci U S A *95*, 15382-15387.
Gleason, D.F., and Mellinger, G.T. (1974). Prediction of prognosis for prostatic adenocarcinoma by combined histological grading and clinical staging. J Urol *111*, 58-64.

Gottlieb, B., Beitel, L.K., Wu, J.H., and Trifiro, M. (2004). The androgen receptor gene mutations database (ARDB): 2004 update. Human mutation *23*, 527-533.

Gottschalk, A.R., Basila, D., Wong, M., Dean, N.M., Brandts, C.H., Stokoe, D., and Haas-Kogan, D.A. (2001). p27Kip1 is required for PTEN-induced G1 growth arrest. Cancer Res *61*, 2105-2111.

Greenberg, N.M., DeMayo, F., Finegold, M.J., Medina, D., Tilley, W.D., Aspinall, J.O., Cunha, G.R., Donjacour, A.A., Matusik, R.J., and Rosen, J.M. (1995). Prostate cancer in a transgenic mouse. Proc Natl Acad Sci U S A *92*, 3439-3443.

Greenlee, R.T., Hill-Harmon, M.B., Murray, T., and Thun, M. (2001). Cancer statistics, 2001. CA Cancer J Clin *51*, 15-36.

Greenlee, R.T., Murray, T., Bolden, S., and Wingo, P.A. (2000). Cancer statistics, 2000. CA Cancer J Clin *50*, 7-33.

Greiner, D.L., Shultz, L.D., Yates, J., Appel, M.C., Perdrizet, G., Hesselton, R.M., Schweitzer, I., Beamer, W.G., Shultz, K.L., Pelsue, S.C., *et al*. (1995). Improved engraftment of human spleen cells in NOD/LtSz-scid/scid mice as compared with C.B-17-scid/scid mice. Am J Pathol *146*, 888-902.

Gstaiger, M., Jordan, R., Lim, M., Catzavelos, C., Mestan, J., Slingerland, J., and Krek, W. (2001). Skp2 is oncogenic and overexpressed in human cancers. Proc Natl Acad Sci U S A *98*, 5043-5048.

Gumerlock, P.H., Poonamallee, U.R., Meyers, F.J., and deVere White, R.W. (1991). Activated ras alleles in human carcinoma of the prostate are rare. Cancer Res *51*, 1632-1637.

Guo, Y., Sklar, G.N., Borkowski, A., and Kyprianou, N. (1997). Loss of the cyclin-dependent kinase inhibitor p27(Kip1) protein in human prostate cancer correlates with tumor grade. Clin Cancer Res *3*, 2269-2274.

Hawksworth, D., Ravindranath, L., Chen, Y., Furusato, B., Sesterhenn, I.A., McLeod, D.G., Srivastava, S., and Petrovics, G. (2010). Overexpression of C-MYC oncogene in prostate cancer predicts biochemical recurrence. Prostate Cancer Prostatic Dis *13*, 311-315.

Hershko, A., and Ciechanover, A. (1998). The ubiquitin system. Annu Rev Biochem *67*, 425-479.

Hoehn, W., Schroeder, F.H., Reimann, J.F., Joebsis, A.C., and Hermanek, P. (1980). Human prostatic adenocarcinoma: some characteristics of a serially transplantable line in nude mice (PC 82). Prostate *1*, 95-104.

Hough, R., Pratt, G., and Rechsteiner, M. (1986). Ubiquitin-lysozyme conjugates. Identification and characterization of an ATP-dependent protease from rabbit reticulocyte lysates. J Biol Chem *261*, 2400-2408.

Hsieh, C.L., Xie, Z., Liu, Z.Y., Green, J.E., Martin, W.D., Datta, M.W., Yeung, F., Pan, D., and Chung, L.W. (2005). A luciferase transgenic mouse model: visualization of prostate development and its androgen responsiveness in live animals. J Mol Endocrinol *35*, 293-304.

Hu, Y., Ippolito, J.E., Garabedian, E.M., Humphrey, P.A., and Gordon, J.I. (2002). Molecular characterization of a metastatic neuroendocrine cell cancer arising in the prostates of transgenic mice. J Biol Chem *277*, 44462-44474.

Huggins, C., and Hodges, C.V. (1972). Studies on prostatic cancer. I. The effect of castration, of estrogen and androgen injection on serum phosphatases in metastatic carcinoma of the prostate. CA Cancer J Clin *22*, 232-240.

Huggins, C., Stevens, R.C., Hodges, C.V. (1941). STUDIES ON PROSTATIC CANCER: II. THE EFFECTS OF CASTRATION ON ADVANCED CARCINOMA OF THE PROSTATE GLAND. Arch Surg *43*, 209-223.

Ingles, S.A., Haile, R.W., Henderson, B.E., Kolonel, L.N., Nakaichi, G., Shi, C.Y., Yu, M.C., Ross, R.K., and Coetzee, G.A. (1997). Strength of linkage disequilibrium between two vitamin D receptor markers in five ethnic groups: implications for association studies. Cancer epidemiology, biomarkers & prevention : a publication of the American Association for Cancer Research, cosponsored by the American Society of Preventive Oncology *6*, 93-98.

Ittmann, M., Huang, J., Radaelli, E., Martin, P., Signoretti, S., Sullivan, R., Simons, B.W., Ward, J.M., Robinson, B.D., Chu, G.C., *et al*. (2013). Animal models of human prostate cancer: the consensus report of the New York meeting of the Mouse Models of Human Cancers Consortium Prostate Pathology Committee. Cancer Res *73*, 2718-2736.

Jemal, A., Murray, T., Samuels, A., Ghafoor, A., Ward, E., and Thun, M.J. (2003). Cancer statistics, 2003. CA Cancer J Clin *53*, 5-26.

Jenkins, R.B., Qian, J., Lieber, M.M., and Bostwick, D.G. (1997). Detection of c-myc oncogene amplification and chromosomal anomalies in metastatic prostatic carcinoma by fluorescence in situ hybridization. Cancer Res *57*, 524-531.

Kallioniemi, A., Visakorpi, T., Karhu, R., Pinkel, D., and Kallioniemi, O.P. (1996). Gene Copy Number Analysis by Fluorescence in Situ Hybridization and Comparative Genomic Hybridization. Methods *9*, 113-121.

Kerr, I.M., and Brown, R.E. (1978). pppA2'p5'A2'p5'A: an inhibitor of protein synthesis synthesized with an enzyme fraction from interferon-treated cells. Proc Natl Acad Sci U S A *75*, 256-260.

Kim, J., Roh, M., Doubinskaia, I., Algarroba, G.N., Eltoum, I.E., and Abdulkadir, S.A. (2012). A mouse model of heterogeneous, c-MYC-initiated prostate cancer with loss of Pten and p53. Oncogene *31*, 322-332.

Kim, S.S., Yoo, N.J., Jeong, E.G., Kim, M.S., and Lee, S.H. (2008). Expression of NEDD4-1, a PTEN regulator, in gastric and colorectal carcinomas. Apmis *116*, 779-784.

King, J.C., Xu, J., Wongvipat, J., Hieronymus, H., Carver, B.S., Leung, D.H., Taylor, B.S., Sander, C., Cardiff, R.D., Couto, S.S., *et al*. (2009). Cooperativity of TMPRSS2-ERG with PI3-kinase pathway activation in prostate oncogenesis. Nat Genet *41*, 524-526.

Klezovitch, O., Chevillet, J., Mirosevich, J., Roberts, R.L., Matusik, R.J., and Vasioukhin, V. (2004). Hepsin promotes prostate cancer progression and metastasis. Cancer Cell *6*, 185-195.

Klezovitch, O., Risk, M., Coleman, I., Lucas, J.M., Null, M., True, L.D., Nelson, P.S., and Vasioukhin, V. (2008). A causal role for ERG in neoplastic transformation of prostate epithelium. Proc Natl Acad Sci U S A *105*, 2105-2110.

Knudson, A.G., Jr. (1971). Mutation and cancer: statistical study of retinoblastoma. Proceedings of the National Academy of Sciences of the United States of America *68*, 820-823.

Kumar-Sinha, C., Tomlins, S.A., and Chinnaiyan, A.M. (2008). Recurrent gene fusions in prostate cancer. Nat Rev Cancer *8*, 497-511.

Kwabi-Addo, B., Giri, D., Schmidt, K., Podsypanina, K., Parsons, R., Greenberg, N., and Ittmann, M. (2001). Haploinsufficiency of the Pten tumor suppressor gene promotes prostate cancer progression. Proc Natl Acad Sci U S A *98*, 11563-11568.

Lalani el, N., Laniado, M.E., and Abel, P.D. (1997). Molecular and cellular biology of prostate cancer. Cancer Metastasis Rev *16*, 29-66.

Lawrence, M.G., Taylor, R.A., Toivanen, R., Pedersen, J., Norden, S., Pook, D.W., Frydenberg, M., Papargiris, M.M., Niranjan, B., Richards, M.G., *et al*. (2013). A preclinical xenograft model of prostate cancer using human tumors. Nat Protoc *8*, 836-848.

Leslie, N.R., Batty, I.H., Maccario, H., Davidson, L., and Downes, C.P. (2008). Understanding PTEN regulation: PIP2, polarity and protein stability. Oncogene *27*, 5464-5476.

Li, J., Yen, C., Liaw, D., Podsypanina, K., Bose, S., Wang, S.I., Puc, J., Miliaresis, C., Rodgers, L., McCombie, R., *et al*. (1997). PTEN, a putative protein tyrosine phosphatase gene mutated in human brain, breast, and prostate cancer. Science *275*, 1943-1947.

Liao, C.P., Zhong, C., Saribekyan, G., Bading, J., Park, R., Conti, P.S., Moats, R., Berns, A., Shi, W., Zhou, Z., *et al*. (2007). Mouse models of prostate adenocarcinoma with the capacity to monitor spontaneous carcinogenesis by bioluminescence or fluorescence. Cancer Res *67*, 7525-7533.

Link, R.E., Shariat, S.F., Nguyen, C.V., Farr, A., Weinberg, A.D., Morton, R.A., Richardson, B., Bernard, D., and Slawin, K.M. (2004). Variation in prostate specific antigen results from 2 different assay platforms: clinical impact on 2304 patients undergoing prostate cancer screening. J Urol *171*, 2234-2238.

Liu, J.L., Sheng, X., Hortobagyi, Z.K., Mao, Z., Gallick, G.E., and Yung, W.K. (2005). Nuclear PTEN-mediated growth suppression is independent of Akt down-regulation. Mol Cell Biol *25*, 6211-6224.

Liu, W., Laitinen, S., Khan, S., Vihinen, M., Kowalski, J., Yu, G., Chen, L., Ewing, C.M., Eisenberger, M.A., Carducci, M.A., *et al*. (2009). Copy number analysis indicates monoclonal origin of lethal metastatic prostate cancer. Nature medicine *15*, 559-565.

Longo, D.L. (2010). New therapies for castration-resistant prostate cancer. N Engl J Med *363*, 479-481.

Lyons, S.K., Lim, E., Clermont, A.O., Dusich, J., Zhu, L., Campbell, K.D., Coffee, R.J., Grass, D.S., Hunter, J., Purchio, T., *et al*. (2006). Noninvasive bioluminescence imaging of normal and spontaneously transformed prostate tissue in mice. Cancer Res *66*, 4701-4707.

Maddison, L.A., Nahm, H., DeMayo, F., and Greenberg, N.M. (2000). Prostate specific expression of Cre recombinase in transgenic mice. Genesis *26*, 154-156.

Maddison, L.A., Sutherland, B.W., Barrios, R.J., and Greenberg, N.M. (2004). Conditional deletion of Rb causes early stage prostate cancer. Cancer Res *64*, 6018-6025.

Majumder, P.K., Yeh, J.J., George, D.J., Febbo, P.G., Kum, J., Xue, Q., Bikoff, R., Ma, H., Kantoff, P.W., Golub, T.R., *et al*. (2003). Prostate intraepithelial neoplasia induced by prostate restricted Akt activation: the MPAKT model. Proc Natl Acad Sci U S A *100*, 7841-7846.

Marino, S., Vooijs, M., van Der Gulden, H., Jonkers, J., and Berns, A. (2000). Induction of medulloblastomas in p53-null mutant mice by somatic inactivation of Rb in the external granular layer cells of the cerebellum. Genes Dev *14*, 994-1004.

Maser, R.S., Choudhury, B., Campbell, P.J., Feng, B., Wong, K.K., Protopopov, A., O'Neil, J., Gutierrez, A., Ivanova, E., Perna, I., *et al*. (2007). Chromosomally unstable mouse tumours have genomic alterations similar to diverse human cancers. Nature *447*, 966-971.

McLeod, D.G., Crawford, E.D., Blumenstein, B.A., Eisenberger, M.A., and Dorr, F.A. (1992). Controversies in the treatment of metastatic prostate cancer. Cancer *70*, 324-328.

Naguib, A., Cooke, J.C., Happerfield, L., Kerr, L., Gay, L.J., Luben, R.N., Ball, R.Y., Mitrou, P.N., McTaggart, A., and Arends, M.J. (2011). Alterations in PTEN and PIK3CA in colorectal cancers in the EPIC Norfolk study: associations with clinicopathological and dietary factors. BMC Cancer *11*, 123.

Nakamura, N., Ramaswamy, S., Vazquez, F., Signoretti, S., Loda, M., and Sellers, W.R. (2000). Forkhead transcription factors are critical effectors of cell death and cell cycle arrest downstream of PTEN. Mol Cell Biol *20*, 8969-8982.

Navin, N., Kendall, J., Troge, J., Andrews, P., Rodgers, L., McIndoo, J., Cook, K., Stepansky, A., Levy, D., Esposito, D., *et al*. (2011). Tumour evolution inferred by single-cell sequencing. Nature *472*, 90-94.

Nguyen, D.X., Bos, P.D., and Massague, J. (2009). Metastasis: from dissemination to organ-specific colonization. Nat Rev Cancer *9*, 274-284.

Ohbo, K., Suda, T., Hashiyama, M., Mantani, A., Ikebe, M., Miyakawa, K., Moriyama, M., Nakamura, M., Katsuki, M., Takahashi, K., *et al*. (1996). Modulation of hematopoiesis in mice with a truncated mutant of the interleukin-2 receptor gamma chain. Blood *87*, 956-967.

Onel, K., and Cordon-Cardo, C. (2004). MDM2 and prognosis. Mol Cancer Res *2*, 1-8.

Perez-Stable, C., Altman, N.H., Mehta, P.P., Deftos, L.J., and Roos, B.A. (1997). Prostate cancer progression, metastasis, and gene expression in transgenic mice. Cancer Res *57*, 900-906.

Perren, A., Weng, L.P., Boag, A.H., Ziebold, U., Thakore, K., Dahia, P.L., Komminoth, P., Lees, J.A., Mulligan, L.M., Mutter, G.L., *et al*. (1999). Immunohistochemical evidence of loss of PTEN expression in primary ductal adenocarcinomas of the breast. Am J Pathol *155*, 1253-1260.

Plafker, S.M., Plafker, K.S., Weissman, A.M., and Macara, I.G. (2004). Ubiquitin charging of human class III ubiquitin-conjugating enzymes triggers their nuclear import. J Cell Biol *167*, 649-659.

Podsypanina, K., Ellenson, L.H., Nemes, A., Gu, J., Tamura, M., Yamada, K.M., Cordon-Cardo, C., Catoretti, G., Fisher, P.E., and Parsons, R. (1999). Mutation of Pten/Mmac1 in mice causes neoplasia in multiple organ systems. Proc Natl Acad Sci U S A *96*, 1563-1568.

Ponce-Castaneda, M.V., Lee, M.H., Latres, E., Polyak, K., Lacombe, L., Montgomery, K., Mathew, S., Krauter, K., Sheinfeld, J., Massague, J., *et al*. (1995). p27Kip1: chromosomal mapping to 12p12-12p13.1 and absence of mutations in human tumors. Cancer Res *55*, 1211-1214.

Rebbeck, T.R., Walker, A.H., Zeigler-Johnson, C., Weisburg, S., Martin, A.M., Nathanson, K.L., Wein, A.J., and Malkowicz, S.B. (2000). Association of HPC2/ELAC2 genotypes and prostate cancer. Am J Hum Genet *67*, 1014-1019.

Reiner, T., de Las Pozas, A., Parrondo, R., and Perez-Stable, C. (2007). Progression of prostate cancer from a subset of p63-positive basal epithelial cells in FG/Tag transgenic mice. Mol Cancer Res *5*, 1171-1179.

Rennert, H., Bercovich, D., Hubert, A., Abeliovich, D., Rozovsky, U., Bar-Shira, A., Soloviov, S., Schreiber, L., Matzkin, H., Rennert, G., *et al*. (2002). A novel founder mutation in the RNASEL gene, 471delAAAG, is associated with prostate cancer in Ashkenazi Jews. Am J Hum Genet *71*, 981-984.

Richardson, T.D., and Oesterling, J.E. (1997). Age-specific reference ranges for serum prostate-specific antigen. Urol Clin North Am *24*, 339-351.

Rokman, A., Ikonen, T., Seppala, E.H., Nupponen, N., Autio, V., Mononen, N., Bailey-Wilson, J., Trent, J., Carpten, J., Matikainen, M.P., *et al*. (2002). Germline alterations of the RNASEL gene, a candidate HPC1 gene at 1q25, in patients and families with prostate cancer. Am J Hum Genet *70*, 1299-1304.

Rundle, A., and Neugut, A.I. (2008). Obesity and screening PSA levels among men undergoing an annual physical exam. Prostate *68*, 373-380.

Ryan, C.J., and Tindall, D.J. (2011). Androgen receptor rediscovered: the new biology and targeting the androgen receptor therapeutically. J Clin Oncol *29*, 3651-3658.
Salmena, L., Carracedo, A., and Pandolfi, P.P. (2008). Tenets of PTEN tumor suppression. Cell *133*, 403-414.
Sato, K., Qian, J., Slezak, J.M., Lieber, M.M., Bostwick, D.G., Bergstralh, E.J., and Jenkins, R.B. (1999). Clinical significance of alterations of chromosome 8 in high-grade, advanced, nonmetastatic prostate carcinoma. J Natl Cancer Inst *91*, 1574-1580.
Saurin, A.J., Borden, K.L., Boddy, M.N., and Freemont, P.S. (1996). Does this have a familiar RING? Trends Biochem Sci *21*, 208-214.
Scheffner, M., Huibregtse, J.M., Vierstra, R.D., and Howley, P.M. (1993). The HPV-16 E6 and E6-AP complex functions as a ubiquitin-protein ligase in the ubiquitination of p53. Cell *75*, 495-505.
Scherl, A., Li, J.F., Cardiff, R.D., and Schreiber-Agus, N. (2004). Prostatic intraepithelial neoplasia and intestinal metaplasia in prostates of probasin-RAS transgenic mice. Prostate *59*, 448-459.
Schleutker, J., Matikainen, M., Smith, J., Koivisto, P., Baffoe-Bonnie, A., Kainu, T., Gillanders, E., Sankila, R., Pukkala, E., Carpten, J., *et al*. (2000). A genetic epidemiological study of hereditary prostate cancer (HPC) in Finland: frequent HPCX linkage in families with late-onset disease. Clinical cancer research : an official journal of the American Association for Cancer Research *6*, 4810-4815.
Schmidt-Kittler, O., Ragg, T., Daskalakis, A., Granzow, M., Ahr, A., Blankenstein, T.J., Kaufmann, M., Diebold, J., Arnholdt, H., Muller, P., *et al*. (2003). From latent disseminated cells to overt metastasis: genetic analysis of systemic breast cancer progression. Proc Natl Acad Sci U S A *100*, 7737-7742.
Schroder, F., Crawford, E.D., Axcrona, K., Payne, H., and Keane, T.E. (2012a). Androgen deprivation therapy: past, present and future. BJU Int *109 Suppl 6*, 1-12.
Schroder, F.H., Hugosson, J., Roobol, M.J., Tammela, T.L., Ciatto, S., Nelen, V., Kwiatkowski, M., Lujan, M., Lilja, H., Zappa, M., *et al*. (2009). Screening and prostate-cancer mortality in a randomized European study. N Engl J Med *360*, 1320-1328.

Schroder, F.H., Hugosson, J., Roobol, M.J., Tammela, T.L., Ciatto, S., Nelen, V., Kwiatkowski, M., Lujan, M., Lilja, H., Zappa, M., *et al*. (2012b). Prostate-cancer mortality at 11 years of follow-up. N Engl J Med *366*, 981-990.

Schwartz, A.L., and Ciechanover, A. (1999). The ubiquitin-proteasome pathway and pathogenesis of human diseases. Annu Rev Med *50*, 57-74.

Serreze, D.V., and Leiter, E.H. (1988). Defective activation of T suppressor cell function in nonobese diabetic mice. Potential relation to cytokine deficiencies. J Immunol *140*, 3801-3807.

Shappell, S.B., Thomas, G.V., Roberts, R.L., Herbert, R., Ittmann, M.M., Rubin, M.A., Humphrey, P.A., Sundberg, J.P., Rozengurt, N., Barrios, R., *et al*. (2004). Prostate pathology of genetically engineered mice: definitions and classification. The consensus report from the Bar Harbor meeting of the Mouse Models of Human Cancer Consortium Prostate Pathology Committee. Cancer Res *64*, 2270-2305.

Shin, I., Yakes, F.M., Rojo, F., Shin, N.Y., Bakin, A.V., Baselga, J., and Arteaga, C.L. (2002). PKB/Akt mediates cell-cycle progression by phosphorylation of p27(Kip1) at threonine 157 and modulation of its cellular localization. Nature medicine *8*, 1145-1152.

Shultz, L.D., Schweitzer, P.A., Christianson, S.W., Gott, B., Schweitzer, I.B., Tennent, B., McKenna, S., Mobraaten, L., Rajan, T.V., Greiner, D.L., *et al*. (1995). Multiple defects in innate and adaptive immunologic function in NOD/LtSz-scid mice. J Immunol *154*, 180-191.

Sikder, H., Huso, D.L., Zhang, H., Wang, B., Ryu, B., Hwang, S.T., Powell, J.D., and Alani, R.M. (2003). Disruption of Id1 reveals major differences in angiogenesis between transplanted and autochthonous tumors. Cancer Cell *4*, 291-299.

Singh, M., and Johnson, L. (2006). Using genetically engineered mouse models of cancer to aid drug development: an industry perspective. Clin Cancer Res *12*, 5312-5328.

Song, M.S., Salmena, L., Carracedo, A., Egia, A., Lo-Coco, F., Teruya-Feldstein, J., and Pandolfi, P.P. (2008). The deubiquitinylation and localization of PTEN are regulated by a HAUSP-PML network. Nature *455*, 813-817.

Stanbrough, M., Leav, I., Kwan, P.W., Bubley, G.J., and Balk, S.P. (2001). Prostatic intraepithelial neoplasia in mice expressing an androgen receptor transgene in prostate epithelium. Proc Natl Acad Sci U S A *98*, 10823-10828.

Steadman, D.J., Giuffrida, D., and Gelmann, E.P. (2000). DNA-binding sequence of the human prostate-specific homeodomain protein NKX3.1. Nucleic Acids Res *28*, 2389-2395.

Stenman, U.H., Hakama, M., Knekt, P., Aromaa, A., Teppo, L., and Leinonen, J. (1994). Serum concentrations of prostate specific antigen and its complex with alpha 1-antichymotrypsin before diagnosis of prostate cancer. Lancet *344*, 1594-1598.

Sternberg, N. (1979). Demonstration and analysis of P1 site-specific recombination using lambda-P1 hybrid phages constructed in vitro. Cold Spring Harb Symp Quant Biol *43 Pt 2*, 1143-1146.

Sternberg, N., and Hamilton, D. (1981). Bacteriophage P1 site-specific recombination. I. Recombination between loxP sites. J Mol Biol *150*, 467-486.

Sun, S., Sprenger, C.C., Vessella, R.L., Haugk, K., Soriano, K., Mostaghel, E.A., Page, S.T., Coleman, I.M., Nguyen, H.M., Sun, H., *et al*. (2010). Castration resistance in human prostate cancer is conferred by a frequently occurring androgen receptor splice variant. J Clin Invest *120*, 2715-2730.

Suzuki, A., de la Pompa, J.L., Stambolic, V., Elia, A.J., Sasaki, T., del Barco Barrantes, I., Ho, A., Wakeham, A., Itie, A., Khoo, W., *et al*. (1998). High cancer susceptibility and embryonic lethality associated with mutation of the PTEN tumor suppressor gene in mice. Curr Biol *8*, 1169-1178.

Tavtigian, S.V., Simard, J., Teng, D.H., Abtin, V., Baumgard, M., Beck, A., Camp, N.J., Carillo, A.R., Chen, Y., Dayananth, P., *et al*. (2001). A candidate prostate cancer susceptibility gene at chromosome 17p. Nat Genet *27*, 172-180.

Taylor, B.S., Schultz, N., Hieronymus, H., Gopalan, A., Xiao, Y., Carver, B.S., Arora, V.K., Kaushik, P., Cerami, E., Reva, B., *et al*. (2010). Integrative genomic profiling of human prostate cancer. Cancer cell *18*, 11-22.

Thalmann, G.N., Anezinis, P.E., Chang, S.M., Zhau, H.E., Kim, E.E., Hopwood, V.L., Pathak, S., von Eschenbach, A.C., and Chung, L.W. (1994). Androgen-independent cancer progression and bone metastasis in the LNCaP model of human prostate cancer. Cancer Res *54*, 2577-2581.

Thompson, I.M., Chi, C., Ankerst, D.P., Goodman, P.J., Tangen, C.M., Lippman, S.M., Lucia, M.S., Parnes, H.L., and Coltman, C.A., Jr. (2006). Effect of finasteride on the sensitivity of PSA for detecting prostate cancer. J Natl Cancer Inst *98*, 1128-1133.

Thompson, I.M., Pauler, D.K., Goodman, P.J., Tangen, C.M., Lucia, M.S., Parnes, H.L., Minasian, L.M., Ford, L.G., Lippman, S.M., Crawford, E.D., *et al*. (2004). Prevalence of prostate

cancer among men with a prostate-specific antigen level < or =4.0 ng per milliliter. N Engl J Med *350*, 2239-2246.

Toledo, F., Krummel, K.A., Lee, C.J., Liu, C.W., Rodewald, L.W., Tang, M., and Wahl, G.M. (2006). A mouse p53 mutant lacking the proline-rich domain rescues Mdm4 deficiency and provides insight into the Mdm2-Mdm4-p53 regulatory network. Cancer Cell *9*, 273-285.

Tomlins, S.A., Laxman, B., Dhanasekaran, S.M., Helgeson, B.E., Cao, X., Morris, D.S., Menon, A., Jing, X., Cao, Q., Han, B., *et al*. (2007). Distinct classes of chromosomal rearrangements create oncogenic ETS gene fusions in prostate cancer. Nature *448*, 595-599.

Tomlins, S.A., Rhodes, D.R., Perner, S., Dhanasekaran, S.M., Mehra, R., Sun, X.W., Varambally, S., Cao, X., Tchinda, J., Kuefer, R., *et al*. (2005). Recurrent fusion of TMPRSS2 and ETS transcription factor genes in prostate cancer. Science *310*, 644-648.

Tran, C., Ouk, S., Clegg, N.J., Chen, Y., Watson, P.A., Arora, V., Wongvipat, J., Smith-Jones, P.M., Yoo, D., Kwon, A., *et al*. (2009). Development of a second-generation antiandrogen for treatment of advanced prostate cancer. Science *324*, 787-790.

Tricoli, J.V., Gumerlock, P.H., Yao, J.L., Chi, S.G., D'Souza, S.A., Nestok, B.R., and deVere White, R.W. (1996). Alterations of the retinoblastoma gene in human prostate adenocarcinoma. Genes Chromosomes Cancer *15*, 108-114.

Trotman, L.C., Alimonti, A., Scaglioni, P.P., Koutcher, J.A., Cordon-Cardo, C., and Pandolfi, P.P. (2006). Identification of a tumour suppressor network opposing nuclear Akt function. Nature *441*, 523-527.

Trotman, L.C., Niki, M., Dotan, Z.A., Koutcher, J.A., Di Cristofano, A., Xiao, A., Khoo, A.S., Roy-Burman, P., Greenberg, N.M., Van Dyke, T., *et al*. (2003). Pten dose dictates cancer progression in the prostate. PLoS Biol *1*, E59.

Trotman, L.C., Wang, X., Alimonti, A., Chen, Z., Teruya-Feldstein, J., Yang, H., Pavletich, N.P., Carver, B.S., Cordon-Cardo, C., Erdjument-Bromage, H., *et al*. (2007). Ubiquitination regulates PTEN nuclear import and tumor suppression. Cell *128*, 141-156.

Ulmert, D., Serio, A.M., O'Brien, M.F., Becker, C., Eastham, J.A., Scardino, P.T., Bjork, T., Berglund, G., Vickers, A.J., and Lilja, H. (2008). Long-term prediction of prostate cancer: prostate-specific antigen (PSA) velocity is predictive but does not improve the predictive accuracy of a single PSA measurement 15 years or more before cancer diagnosis in a large, representative, unscreened population. J Clin Oncol *26*, 835-841.

Valkenburg, K.C., and Williams, B.O. (2011). Mouse models of prostate cancer. Prostate Cancer *2011*, 895238.

Van Themsche, C., Leblanc, V., Parent, S., and Asselin, E. (2009). X-linked inhibitor of apoptosis protein (XIAP) regulates PTEN ubiquitination, content, and compartmentalization. J Biol Chem *284*, 20462-20466.

Vassilev, L.T. (2004). Small-molecule antagonists of p53-MDM2 binding: research tools and potential therapeutics. Cell Cycle *3*, 419-421.

Vazquez, F., Grossman, S.R., Takahashi, Y., Rokas, M.V., Nakamura, N., and Sellers, W.R. (2001). Phosphorylation of the PTEN tail acts as an inhibitory switch by preventing its recruitment into a protein complex. The Journal of biological chemistry *276*, 48627-48630.

Vivanco, I., and Sawyers, C.L. (2002). The phosphatidylinositol 3-Kinase AKT pathway in human cancer. Nat Rev Cancer *2*, 489-501.

Vogelstein, B., Papadopoulos, N., Velculescu, V.E., Zhou, S., Diaz, L.A., Jr., and Kinzler, K.W. (2013). Cancer genome landscapes. Science *339*, 1546-1558.

Wang, L., McDonnell, S.K., Cunningham, J.M., Hebbring, S., Jacobsen, S.J., Cerhan, J.R., Slager, S.L., Blute, M.L., Schaid, D.J., and Thibodeau, S.N. (2003). No association of germline alteration of MSR1 with prostate cancer risk. Nat Genet *35*, 128-129.

Wang, X., and Jiang, X. (2008). Post-translational regulation of PTEN. Oncogene *27*, 5454-5463.

Wang, X., Kruithof-de Julio, M., Economides, K.D., Walker, D., Yu, H., Halili, M.V., Hu, Y.P., Price, S.M., Abate-Shen, C., and Shen, M.M. (2009). A luminal epithelial stem cell that is a cell of origin for prostate cancer. Nature *461*, 495-500.

Wang, X., Trotman, L.C., Koppie, T., Alimonti, A., Chen, Z., Gao, Z., Wang, J., Erdjument-Bromage, H., Tempst, P., Cordon-Cardo, C., *et al*. (2007). NEDD4-1 is a proto-oncogenic ubiquitin ligase for PTEN. Cell *128*, 129-139.

Werny, D.M., Saraiya, M., Chen, X., and Platz, E.A. (2007). Prostate-specific antigen, sexual behavior, and sexually transmitted infections in US men 40-59 years old, 2001-2004: a cross-sectional study. Infect Agent Cancer *2*, 19.

Wu, C.T., Altuwaijri, S., Ricke, W.A., Huang, S.P., Yeh, S., Zhang, C., Niu, Y., Tsai, M.Y., and Chang, C. (2007). Increased prostate cell proliferation and loss of cell differentiation in mice lacking prostate epithelial androgen receptor. Proc Natl Acad Sci U S A *104*, 12679-12684.

Wu, X., Wu, J., Huang, J., Powell, W.C., Zhang, J., Matusik, R.J., Sangiorgi, F.O., Maxson, R.E., Sucov, H.M., and Roy-Burman, P. (2001). Generation of a prostate epithelial cell-specific Cre transgenic mouse model for tissue-specific gene ablation. Mech Dev *101*, 61-69.

Xu, J., Zheng, S.L., Komiya, A., Mychaleckyj, J.C., Isaacs, S.D., Hu, J.J., Sterling, D., Lange, E.M., Hawkins, G.A., Turner, A., *et al*. (2002). Germline mutations and sequence variants of the macrophage scavenger receptor 1 gene are associated with prostate cancer risk. Nat Genet *32*, 321-325.

Yanagawa, N., Leduc, C., Kohler, D., Saieg, M.A., John, T., Sykes, J., Yoshimoto, M., Pintilie, M., Squire, J., Shepherd, F.A., *et al*. (2012). Loss of phosphatase and tensin homolog protein expression is an independent poor prognostic marker in lung adenocarcinoma. J Thorac Oncol *7*, 1513-1521.

Yen, H.C., and Elledge, S.J. (2008). Identification of SCF ubiquitin ligase substrates by global protein stability profiling. Science *322*, 923-929.

Yen, H.C., Xu, Q., Chou, D.M., Zhao, Z., and Elledge, S.J. (2008). Global protein stability profiling in mammalian cells. Science *322*, 918-923.

Yoshidome, K., Shibata, M.A., Maroulakou, I.G., Liu, M.L., Jorcyk, C.L., Gold, L.G., Welch, V.N., and Green, J.E. (1998). Genetic alterations in the development of mammary and prostate cancer in the C3(1)/Tag transgenic mouse model. Int J Oncol *12*, 449-453.

Yoshimoto, M., Cutz, J.C., Nuin, P.A., Joshua, A.M., Bayani, J., Evans, A.J., Zielenska, M., and Squire, J.A. (2006). Interphase FISH analysis of PTEN in histologic sections shows genomic deletions in 68% of primary prostate cancer and 23% of high-grade prostatic intra-epithelial neoplasias. Cancer Genet Cytogenet *169*, 128-137.

You, M.J., Castrillon, D.H., Bastian, B.C., O'Hagan, R.C., Bosenberg, M.W., Parsons, R., Chin, L., and DePinho, R.A. (2002). Genetic analysis of Pten and Ink4a/Arf interactions in the suppression of tumorigenesis in mice. Proc Natl Acad Sci U S A *99*, 1455-1460.

Yuan, T.L., and Cantley, L.C. (2008). PI3K pathway alterations in cancer: variations on a theme. Oncogene *27*, 5497-5510.

Zhang, J., Thomas, T.Z., Kasper, S., and Matusik, R.J. (2000). A small composite probasin promoter confers high levels of prostate-specific gene expression through regulation by androgens and glucocorticoids in vitro and in vivo. Endocrinology *141*, 4698-4710.

Zhang, Q., Yang, X.J., Kundu, S.D., Pins, M., Javonovic, B., Meyer, R., Kim, S.J., Greenberg, N.M., Kuzel, T., Meagher, R., *et al*. (2006). Blockade of transforming growth factor-{beta} signaling in tumor-reactive CD8(+) T cells activates the antitumor immune response cycle. Mol Cancer Ther *5*, 1733-1743.

Zhau, H.E., Li, C.L., and Chung, L.W. (2000). Establishment of human prostate carcinoma skeletal metastasis models. Cancer *88*, 2995-3001.

Zhou, A., Paranjape, J., Brown, T.L., Nie, H., Naik, S., Dong, B., Chang, A., Trapp, B., Fairchild, R., Colmenares, C., *et al*. (1997). Interferon action and apoptosis are defective in mice devoid of 2',5'-oligoadenylate-dependent RNase L. Embo J *16*, 6355-6363.

Zhou, X.P., Loukola, A., Salovaara, R., Nystrom-Lahti, M., Peltomaki, P., de la Chapelle, A., Aaltonen, L.A., and Eng, C. (2002). PTEN mutational spectra, expression levels, and subcellular localization in microsatellite stable and unstable colorectal cancers. Am J Pathol *161*, 439-447.

Zhu, M.L., and Kyprianou, N. (2008). Androgen receptor and growth factor signaling cross-talk in prostate cancer cells. Endocr Relat Cancer *15*, 841-849.

VIII. Appendix

1. Submitted manuscript related Part II : The following abstract and figures were submitted to *Cancer Discovery*.

RapidCaP, a Genetically engineered mouse model for analysis and therapy of metastatic prostate cancer reveals drivers of *Pten*-mutant metastasis.

Hyejin Cho[1], Tali Herzka[1], Wu Zheng[1], Mireia Castillo-Martin[2], Carlos Cordon-Cardo[2], Lloyd C. Trotman[1]

[1]Cold Spring Harbor Laboratory, One Bungtown Road, Cold Spring Harbor, NY 11724, USA.

[2]Mount Sinai School of Medicine, One Gustave L. Levy Place, New York, NY 10029, USA.

Genetically Engineered Mouse (GEM) models are the gold standard for functional cancer research. GEM models for *Pten*-deficient Cancers of the Prostate (CaP) have greatly helped us understand the biology of tumor initiation, but their characteristic of developing lethal primary disease is obstructing research and therapy of the advanced metastatic disease stages. Thus, the genetic requirements needed to trigger metastatic prostate cancer have remained ill defined. Here we developed RapidCaP, a GEM modeling approach that uses surgical injection for viral gene delivery. We show that in *Pten*-deficiency, complete loss of the p53 tumor suppressor triggers CaP metastasis to distant sites at greater than 50% penetrance by 4 months, entirely consistent with results from human genome analysis. Through live tracking of the endogenous prostate metastasis *via* bioluminescence imaging, we find that both primary and metastatic disease first respond to castration, but later relapse to produce lethal, castration resistant disease, as seen in human. To our surprise, analysis of these lesions and of metastatic nodules in lung consistently failed to reveal activation of Akt, the signature oncogene downstream of *Pten*-loss. Instead, these metastases showed strong activation of the Myc oncogene, which was even more pronounced in the castration resistant tumors.

Taken together, these data suggest that an 'Akt-switch' to Myc is a critical event in prostate cancer metastasis and resistance to castration therapy. Thus, the RapidCaP system greatly helps address the hitherto unmet need for analysis, gene validation and therapy of prostate cancer metastasis in genetically engineered mice.

2. List of hairpins and primers used in chapter IV

Table 4.1 List of pGIPZ lentiviral shRNA expressing construct

	shRNA Accession	***pGIPZ Clone IDs***
USP15	NM_006313	V2LHS_196921
	NM_006313	V2LHS_5710
	NM_006313	V2LHS_13436
	NM_006313	V2LHS_13437
	NM_027604	V2LHS_196921
USP28	NM_020886	V2LHS_14019
	NM_020886	V2LHS_14020
	NM_020886	V2LHS_6063
USP28	NM_175482	V2LHS_14020
	NM_175482	V2LHS_6063
BAP1	NM_004656	V2LHS_246612
	NM_004656	V2LHS_41473
	NM_004656	V2LHS_41478
	NM_004656	V2LHS_41476
USP8	NM_005154=XM_215821	V2LHS_13384
	NM_005154=XM_215821	V2LHS_254594
	NM_005154=XM_215821	V2LHS_49252
	NM_005154=XM_215821	V2LHS_49323
	NM_005154=XM_215821	V2LHS_49253
	NM_005154=XM_215821	V2LHS_49254
	NM_005154=XM_215821	V2LHS_49250
	NM_005154=XM_215821	V2LHS_49251
	NM_005154=XM_215821	V2LMM_37945
NEDD4-1	NM_006154	V2LHS_254872

	shRNA Accession	*pGIPZ Clone IDs*
	NM_006154	V2LHS_72555
	NM_006154	V2LHS_72553
USP4	NM_003363=U20657	V2LHS_221699
	NM_003363=U20657	V2LHS_171855
	NM_003363=U20657	V2LHS_171854
USP14	NM_005151	V2LHS_49355
	NM_005151	V2LHS_254586
	NM_005151	V2LHS_49357
	NM_005151	V2LHS_49358
E2E1	NM_003341=BC079134=NM_009455	V2LHS_13163
	NM_003341=BC079134=NM_009455	V2LHS_171754
	NM_003341=BC079134=NM_009455	V2LHS_220497
	NM_003341=BC079134=NM_009455	V2LHS_171755
	NM_003341=BC079134=NM_009455	V2LHS_171757
	NM_003341=BC079134=NM_009455	V2LHS_171753
E2E2	NM_152653	V2LHS_43620
	NM_152653	V2LHS_243310
	NM_003341 = B079134	V2LHS_13163
	NM_003341 = B079134	V2LHS_171754
	NM_003341 = B079134	V2LHS_220497
	NM_003341 = B079134	V2LHS_171755
	NM_003341 = B079134	V2LHS_171757
	NM_003341 = B079134	V2LHS_171753
	NM_152653	V2LHS_43620
	NM_152653	V2LHS_243310

	shRNA Accession	*pGIPZ Clone IDs*
	NM_144839 = XM_341288 = NM_152653	Only GIPZ Mm EXCEPT NM_152653
	NM_152653	V2LHS_43620
	NM_152653	V2LHS_243310
USP7	XM_340747 = NM_001003918 = NM_003470	V2LHS_222871
	XM_340747 = NM_001003918 = NM_003470	V2LMM_214243
USP7	NM_003470	V2LHS_222871
	NM_003470	V2LHS_172409
	NM_003470	V2LHS_172411
PTEN	AF019083,NM_000314,NM_008960,NM_031606	V2LHS_531
	AF019083,NM_000314,NM_008960	V2LHS_529
	AF019083,NM_000314,NM_008960	V2LHS_192536
	NM_000314,AF019083,NM_008960,NM_031606	V2LHS_531
	NM_000314,NM_008960	V2LHS_231477
	NM_000314	V2LHS_92314
	NM_000314	V2LHS_231772
	NM_000314,AF019083,NM_008960	V2LHS_529
	NM_000314,XM_071675	V2LHS_92319
	NM_000314	V2LHS_92317
	NM_000314,AF019083,NM_008960	V2LHS_192536
	NM_008960,NM_031606,AF019083,NM_000314	V2LHS_531
	NM_008960,NM_000314	V2LHS_231477
	NM_008960,NM_000314,AF019083	V2LHS_529
	NM_008960,NM_000314,AF019083	V2LHS_192536

Table 4.2 Primer sequence for RT-qPCR

	GenBank Accession	Primer Bank ID	Forward Primer	Reverse Primer
BAP1	NM_004656	4757836a1	ACCCTGCTCGTGGAAGATTTC	TCATCAATCACGGACGTATCATC
		4757836a2	GATACGTCCGTGATTGATGATGA	GCATATCCTTTGCTCTCAGGG
		4757836a3	TGAGAGCAAAGGATATGCGATTG	GCACTAAGGCCATTCTGCTTCT
E2E 1	NM_003341	4507779a1	ATGTCGGATGACGATTCGAGG	AGGTGGAGGGTCTAAAGTGATG
		4507779a2	GGAGAGTAAAGTCAGCATGAGC	AGGTGGAGGGTCTAAAGTGATG
		4507779a3	TCGGATGACGATTCGAGGG	TGCAATTAGGTGGAGGGTCTAAA
E2E 2	NM_152653	22749327a1	GAGGCACAAAGAGTTGATGACA	GCGGTTTTGCTGGATATTTTTCC
		22749327a2	AGCAAAACCGCTGCTAAATTG	CTTTGGGTCCAGCACTACAGT
		22749327a3	TACCTTTTCACCAGACTATCCGT	GTCCAGACAGATCACACCTTG
hPTEN	NM_000314	4506249a1	TGGATTCGACTTAGACTTGACCT	TTTGGCGGTGTCATAATGTCTT
		4506249a2	TGCAGAGTTGCACAATATCCTT	GTCATCTTCACTTAGCCATTGGT
		4506249a3	GACAATCATGTTGCAGCAATTCA	CCCATAGAAATCTAGGGCCTCT
NEDD4-1	NM_006154	577313a1	GGAAGCGTTCGGAAATGGC	CGTAAGGATCACTAGCTCCCA
		577313a2	GAGCTAGTGATCCTTACGTGAGA	TCGGTTTTCGTCAAACACTTCA
		577313a3	AGTGTTTGACGAAAACCGATTGA	CAGCCTGTTCTGCATTATCATCT
USP4	NM_003363	4507853a1	TCAGCAAGTCCCTATTCCTCA	GGCTCCTGACAATTATACGAAGC
		4507853a2	TCAGCAAGTCCCTATTCCTCA	GAGAAAGTAGTCAGTCAGTGGTG
		4507853a3	GCTTCGTATAATTGTCAGGAGCC	TGAGTTTTGAACATCGAGGGTG
USP7	NM_003470	4507857a1	GGAAGCGGGAGATACAGATGA	AAGGACCGACTCACTCAGTCT
		4507857a2	CCTTAGCCCTCCGTGTTTTGT	GACGACTGAACGACTTTTCATCA
		4507857a3	TGAAAAGTCGTTCAGTCGTCG	CTCAGGATCGGTCACTTCACT

	GenBank Accession	Primer Bank ID	Forward Primer	Reverse Primer
USP8	NM_005154	4827054a1	AAAAAGCTGTCGAAGAAGCTGA	CCAAAGAGCCTTTAGCCAATGT
		4827054a2	TTGGCTAAAGGCTCTTTGGAG	TGCATTCTTCGAGCATCCATTAT
		4827054a3	GTCCAGGAGTCACTGCTAGTT	GCCTCCCTCTAAAACCAAAGG
USP14	NM_005151	4827050a1	ATGCCGCTCTACTCCGTTACT	GACTCCAGTCAACGCAAACAG
		4827050a2	GTGAAAGGAGGAACGCTAAAGG	TCCACATGGTAACTCCATAGCA
		4827050a3	CTGTGCCTGAACTCAAAGATGC	GGAAAGCCATGTGCAAAAACTG
USP15	NM_006313	14149627a1	CGACGCTGCTCAAAACCTC	TCCCATCTGGTATTTGTCCCAA
		14149627a2	ACCTAGTCGATAGTCGCTGGT	TCCCATCTGGTATTTGTCCCAA
		14149627a3	CTGGAAGAAACAATGAACAGCCA	AGTGGAGGTGTGTTGCTCAAA
USP28	NM_020886	16507200a1	GCACTGAGTGAGGTGATGCTG	CAAAGGTCTGACGGGCTTTAG
		16507200a2	GCACTGAGTGAGGTGATGCTG	TGCTTCAGACCCATCTCGGT
		16507200a3	ACCCTTCCTTTCTCCATGAAGC	GGGCTCCTTAACTCTCTCATCA

Table 4.3 The big library - Ubiquitin Proteasome System (UPS)

symbol	name
SH3MD2	SH3 multiple domains 2
CHFR	checkpoint with forkhead and ring finger domains
KIAA1333	KIAA1333
UBE3C	ubiquitin protein ligase E3C
ISGF3G	interferon-stimulated transcription factor 3, gamma 48kDa
FBXO21	F-box protein 21
FBXO7	F-box protein 7
RBBP6	retinoblastoma binding protein 6
BRAP	BRCA1 associated protein
ZNRF2	zinc and ring finger 2
|LOC244421|FLJ23749|LOC306505	similar to hypothetical protein FLJ23749; hypothetical protein FLJ23749
FAF1	Fas (TNFRSF6) associated factor 1
FBXO9	F-box protein 9
UBE4B	ubiquitination factor E4B (UFD2 homolog, yeast)
Socs6|SOCS6	suppressor of cytokine signaling 6
TRIM8	tripartite motif-containing 8
WSB1	WD repeat and SOCS box-containing 1
RNF128	ring finger protein 128
FBXO10	F-box protein 10
FAF1	Fas (TNFRSF6) associated factor 1
RNF7	ring finger protein 7
RNF25	ring finger protein 25
UBXD2	UBX domain containing 2
SOCS3	suppressor of cytokine signaling 3
FBXL6	F-box and leucine-rich repeat protein 6
BIRC4	baculoviral IAP repeat-containing 4
FBXW7	F-box and WD-40 domain protein 7 (archipelago homolog, Drosophila)
RNF128	ring finger protein 128
SKP2	S-phase kinase-associated protein 2 (p45)
RNF166	ring finger protein 166
KIAA0794	KIAA0794 protein
RAF1	v-raf-1 murine leukemia viral oncogene homolog 1
RNF7	ring finger protein 7
RBX1	ring-box 1
RNF111	ring finger protein 111
FBXO46	F-box protein 46
FBXW11	F-box and WD-40 domain protein 11
HECTD1	HECT domain containing 1
RCHY1	ring finger and CHY zinc finger domain containing 1
MAP3K1	mitogen-activated protein kinase kinase kinase 1
DZIP3	zinc finger DAZ interacting protein 3
NFX1	nuclear transcription factor, X-box binding 1
TRIM55	tripartite motif-containing 55
RNF167	ring finger protein 167
FBXL5	F-box and leucine-rich repeat protein 5

symbol	name
ATRX	alpha thalassemia/mental retardation syndrome X-linked (RAD54 homolog, S. cerevisiae)
PEX12	peroxisomal biogenesis factor 12
RNF139	ring finger protein 139
RKHD2	ring finger and KH domain containing 2
C20orf18	chromosome 20 open reading frame 18
RNF146	ring finger protein 146
Raf1|RAF1	murine leukemia viral (v-raf-1) oncogene homolog 1 (3611-MSV); v-raf-1 leukemia viral oncogene 1; v-raf-1 murine leukemia viral oncogene homolog 1
KIAA1542	CTD-binding SR-like protein rA9
TRAF5	TNF receptor-associated factor 5
MLL3	myeloid/lymphoid or mixed-lineage leukemia 3
RGD:621856|RNF38	RING finger protein OIP1; ring finger protein 38
MKRN3	makorin, ring finger protein, 3
PXMP3	peroxisomal membrane protein 3, 35kDa (Zellweger syndrome)
IBRDC3	IBR domain containing 3
HACE1	HECT domain and ankyrin repeat containing, E3 ubiquitin protein ligase 1
Rchy1|RCHY1	ring finger and CHY zinc finger domain containing 1
BIRC7	baculoviral IAP repeat-containing 7 (livin)
WHSC1L1	Wolf-Hirschhorn syndrome candidate 1-like 1
RNF125	ring finger protein 125
TRIM31	tripartite motif-containing 31
ZNF183|LOC313450	zinc finger protein 183 (RING finger, C3HC4 type); similar to RIKEN cDNA 2810428C21
FLJ30092	AF-1 specific protein phosphatase
FLJ12875	hypothetical protein FLJ12875
TRAF3	TNF receptor-associated factor 3
ARIH1	ariadne homolog, ubiquitin-conjugating enzyme E2 binding protein, 1 (Drosophila)
DTX4	deltex 4 homolog (Drosophila)
RNF13	ring finger protein 13
FBXO30|Fbxo30	F-box protein 30
FBXL15	F-box and leucine-rich repeat protein 15
FBXL5	F-box and leucine-rich repeat protein 5
HERC6	hect domain and RLD 6
TRIM49	tripartite motif-containing 49
BTRC	beta-transducin repeat containing
RKHD2	ring finger and KH domain containing 2
ISGF3G	interferon-stimulated transcription factor 3, gamma 48kDa
RGD:1307339|-|TRIM33|Trim33	tripartite motif protein 33 (predicted); -; tripartite motif protein 33; tripartite motif-containing 33
UHRF1	ubiquitin-like, containing PHD and RING finger domains, 1
KIAA0317|1110018G07Rik	KIAA0317; RIKEN cDNA 1110018G07 gene
WHSC1L1	Wolf-Hirschhorn syndrome candidate 1-like 1
WSB2	WD repeat and SOCS box-containing 2
MID1	midline 1 (Opitz/BBB syndrome)
TRIM26	tripartite motif-containing 26
RNF170	ring finger protein 170

symbol	name
MRPL49	mitochondrial ribosomal protein L49
KIAA1333	KIAA1333
LRSAM1	leucine rich repeat and sterile alpha motif containing 1
SOCS2	suppressor of cytokine signaling 2
MAP3K1	mitogen-activated protein kinase kinase kinase 1
KIAA0317	KIAA0317
D6Ertd365e|ZNRF2	DNA segment, Chr 6, ERATO Doi 365, expressed; zinc and ring finger 2
PCGF3	polycomb group ring finger 3
TRIM32	tripartite motif-containing 32
VHL	von Hippel-Lindau tumor suppressor
Ube3c|UBE3C	ubiquitin protein ligase E3C
ASPSCR1	alveolar soft part sarcoma chromosome region, candidate 1
FBXL12	F-box and leucine-rich repeat protein 12
TRIM38	tripartite motif-containing 38
FBXO7	F-box protein 7
RNF8	ring finger protein (C3HC4 type) 8
DTX3L	deltex 3-like (Drosophila)
ATRX	alpha thalassemia/mental retardation syndrome X-linked (RAD54 homolog, S. cerevisiae)
NEDD4L	neural precursor cell expressed, developmentally down-regulated 4-like
RNF12	ring finger protein 12
DZIP3	zinc finger DAZ interacting protein 3
FBXW11	F-box and WD-40 domain protein 11
RING1	ring finger protein 1
UBE3C	ubiquitin protein ligase E3C
RNF146	ring finger protein 146
ZNRF1	zinc and ring finger 1
UBE3A	ubiquitin protein ligase E3A (human papilloma virus E6-associated protein, Angelman syndrome)
RNF26	ring finger protein 26
TRIM36	tripartite motif-containing 36
CISH	cytokine inducible SH2-containing protein
D8S2298E	reproduction 8
BIRC3	baculoviral IAP repeat-containing 3
FLJ23749	hypothetical protein FLJ23749
BAZ1B	bromodomain adjacent to zinc finger domain, 1B
UBE3B	ubiquitin protein ligase E3B
FBXO7	F-box protein 7
RAG1|RGD:1308224|Rag1	recombination activating gene 1; recombination activating gene 1 (predicted)
FBXO9	F-box protein 9
ATRX|Atrx	alpha thalassemia/mental retardation syndrome X-linked (RAD54 homolog, S. cerevisiae); alpha thalassemia/mental retardation syndrome X-linked homolog (human)
BRCA1	breast cancer 1, early onset
FBXO5	F-box protein 5
BTRC	beta-transducin repeat containing
RGD:1310460|Fbxw2|FBXW2	F-box and WD-40 domain protein 2; F-box and WD-40 domain protein 2 (predicted)
LOC339843|WWP1	WW domain containing E3 ubiquitin protein ligase 1; similar to Nedd-4-like E3 ubiquitin-protein ligase WWP1 (WW domain-containing protein 1)

symbol	name
FBXO4	F-box protein 4
BARD1	BRCA1 associated RING domain 1
BRCA1	breast cancer 1, early onset
FLJ10597	hypothetical protein FLJ10597
TRIM9|Trim9	tripartite motif-containing 9; tripartite motif protein 9
SOCS3	suppressor of cytokine signaling 3
RNF6|Rnf6	ring finger protein (C3H2C3 type) 6
RBX1	ring-box 1
FBXL6	F-box and leucine-rich repeat protein 6
TRIM52	tripartite motif-containing 52
BIRC2	baculoviral IAP repeat-containing 2
FLJ21156	hypothetical protein FLJ21156
TRIM46	tripartite motif-containing 46
HECW1	HECT, C2 and WW domain containing E3 ubiquitin protein ligase 1
TRIM36	tripartite motif-containing 36
FBXL2|Fbxl2	F-box and leucine-rich repeat protein 2
KIAA0804	KIAA0804 protein
LMO7	LIM domain 7
MLL3	myeloid/lymphoid or mixed-lineage leukemia 3
ZMYND11	zinc finger, MYND domain containing 11
SOCS5	suppressor of cytokine signaling 5
PRP19	PRP19/PSO4 homolog (S. cerevisiae)
TRIM9	tripartite motif-containing 9
HERC1	hect (homologous to the E6-AP (UBE3A) carboxyl terminus) domain and RCC1 (CHC1)-like domain (RLD) 1
TRAF6|Traf6	TNF receptor-associated factor 6; Tnf receptor-associated factor 6
PCGF3	polycomb group ring finger 3
RNF13	ring finger protein 13
- |LOC260337|UHRF2	zinc finger protein Np97 pseudogene; ubiquitin-like, containing PHD and RING finger domains, 2
RNF111	ring finger protein 111
RNF125	ring finger protein 125
DPF2	D4, zinc and double PHD fingers family 2
MLL3	myeloid/lymphoid or mixed-lineage leukemia 3
RNF103|Rnf103	ring finger protein 103
AMFR	autocrine motility factor receptor
FBXO10	F-box protein 10
RCHY1	ring finger and CHY zinc finger domain containing 1
RGD:1306453|TRIM54	ring finger protein 30 (predicted); tripartite motif-containing 54
NEDD4	neural precursor cell expressed, developmentally down-regulated 4
NEDD4L	neural precursor cell expressed, developmentally down-regulated 4-like
BARD1	BRCA1 associated RING domain 1
TRAF2	TNF receptor-associated factor 2
ZNF183L1	zinc finger protein 183-like 1

symbol	name
RGD:1306607|Trip12|TRIP12	thyroid hormone receptor interactor 12; gene trap locus 6 (predicted)
RNF26	ring finger protein 26
UBOX5|Ubox5	U box domain containing 5; U-box domain containing 5
FADS1	fatty acid desaturase 1
UBE4B	ubiquitination factor E4B (UFD2 homolog, yeast)
PCGF4|Bmi1	polycomb group ring finger 4; B lymphoma Mo-MLV insertion region 1
PDZRN3	PDZ domain containing RING finger 3
RNF32	ring finger protein 32
Brca1|BRCA1	breast cancer 1; breast cancer 1, early onset
HACE1	HECT domain and ankyrin repeat containing, E3 ubiquitin protein ligase 1
ASB3	ankyrin repeat and SOCS box-containing 3
RNF127	ring finger protein 127
RGD:727935|Fbxo11|FBXO11	F-box only protein 11; F-box protein 11
CCNF	cyclin F
RNF26	ring finger protein 26
FBXL5	F-box and leucine-rich repeat protein 5
RNF150	ring finger protein 150
TRAF6	TNF receptor-associated factor 6
MAP3K1	mitogen-activated protein kinase kinase kinase 1
RNF128	ring finger protein 128
FBXO32	F-box protein 32
RNF126	ring finger protein 126
PEX10	peroxisome biogenesis factor 10
FADS1	fatty acid desaturase 1
FBXO30	F-box protein 30
LMO7	LIM domain 7
BAZ1A	bromodomain adjacent to zinc finger domain, 1A
FLJ10597	hypothetical protein FLJ10597
TRAF6	TNF receptor-associated factor 6
FBXO40	F-box protein 40
TRIM55	tripartite motif-containing 55
FBXO3	F-box protein 3
VHL	von Hippel-Lindau tumor suppressor
RNF150	ring finger protein 150
CUL7	cullin 7
PAK6	p21(CDKN1A)-activated kinase 6
HACE1	HECT domain and ankyrin repeat containing, E3 ubiquitin protein ligase 1
HECW1	HECT, C2 and WW domain containing E3 ubiquitin protein ligase 1
FBXO38	F-box protein 38
CHD6	chromodomain helicase DNA binding protein 6
MNAB	membrane associated DNA binding protein
FBXL17	F-box and leucine-rich repeat protein 17
RFFL	fring
Huwe1|UREB1	upstream regulatory element binding protein 1; HECT, UBA and WWE domain containing 1

symbol	name
TRIM6|TRIM6-TRIM34	tripartite motif-containing 6; tripartite motif-containing 6 and tripartite motif-containing 34
FBXO18	F-box protein, helicase, 18
BTRC	beta-transducin repeat containing
Fbxl5|FBXL5	F-box and leucine-rich repeat protein 5
TRIM62	tripartite motif-containing 62
FBXO9	F-box protein 9
RNF34	ring finger protein 34
ZNRF2	zinc and ring finger 2
UREB1	upstream regulatory element binding protein 1
TPT1|UREB1	upstream regulatory element binding protein 1; tumor protein, translationally-controlled 1
RNF135	ring finger protein 135
RNF130|Rnf130	ring finger protein 130
WHSC1L1	Wolf-Hirschhorn syndrome candidate 1-like 1
RAB40B	RAB40B, member RAS oncogene family
Mdm2	transformed mouse 3T3 cell double minute 2
MNAT1	menage a trois 1 (CAK assembly factor)
FBXL11|RGD:1309419	F-box and leucine-rich repeat protein 11; F-box and leucine-rich repeat protein 11 (predicted)
TRIM8	tripartite motif-containing 8
ZNRF1	zinc and ring finger 1
DTX3L	deltex 3-like (Drosophila)
RNF144	ring finger protein 144
MDM4	Mdm4, transformed 3T3 cell double minute 4, p53 binding protein (mouse)
D8S2298E	reproduction 8
TRIM49|LOC283116	similar to RING finger protein 18 (Testis-specific ring-finger protein); tripartite motif-containing 49
SOCS5	suppressor of cytokine signaling 5
TTC3	tetratricopeptide repeat domain 3
RGD:1308638|MTAP|Phf7|PHF7	PHD finger protein 7 (predicted); PHD finger protein 7; methylthioadenosine phosphorylase
HERC6	hect domain and RLD 6
VHL	von Hippel-Lindau tumor suppressor
RNF19	ring finger protein 19
SH3MD2	SH3 multiple domains 2
HECW2	HECT, C2 and WW domain containing E3 ubiquitin protein ligase 2
RNF133	ring finger protein 133
CHD6	chromodomain helicase DNA binding protein 6
FBXL7	F-box and leucine-rich repeat protein 7
SPPL2B	SPPL2b
ZNF313	zinc finger protein 313
BARD1	BRCA1 associated RING domain 1
RNF133	ring finger protein 133
RNF130|Rnf130	ring finger protein 130
RNF34	ring finger protein 34
Smarca3|RGD:1309031|SMARCA3	SWI/SNF related, matrix associated, actin dependent regulator of chromatin, subfamily a, member 3; SWI/SNF related, matrix associated, actin dependent regulator of chromatin, subfamily a, member 3 (predicted)

symbol	name
C20orf18	chromosome 20 open reading frame 18
TRAF3	TNF receptor-associated factor 3
LOC291860_predicted|KIAA1972|4930470D19Rik	similar to SPla/RYanodine receptor SPRY (1J970) (predicted); KIAA1972 protein; RIKEN cDNA 4930470D19 gene
SKP2	S-phase kinase-associated protein 2 (p45)
RNF41	ring finger protein 41
RNF127	ring finger protein 127
HECW1	HECT, C2 and WW domain containing E3 ubiquitin protein ligase 1
BAZ1A	bromodomain adjacent to zinc finger domain, 1A
FBXL12	F-box and leucine-rich repeat protein 12
TRIM39	tripartite motif-containing 39
TTC3|LOC286495	similar to Tetratricopeptide repeat protein 3 (TPR repeat protein D); tetratricopeptide repeat domain 3
Rnf139|RNF139	ring finger protein 139
RNF26	ring finger protein 26
BAZ1A	bromodomain adjacent to zinc finger domain, 1A
FBXW2	F-box and WD-40 domain protein 2
RNF139|TATDN1	TatD DNase domain containing 1; ring finger protein 139
KIAA0794	KIAA0794 protein
RGD:621856|RNF38|Rnf38	RING finger protein OIP1; ring finger protein 38
DTX3L	deltex 3-like (Drosophila)
TRIM6	tripartite motif-containing 6
HERC5	hect domain and RLD 5
PEX10	peroxisome biogenesis factor 10
ASPSCR1	alveolar soft part sarcoma chromosome region, candidate 1
RGD:1306361|UBE3A	ubiquitin protein ligase E3A (predicted); ubiquitin protein ligase E3A (human papilloma virus E6-associated protein, Angelman syndrome)
FBXO38	F-box protein 38
PCGF2	polycomb group ring finger 2
UBXD2	UBX domain containing 2
UBE3A	ubiquitin protein ligase E3A (human papilloma virus E6-associated protein, Angelman syndrome)
VHL	von Hippel-Lindau tumor suppressor
SOCS3|Socs3	suppressor of cytokine signaling 3
UBE3B	ubiquitin protein ligase E3B
TRAF6	TNF receptor-associated factor 6
RNF32	ring finger protein 32
MAFK|PPIL2	v-maf musculoaponeurotic fibrosarcoma oncogene homolog K (avian); peptidylprolyl isomerase (cyclophilin)-like 2
BIRC3	baculoviral IAP repeat-containing 3
RNF138	ring finger protein 138
LOC51255	hypothetical protein LOC51255
RFFL	fring
FBXL4	F-box and leucine-rich repeat protein 4
FBXL10	F-box and leucine-rich repeat protein 10
ANAPC11	APC11 anaphase promoting complex subunit 11 homolog (yeast)
FBXO18	F-box protein, helicase, 18
Cbll1|CBLL1	Casitas B-lineage lymphoma-like 1; Cas-Br-M (murine) ecotropic retroviral transforming sequence-like 1

symbol	name
RNF13	ring finger protein 13
TRIM23	tripartite motif-containing 23
FBXL12	F-box and leucine-rich repeat protein 12
KIAA1333	KIAA1333
Socs7|SOCS7|RGD:1307720	suppressor of cytokine signaling 7 (predicted); suppressor of cytokine signaling 7
RNF121	ring finger protein 121
RNF19	ring finger protein 19
RFFL	fring
C20orf55	chromosome 20 open reading frame 55
TRIM49	tripartite motif-containing 49
LRSAM1	leucine rich repeat and sterile alpha motif containing 1
RNF10	ring finger protein 10
FBXW7|Fbxw7	F-box and WD-40 domain protein 7 (archipelago homolog, Drosophila); F-box and WD-40 domain protein 7, archipelago homolog (Drosophila)
VHL	von Hippel-Lindau tumor suppressor
RNF19	ring finger protein 19
RAPSN	receptor-associated protein of the synapse, 43kD
LOC288469_predicted|Smurf1|SMURF1	SMAD specific E3 ubiquitin protein ligase 1; similar to RIKEN cDNA 4930431E10 (predicted)
CUL7	cullin 7
PCGF4|Bmi1	polycomb group ring finger 4; B lymphoma Mo-MLV insertion region 1
PDZRN3	PDZ domain containing RING finger 3
FBXO40	F-box protein 40
FBXO46	F-box protein 46
FBXO8	F-box protein 8
RGD:1308654|Ttc3|TTC3|LOC286495	similar to Tetratricopeptide repeat protein 3 (TPR repeat protein D); tetratricopeptide repeat domain 3; tetratricopeptide repeat domain 3 (predicted)
ZZANK1	zinc finger, ZZ type with ankyrin repeat domain 1
RNF41	ring finger protein 41
FLJ20225	hypothetical protein FLJ20225
0610009K11Rik|FLJ12875	hypothetical protein FLJ12875; RIKEN cDNA 0610009K11 gene
FBXL7	F-box and leucine-rich repeat protein 7
PML	promyelocytic leukemia
FBXW11	F-box and WD-40 domain protein 11
ZNF183L1	zinc finger protein 183-like 1
ASB3	ankyrin repeat and SOCS box-containing 3
ATRX|RGD:619795|Atrx	alpha thalassemia/mental retardation syndrome X-linked (RAD54 homolog, S. cerevisiae); alpha thalassemia/mental retardation syndrome X-linked (RAD54 homolog, S.cerevisiae); alpha thalassemia/mental retardation syndrome X-linked homolog (human)
RNF40	ring finger protein 40
TRIM56	tripartite motif-containing 56
ZNRF3|BC019575	zinc and ring finger 3; cDNA sequence BC019575
FBXL17	F-box and leucine-rich repeat protein 17
FBXO28	F-box protein 28
RGD:1308885|Trim41|TRIM41	tripartite motif-containing 41; tripartite motif-containing 41 (predicted)

symbol	name
RAG1	recombination activating gene 1
NEDD4	neural precursor cell expressed, developmentally down-regulated 4
FBXO42	F-box protein 42
ZNF183	zinc finger protein 183 (RING finger, C3HC4 type)
Zmynd11|RGD:1303252|ZMYND11	zinc finger, MYND domain containing 11; BS69 protein
UBE4A	ubiquitination factor E4A (UFD2 homolog, yeast)
TRIM68	tripartite motif-containing 68
TRIM10	tripartite motif-containing 10
MNAT1	menage a trois 1 (CAK assembly factor)
ARIH1	ariadne homolog, ubiquitin-conjugating enzyme E2 binding protein, 1 (Drosophila)
DZIP3	zinc finger DAZ interacting protein 3
UBE3B	ubiquitin protein ligase E3B
BTRC	beta-transducin repeat containing
RNF20	ring finger protein 20
SOCS3	suppressor of cytokine signaling 3
FBXO5	F-box protein 5
RNF149	ring finger protein 149
SOCS6	suppressor of cytokine signaling 6
RAD18	RAD18 homolog (S. cerevisiae)
NEDD4L	neural precursor cell expressed, developmentally down-regulated 4-like
HACE1	HECT domain and ankyrin repeat containing, E3 ubiquitin protein ligase 1
HACE1|Hace1|RGD:1306114	HECT domain and ankyrin repeat containing, E3 ubiquitin protein ligase 1; HECT domain and ankyrin repeat containing, E3 ubiquitin protein ligase 1 (predicted)
ITCH	itchy homolog E3 ubiquitin protein ligase (mouse)
UBOX5	U-box domain containing 5
RNF26	ring finger protein 26
Fbxw2|FBXW2	F-box and WD-40 domain protein 2
DTX4	deltex 4 homolog (Drosophila)
KIAA0794	KIAA0794 protein
FBXO3	F-box protein 3
FBXO24	F-box protein 24
FBXL5	F-box and leucine-rich repeat protein 5
RNF39	ring finger protein 39
MKRN3	makorin, ring finger protein, 3
RNF19	ring finger protein 19
RNF2	ring finger protein 2
RNF138	ring finger protein 138
LMO7	LIM domain 7
PAK6	p21(CDKN1A)-activated kinase 6
RGD:1306366|HERC1	hect (homologous to the E6-AP (UBE3A) carboxyl terminus) domain and RCC1 (CHC1)-like domain (RLD) 1 (predicted); hect (homologous to the E6-AP (UBE3A) carboxyl terminus) domain and RCC1 (CHC1)-like domain (RLD) 1
TIF1	transcriptional intermediary factor 1
UBE3B	ubiquitin protein ligase E3B
HERC2	hect domain and RLD 2
RNF8	ring finger protein (C3HC4 type) 8
FBXO11	F-box protein 11

symbol	name
RFP2	ret finger protein 2
SOCS2	suppressor of cytokine signaling 2
SMARCA3	SWI/SNF related, matrix associated, actin dependent regulator of chromatin, subfamily a, member 3
FBXW11	F-box and WD-40 domain protein 11
TRIM22	tripartite motif-containing 22
UBE3B	ubiquitin protein ligase E3B
MGC4734	hypothetical protein MGC4734
FLJ30092	AF-1 specific protein phosphatase
TRIM5	tripartite motif-containing 5
FBXO7	F-box protein 7
WSB1	WD repeat and SOCS box-containing 1
FBXO28	F-box protein 28
PCGF3	polycomb group ring finger 3
ZNF364	zinc finger protein 364
BRAP	BRCA1 associated protein
TRIM6|TRIM6-TRIM34	tripartite motif-containing 6; tripartite motif-containing 6 and tripartite motif-containing 34
WHSC1L1	Wolf-Hirschhorn syndrome candidate 1-like 1
BRCA1	breast cancer 1, early onset
FLJ31951	hypothetical protein FLJ31951
FBXO3|Fbxo3|RGD:1306352	F-box protein 3; F-box only protein 3 (predicted); F-box only protein 3
UBE3C	ubiquitin protein ligase E3C
VPS41	vacuolar protein sorting 41 (yeast)
RFFL	fring
Trim23|TRIM23	tripartite motif-containing 23; tripartite motif protein 23
ZNRF4	zinc and ring finger 4
FBXO28	F-box protein 28
Rnf19|RNF19	ring finger protein (C3HC4 type) 19; ring finger protein 19
BRCA1	breast cancer 1, early onset
PDZRN4	PDZ domain containing RING finger 4
PCGF4	polycomb group ring finger 4
Trim8|TRIM8	tripartite motif protein 8; tripartite motif-containing 8
RNF146	ring finger protein 146
RFFL	fring
KIAA1333	KIAA1333
4432411E13Rik|EDD|RGD:621236	E3 identified by differential display; RIKEN cDNA 4432411E13 gene; progestin induced protein
FLJ30092	AF-1 specific protein phosphatase
RNF167|Rnf167|RGD:1305972	similar to RIKEN cDNA 5730408C10 (predicted); ring finger protein 167
ASB1	ankyrin repeat and SOCS box-containing 1
RNF11	ring finger protein 11
SOCS1	suppressor of cytokine signaling 1
FBXO22	F-box protein 22
UHRF2	ubiquitin-like, containing PHD and RING finger domains, 2
LMO7	LIM domain 7
TRIM52	tripartite motif-containing 52
BIRC7	baculoviral IAP repeat-containing 7 (livin)

symbol	name
CISH	cytokine inducible SH2-containing protein
FBXO46	F-box protein 46
FBXO3	F-box protein 3
RNF20	ring finger protein 20
WSB2	WD repeat and SOCS box-containing 2
CHD6	chromodomain helicase DNA binding protein 6
RNF44	ring finger protein 44
FBXO32	F-box protein 32
4931406I20Rik|FLJ10597	hypothetical protein FLJ10597; RIKEN cDNA 4931406I20 gene
ZC3HDC5	zinc finger CCCH type domain containing 5
FBXL4	F-box and leucine-rich repeat protein 4
RNF150	ring finger protein 150
TRIM5	tripartite motif-containing 5
FBXL11|RGD:1309419	F-box and leucine-rich repeat protein 11; F-box and leucine-rich repeat protein 11 (predicted)
ARIH1|Arih1	ariadne homolog, ubiquitin-conjugating enzyme E2 binding protein, 1 (Drosophila); ariadne ubiquitin-conjugating enzyme E2 binding protein homolog 1 (Drosophila)
ZNRF2	zinc and ring finger 2
FBXL11	F-box and leucine-rich repeat protein 11
RNF7	ring finger protein 7
LRRC29|Lrrc29	leucine rich repeat containing 29
FLJ32785	hypothetical protein FLJ32785
SOCS2	suppressor of cytokine signaling 2
RNF149	ring finger protein 149
WSB2	WD repeat and SOCS box-containing 2
RNF144	ring finger protein 144
PCGF6	polycomb group ring finger 6
RNF122	ring finger protein 122
RNF167	ring finger protein 167
PCGF3	polycomb group ring finger 3
RNF138	ring finger protein 138
NOSIP	nitric oxide synthase interacting protein
MRPL49	mitochondrial ribosomal protein L49
FLJ30092	AF-1 specific protein phosphatase
FBXW8	F-box and WD-40 domain protein 8
RGD:1310374|FBXO9	f-box only protein 9 (predicted); F-box protein 9
HERC1	hect (homologous to the E6-AP (UBE3A) carboxyl terminus) domain and RCC1 (CHC1)-like domain (RLD) 1
PDZRN3	PDZ domain containing RING finger 3
PJA2	praja 2, RING-H2 motif containing
FBXL17	F-box and leucine-rich repeat protein 17
ANKIB1	ankyrin repeat and IBR domain containing 1
RNF38	ring finger protein 38
FBXO40	F-box protein 40
C20orf18	chromosome 20 open reading frame 18
RNF10	ring finger protein 10

symbol	name
SH3MD2	SH3 multiple domains 2
MNAB	membrane associated DNA binding protein
Socs2|SOCS2	suppressor of cytokine signaling 2
RNF6	ring finger protein (C3H2C3 type) 6
UBE3A	ubiquitin protein ligase E3A (human papilloma virus E6-associated protein, Angelman syndrome)
TRIM26	tripartite motif-containing 26
ITCH	itchy homolog E3 ubiquitin protein ligase (mouse)
TRIM33	tripartite motif-containing 33
HACE1	HECT domain and ankyrin repeat containing, E3 ubiquitin protein ligase 1
FBXO8	F-box protein 8
FBXO25	F-box protein 25
LRRC29	leucine rich repeat containing 29
MYLIP	myosin regulatory light chain interacting protein
PEX12	peroxisomal biogenesis factor 12
TTC3|LOC286495	similar to Tetratricopeptide repeat protein 3 (TPR repeat protein D); tetratricopeptide repeat domain 3
CISH	cytokine inducible SH2-containing protein
WSB1	WD repeat and SOCS box-containing 1
MRPL49	mitochondrial ribosomal protein L49
DTX3L	deltex 3-like (Drosophila)
FBXO4	F-box protein 4
FBXO11	F-box protein 11
RNF150	ring finger protein 150
WWP1	WW domain containing E3 ubiquitin protein ligase 1
TRIM45	tripartite motif-containing 45
ATRX	alpha thalassemia/mental retardation syndrome X-linked (RAD54 homolog, S. cerevisiae)
BIRC2	baculoviral IAP repeat-containing 2
LMO7	LIM domain 7
Cbll1|CBLL1	Casitas B-lineage lymphoma-like 1; Cas-Br-M (murine) ecotropic retroviral transforming sequence-like 1
MGRN1	mahogunin, ring finger 1
ASPSCR1	alveolar soft part sarcoma chromosome region, candidate 1
RNF150	ring finger protein 150
FBXO44	F-box protein 44
HECTD1	HECT domain containing 1
ARIH1	ariadne homolog, ubiquitin-conjugating enzyme E2 binding protein, 1 (Drosophila)
FBXL5|RGD:1306887	F-box and leucine-rich repeat protein 5 (predicted); F-box and leucine-rich repeat protein 5
Zmynd11|ZMYND11	zinc finger, MYND domain containing 11
FBXW11	F-box and WD-40 domain protein 11
ASB2	ankyrin repeat and SOCS box-containing 2
FBXW7	F-box and WD-40 domain protein 7 (archipelago homolog, Drosophila)
KIAA1333	KIAA1333
RNF44	ring finger protein 44
FBXL10	F-box and leucine-rich repeat protein 10
WWP2	WW domain containing E3 ubiquitin protein ligase 2
RNF38|Rnf38	ring finger protein 38
ZFYVE19	zinc finger, FYVE domain containing 19
RNF128	ring finger protein 128

symbol	name
TRAF6	TNF receptor-associated factor 6
FBXL5	F-box and leucine-rich repeat protein 5
RKHD2	ring finger and KH domain containing 2
SMURF1	SMAD specific E3 ubiquitin protein ligase 1

Table 4.4 The priority set-shRNA library

Target	blastID	Target	blastID	Target	blastID
CUL1	CUL1.1201		LMO7.6395	STAMBP1	STAMBPL1.1091
	CUL1.2227	LONRF1	LONRF1.1239		STAMBPL1.1919
	CUL1.2599		LONRF1.1923		STAMBPL1.1958
	CUL1.3048		LONRF1.2552		STAMBPL1.695
CDUB3	DUB3.1007		LONRF1.2564		STAMBPL1.812
	DUB3.1023		LONRF1.3153		STAMBPL1.175
	DUB3.1385	PSMA2	PSMA2.1164	TCEB1	TCEB1.161
	DUB3.598		PSMA2.1424		TCEB1.286
	DUB3.790		PSMA2.649		TCEB1.404
	DUB3.851		PSMA2.656		TCEB1.408
FBXL4	FBXL4.1645		PSMA2.741		TCEB1.62
	FBXL4.2349	PSMD7	PSMD7.1339	TRIM13	TRIM13.3487
	FBXL4.338		PSMD7.342		TRIM13.4494
	FBXL4.771		PSMD7.369		TRIM13.5301
	FBXL4.934		PSMD7.370		TRIM13.5308
FBXO25	FBXO25.1989		PSMD7.380		TRIM13.752
	FBXO25.2021		PSMD7.653		TRIM13.848
	FBXO25.2196	PXMP3	PXMP3.1646	UBAP1	UBAP1.1618
	FBXO25.2240		PXMP3.1647		UBAP1.217
	FBXO25.758		PXMP3.1648		UBAP1.2417
FRK	FRK.1365		PXMP3.2619		UBAP1.296
	FRK.1604		PXMP3.2684		UBAP1.893
	FRK.1608		PXMP3.542	UBAP2	UBAP2.1647
	FRK.1666	RNF122	RNF122.1366		UBAP2.3002
	FRK.1709		RNF122.1580		UBAP2.3303
	FRK.472		RNF122.1581		UBAP2.4038
LMO7	LMO7.187		RNF122.649	USP45	USP45.2805
	LMO7.5433		RNF122.833		USP45.3824
	LMO7.5494	TPT1	TPT1.358		USP45.538
	LMO7.5545		TPT1.365		USP45.5952
	LMO7.5783		TPT1.488		USP45.4470
UBXN8	[illegible]	SIAH3	[illegible]		[illegible]
	UBXN8.490		SIAH3.2195	UCHL3	UCHL3.335
	UBXN8.538		SIAH3.3410		UCHL3.497
	UBXN8.557		SIAH3.3429		UCHL3.678

Target	blastID	Target	blastID	Target	blastID
	UBXN8.675	UFM1	UFM1.1188		UCHL3.679
	UBXN8.577		UFM1.1972		UCHL3.715
UBE2J1	UBE2J1.2135		UFM1.1973	ZNRF1	ZNRF1.2018
	UBE2J1.2856		UFM1.2242		ZNRF1.2211
	UBE2J1.4153		UFM1.448		ZNRF1.2537
	UBE2J1.4325		UFM1.475		ZNRF1.3180
	UBE2J1.567	USP10	USP10.1333		ZNRF1.4280
	UBE2J1.881		USP10.1532		ZNRF1.4433
UBE2R2	UBE2R2.1134		USP10.1750	HACE1	HACE1.1602
	UBE2R2.1782		USP10.3003		HACE1.2496
	UBE2R2.2366		USP10.3101		HACE1.2933
	UBE2R2.4399		USP10.613		HACE1.3979
	UBE2R2.950	USP33	USP33.1007		HACE1.609
UBE2W	UBE2W.1045		USP33.1302		HACE1.3456
	UBE2W.1078		USP33.1358	UBE2CBP	UBE2CBP.1358
	UBE2W.2614		USP33.2176		UBE2CBP.1581
	UBE2W.262		USP33.2507		UBE2CBP.1582
	UBE2W.2810		USP33.624		UBE2CBP.1584
	UBE2W.3779	USP42	USP42.121		UBE2CBP.1813
UBR5	UBR5.161		USP42.4144	WHSC1L1	WHSC1L1.1233
	UBR5.1629		USP42.4569		WHSC1L1.1396
	UBR5.7005		USP42.4745		WHSC1L1.1501
	UBR5.7606		USP42.4972		WHSC1L1.1718
	UBR5.7682	UBE2H	UBE2H.1148		WHSC1L1.768
RNF166	RNF166.1316		UBE2H.1389		WHSC1L1.845
	[illegible]		[illegible]		
	[illegible]		[illegible]		